BLEJSKE DELAVNICE IZ FIZIKE LETNIK 5, ŠT. 1
BLED WORKSHOPS IN PHYSICS VOL. 5, NO. 1

ISSN 1580–4992

Proceedings of the Mini-Workshop

Quark Dynamics

Bled, Slovenia, July 12–19, 2004

Edited by

Bojan Golli
Mitja Rosina
Simon Širca

University of Ljubljana and Jožef Stefan Institute

DMFA – ZALOŽNIŠTVO
LJUBLJANA, NOVEMBER 2004

The Mini-Workshop *Quark Dynamics*

was organized by

Jožef Stefan Institute, Ljubljana

Department of Physics, Faculty of Mathematics and Physics, University of Ljubljana

and sponsored by

Ministry of Education, Science and Sport of Slovenia

Department of Physics, Faculty of Mathematics and Physics, University of Ljubljana

Society of Mathematicians, Physicists and Astronomers of Slovenia

Organizing Committee

Mitja Rosina
Bojan Golli
Simon Širca

List of participants

José Amoreira, Covilhã, amoreira@dfisica.ubi.pt
Enrique Ruiz Arriola, Granada, earriola@ugr.es
Wojciech Broniowski, Krakow, b4bronio@cyf-kr.edu.pl
Luciano Canton, Padova, luciano.canton@pd.infn.it
Manuel Fiolhais, Coimbra, tmanuel@teor.fis.uc.pt
Harald Fritzsch, München, fritzsch@mppmu.mpg.de
Leonid Glozman, Graz, leonid.glozman@uni-graz.at
Dubravko Klabučar, Zagreb, klabucar@phy.hr
William Klink, Iowa, william-klink@uiowa.edu
Thomas Melde, Graz, thomas.melde@uni-graz.at
Willibald Plessas, Graz, plessas@bkfug.kfunigraz.ac.at
Dan-Olof Riska, Helsinki, riska@pcu.helsinki.fi
Bojan Golli, Ljubljana, bojan.golli@ijs.si
Damijan Janc, Ljubljana, damijan.janc@ijs.si
Mitja Rosina, Ljubljana, mitja.rosina@ijs.si
Simon Širca, Ljubljana, simon.sirca@fmf.uni-lj.si
Tomo Živko, Ljubljana, tomi.zivko@ijs.si

Electronic edition

http://www-f1.ijs.si/BledPub/

Contents

Preface V

Polyakov Loop at Finite Temperature in Chiral Quark Models
E. Megías, E. Ruiz Arriola, and L.L. Salcedo 1

Application of chiral quark models to high-energy processes
W. Broniowski and E. Ruiz Arriola 7

On the Meson-Few-Body Problem From a Few-Nucleon Perspective
L. Canton and L. G. Levchuk 11

Quark matter and quark stars
M. Fiolhais, L. P. Linares, M. Malheiro, A. Taurines 18

A Time Dependence of the Scale of QCD
H. Fritzsch 22

Critical Review of Pentaquarks
L. Ya. Glozman 27

Excited Hadrons on the Lattice
L. Ya. Glozman (for BGR collaboration) 28

A heuristic derivation of an effective QCD coupling dominated by gluon condensates
D. Kekez and D. Klabučar 29

Vertex Interactions and Applications
W. H. Klink 36

Strong Decays of Baryons
T. Melde, L. Canton, W. Plessas, and R. F. Wagenbrunn 43

Relativistic Treatment of Baryon Reactions
W. Plessas 49

The Double-Charm Hyperons and Their Interactions
D.-O. Riska 58

Calculation of electroproduction amplitudes in the K-matrix formalism
B. Golli, P. Alberto, L. Amoreira, M. Fiolhais and S. Širca 62

Molecular binding of $T_{cc} = DD^*$ tetraquark
D. Janc, M. Rosina 70

New ideas about production and detection of cc-tetraquarks
M. Rosina , D. Janc 74

Recent results on Δ resonance production at MIT-Bates, MAMI, and JLab (Hall A)
S. Širca 77

Search for Pentaquarks at HERA-B
T. Živko 83

Preface

This summer's Mini-Workshop on Quark Dynamics has been another in the traditional series of meetings held at Bled, in the inspiring atmosphere of Villa Plemelj. The Workshop, virtually free of the time constraints imposed on speakers at large-scale venues, has retained the spirit of "friendly confrontation" among physicists working on closely related problems in hadronic physics. With respect to the previous Workshops, the emphasis has shifted from the structure of hadrons to the dynamics of their production and detection, and a colorful set of topics has been covered.

The relativistic approach has been advanced one step further, using the spectator approximation and the point form. Yet, a few "naughty" electro-magnetic and mesonic decays of baryons remain to be open problems. To see, or not to see a pentaquark was an unbalanced issue with prevailing arguments against the sightings. On the other hand, the tetraquark proponents were optimistic about the conclusion that the DD^* state is probably bound. The Roper resonance has been observed in lattice QCD. Production of pions was shown to be a three-body problem sensitive to spin-orbit and tensor forces. Does the strong coupling change over time? Maybe a laser can tell. High energies, high temperatures, high densities, the chiral phase transition, and quark stars still excite our phantasy. Can effective interactions be parameterized directly by Feynman graphs? What is the role of the gluon condensate?

These Proceedings represent a succinct record of the broad range of issues discussed at the Workshop.

Ljubljana, November 2004

M. Rosina
B. Golli
S. Širca

Workshops organized at Bled

- *What Comes beyond the Standard Model* (June 29–July 9, 1998)
  Bled Workshops in Physics **0** (1999) No. 1
- *Hadrons as Solitons* (July 6–17, 1999)
- *What Comes beyond the Standard Model* (July 22–31, 1999)
- *Few-Quark Problems* (July 8–15, 2000)
  Bled Workshops in Physics **1** (2000) No. 1
- *What Comes beyond the Standard Model* (July 17–31, 2000)
- *Statistical Mechanics of Complex Systems* (August 27–September 2, 2000)
- *Selected Few-Body Problems in Hadronic and Atomic Physics* (July 7–14, 2001)
  Bled Workshops in Physics **2** (2001) No. 1
- *What Comes beyond the Standard Model* (July 17–27, 2001)
  Bled Workshops in Physics **2** (2001) No. 2
- *Studies of Elementary Steps of Radical Reactions in Atmospheric Chemistry*
- *Quarks and Hadrons* (July 6–13, 2002)
  Bled Workshops in Physics **3** (2002) No. 3
- *What Comes beyond the Standard Model* (July 15–25, 2002)
  Bled Workshops in Physics **3** (2002) No. 4
- *Effective Quark-Quark Interaction* (July 7–14, 2003)
  Bled Workshops in Physics **4** (2003) No. 1
- *What Comes beyond the Standard Model* (July 17–27, 2003)
  Bled Workshops in Physics **4** (2003) No. 2-3
- *Quark Dynamics* (July 12–19, 2004)
  Bled Workshops in Physics **5** (2004) No. 1
- *What Comes beyond the Standard Model* (July 19–29, 2004)

Also published in this series

- Book of Abstracts, *XVIII European Conference on Few-Body Problems in Physics*, Bled, Slovenia, September 8–14, 2002, Edited by Rajmund Krivec, Bojan Golli, Mitja Rosina, and Simon Širca
  Bled Workshops in Physics **3** (2002) No. 1–2

BLED WORKSHOPS
IN PHYSICS
VOL. 5, NO. 1

Proceedings of the Mini-Workshop
Quark Dynamics *(p. 1)*
Bled, Slovenia, July 12-19, 2004

Polyakov Loop at Finite Temperature in Chiral Quark Models*

E. Megías, E. Ruiz Arriola, and L.L. Salcedo

Departamento de Física Moderna, Universidad de Granada, E-18071 Granada, Spain

Abstract. At finite temperature, chiral quark models do not incorporate large gauge invariance which implies genuinely non-perturbative finite temperature gluonic degrees of freedom. Motivated by this observation, we describe how the coupling of the Polyakov loop as an independent degree of freedom to quarks not only accounts for large gauge invariance, but also allows to establish in a dynamical way the interaction between composite hadronic states such as Goldstone bosons to finite temperature non-perturbative gluons in a medium which can undergo a confinement-deconfinement phase transition.

1 Large Gauge Transformations

One feature of gauge theories like QCD at finite temperatures in the imaginary time formulation [1–3] is the non-perturbative manifestation of the non Abelian gauge symmetry. In the Polyakov gauge, where $\partial_4 A_4 = 0$ and A_4 is a diagonal and traceless $N_c \times N_c$ matrix, and N_c is the number of colors, there is still some freedom in choosing the gluon field. Let us consider for instance the periodic gauge transformation [4,5]

$$g(x_4) = e^{i2\pi x_4 \Lambda/\beta}\,, \tag{1}$$

where Λ is a color traceless diagonal matrix of integers. We call it a large gauge transformation (LGT) since it cannot be considered to be close to the identity[1]. The gauge transformation on the A_4 component of the gluon field is

$$A_4 \to A_4 + \frac{2\pi}{\beta}\Lambda\,. \tag{2}$$

Thus, invariance under the LGT, Eq. (1), implies a constant shift in the A_4 gluon amplitudes, meaning that A_4 is not uniquely defined by the Polyakov gauge condition. These ambiguities on the choice of the gauge field within a given gauge fixing are usually called Gribov copies. The requirement of gauge invariance actually implies identifying all amplitudes differing by a multiple of $2\pi/\beta$, which means periodicity in the diagonal amplitudes of A_4 of period $2\pi/\beta$. Perturbation theory, which corresponds to expanding in powers of small A_4 fields manifestly breaks gauge invariance at finite temperature, because a Taylor expansion on a periodic function violates the periodicity behavior. Thus, taking into

* Talk delivered by E. Ruiz Arriola

[1] Note that they are not large in the topological sense, as discussed in [4,5].

account these Gribov replicas is equivalent to explicitly deal with genuine non-perturbative finite temperature gluonic degrees of freedom. A way of automatically taking into account LGT is by considering the Polyakov loop Ω as an independent variable, which in the Polyakov gauge becomes a diagonal unitary matrix

$$\Omega = e^{i\beta A_4(\mathbf{x})} \tag{3}$$

invariant under the set of transformations given by Eq. (1). The relevance of the Polyakov loop in practical calculations is well recognized [1] but seldomly taken into account in high temperature calculations where large gauge invariance is manifestly broken since the gluon field is considered to be small. We have recently developed an expansion keeping these symmetries in general theories and applied it to QCD at the one quark+gluon loop level [6,7].

2 The Center Symmetry

In pure gluodynamics, or in the quenched approximation (valid for heavy quarks) at finite temperature there is actually a larger symmetry since one can extend the periodic transformations to aperiodic ones [3],

$$g(x_4+\beta) = zg(x_4)\,, \qquad z^{N_c} = 1 \tag{4}$$

so that z is an element of the center $Z(N_c)$ of the group $SU(N_c)$. This center symmetry is a symmetry of the action as well as the gluon field boundary conditions. An example of such a transformation in the Polyakov gauge is given by

$$g(x_4) = e^{i2\pi x_4 \Lambda/N_c\beta}\,. \tag{5}$$

On the A_4 component of the gluon field produces

$$A_4 \to A_4 + \frac{2\pi}{N_c\beta}\Lambda\,. \tag{6}$$

Thus, in the quenched approximation the period is N_c times smaller than in full QCD. Under these transformations the gluonic action, measure and boundary conditions are invariant. The Polyakov loop, however, transforms as the fundamental representation of the $Z(N_c)$ group, i.e. $\Omega \to z\Omega$, yielding $\langle\Omega\rangle = z\langle\Omega\rangle$ and hence $\langle\Omega\rangle = 0$ in the unbroken center symmetry phase. At high temperatures one expects perturbation theory to hold, the gluon field amplitude becomes small and hence $\langle\Omega\rangle \to 1$, justifying the choice of Ω as an order parameter for a confinement-deconfinement phase transition. More generally, in the confining phase

$$\langle\Omega^n\rangle = 0 \qquad \text{for} \qquad n \neq mN_c \tag{7}$$

with m an arbitrary integer. The antiperiodic quark fields at the end of the Euclidean imaginary interval transform as $q(\mathbf{x},\beta) = -q(\mathbf{x},0) \to zq(\mathbf{x},\beta) = -q(\mathbf{x},0)$,

so that the center symmetry is explicitly broken by the presence of dynamical quarks. A direct consequence of such a property is that, in the quenched approximation non-local condensates fulfill a selection rule of the form,

$$\langle \bar{q}(n\beta)q(0)\rangle = 0 \qquad \text{for} \qquad n \neq mN_c \tag{8}$$

since under the large aperiodic transformations given by Eq. (5) we have $\bar{q}(n\beta)q(0) \to z^{-n}\bar{q}(n\beta)q(0)$. This selection rule has some impact on chiral quark models.

3 Chiral quark models at finite temperature

To fully appreciate the role played by the center symmetry in chiral quark models (for a recent review on such models see e.g. Ref. [8] and references therein) let us evaluate the chiral condensate at finite temperature. At the one loop level one has[2]

$$\langle \bar{q}q\rangle^* = 4MTTr_c \sum_{\omega_n} \int \frac{d^3k}{(2\pi)^3} \frac{1}{\omega_n^2 + k^2 + M^2} \tag{9}$$

where $\omega_n = 2\pi T(n + 1/2)$ are the fermionic Matsubara frequencies, M is the constituent quark mass and Tr_c stands for the color trace in the fundamental representation which in this case trivially yields a N_c factor. Possible finite cut-off corrections, appearing in the chiral quark models such as the NJL model at finite temperature have been neglected. This is a reasonable approximation as long as the temperature is low enough $T \ll \Lambda \sim 1\text{GeV}$. The condensate can be rewritten as

$$\langle \bar{q}q\rangle^* = \sum_n (-1)^n \langle \bar{q}(n\beta)q(0)\rangle \tag{10}$$

in terms of nonlocal Euclidean condensates at zero temperature. After Poisson resummation, at low temperatures we have

$$\begin{aligned} \langle \bar{q}q\rangle^* &= \langle \bar{q}q\rangle + 8N_c \sum_{n=1}^{\infty} (-)^n \frac{TM^2}{\pi^2} K_1(Mn/T)\,, \\ &\sim \langle \bar{q}q\rangle - \sum_{n=1}^{\infty} (-)^n \frac{N_c}{2} \left(\frac{2Mn T}{\pi}\right)^{3/2} e^{-nM/T}\,, \end{aligned} \tag{11}$$

where the asymptotic expansion of the modified Bessel function K_1 has been used. One can interpret the previous formula for the condensate in terms of statistical Boltzmann factors, since at large Euclidean coordinates the fermion propagator behaves as $S(i\beta, \boldsymbol{x}) \sim e^{-M\beta}$, so that we have contributions from multiquark states. This is a problem since it means that the heat bath is made out of free

[2] We use an asterisk to denote finite temperature observables.

constituent quarks without any color clustering[3]. Another problem comes from comparison with Chiral Perturbation Theory at Finite Temperature [10]. In the chiral limit, i.e., for $m_\pi \ll 2\pi T \ll 4\pi f_\pi$ the leading thermal corrections to the quark condensate are given by

$$\langle \bar{q}q \rangle^* \Big|_{\rm ChPT} = \langle \bar{q}q \rangle \left(1 - \frac{T^2}{8f_\pi^2} - \frac{T^4}{384 f_\pi^4} + \dots \right) . \tag{13}$$

This formula is derived under the assumption that there is no temperature dependence of the low energy constants, i.e. $L_i^* \simeq L_i$ so that the whole effect is due to thermal pion loops. Thus, the finite temperature correction is N_c-suppressed as compared to the zero temperature value. This *is not* what one sees in chiral quark model calculations; in the large N_c limit *there is* a finite temperature correction, which would mean that the low energy constants which appear in the chiral Lagrangian would have a genuine tree level temperature dependence, $L_i^* - L_i \simeq N_c e^{-M/T}$. To obtain the ChPT result of Eq. (13) pion loops have to be considered [11] and dominate for $T \ll M$. The problem is that already without pion loops chiral quark models predict a chiral phase transition at about $T_c \sim 170$ MeV, in remarkable but perhaps unjustified agreement with lattice calculations.

4 Coupling the Polyakov loop

In the Polyakov gauge one can formally keep track of large gauge invariance at finite temperature by coupling gluons to the model in a minimal way. This means in practice using the modified fermionic Matsubara frequencies [4,5]

$$\hat{\omega}_n = 2\pi T(n + 1/2 + \nu) , \quad \nu = (2\pi i)^{-1} \log \Omega \tag{14}$$

which are shifted by the logarithm of the Polyakov loop which we assume for simplicity to be $\boldsymbol{x}$ independent. Previous work have coupled similarly Ω on pure phenomenological grounds [12–14], but the key role played by the implementation of large gauge invariance was not recognized. This is the only place where explicit dependence on colour degrees of freedom appear. This coupling introduces a colour source into the problem for a fixed A_0 field and projection onto the colour neutral states by integrating over the A_0 field, in a gauge invariant manner, as required. Actually, at the one quark loop level there is an accidental $Z(N_c)$ symmetry in the model which generates a similar selection rule as in pure gluodynamics, from which a strong thermal suppression, $\mathcal{O}(e^{-N_c M/T})$ follows.

[3] One could think that this is a natural consequence of the lack of confinement in chiral quark models such as NJL. Contrary to naive expectations this is not necessarily the case; Boltzmann factors occur in quark models with analytic confinement such as the Spectral Quark Model [9]. There the condensate is given by

$$\frac{\langle \bar{q}q \rangle_*}{\langle \bar{q}q \rangle} = \tanh(M/2T) = 1 - 2e^{-M/T} + 2e^{-2M/T} + \dots \tag{12}$$

where $M = M_S/2$, despite the absence of poles in the quark propagator.

In this way compliance with ChPT can be achieved since now $L_i^* - L_i \simeq e^{-N_c M/T}$ but also puts some doubts on whether chiral quark models still predict a chiral phase transition at realistic temperatures. This question has been addressed using specific potentials for the Polyakov loop either based on one loop perturbation theory for massive gluons [13] in the high temperature approximation or on strong coupling expansions on the lattice [14]. In both cases similar mean field qualitative features are displayed; the low temperature evolution is extremely flat, but there appears a rapid change in the critical region, so that $\langle \bar{q} q \rangle^* \simeq \langle \bar{q} q \rangle$ when $\langle \Omega \rangle \simeq 0$ and $\langle \bar{q} q \rangle \simeq 0$ when $\langle \Omega \rangle \simeq 1$. A more general discussion and diagramatic interpretation of these issues as well as the influence of higher quark loop effects and dynamical Polyakov loop contributions will be presented elsewhere [15] providing a justification of the one quark loop approximation at least at low temperatures. There one obtains that the Polyakov loop effect can be factored out as follows[4]

$$\langle \bar{q} q \rangle^* = \sum_n \frac{1}{N_c} \mathrm{Tr}_c((-\Omega)^n) \langle \bar{q}(n\beta) q(0) \rangle \, . \tag{15}$$

This result is consistent with applying the center symmetry selection rule, Eq. (8), to the $Z(N_c)$ breaking condensate, Eq. (10), of the chiral quark model without Polyakov loops. If one now takes a suitable average on Polyakov loop configurations consistent with center symmetry, i.e., including for each such configuration all its Gribov replicas, Eq. (7) applies. Schematically, this yields

$$\langle \bar{q} q \rangle^* \sim \sum_n \langle \bar{q}(n N_c \beta) q(0) \rangle \sim \sum_n e^{-n N_c M/T} \tag{16}$$

in the confining phase. (In the above sums each term carries a weight coming from the Polyakov loop average and phase space factors.) On the other hand in the unconfining phase, where the center symmetry is spontaneously broken, the Polyakov loop is nearly unity and one recovers the standard chiral quark models results, without Polyakov loop coupling.

5 Chiral Lagrangians at finite temperature

It is interesting to construct the coupling of Polyakov loops with composite pion fields at finite temperature. Using the heat kernel techniques presented in Ref. [6] and already applied to massless QCD [7], we can obtain the lowest order chiral Lagrangian

$$\mathcal{L}_q^{(2)} = \frac{f_\pi^{*\,2}}{4} \mathrm{tr}_f \left(\mathbf{D}_\mu U^\dagger \mathbf{D}_\mu U + (\overline{\chi}^\dagger U + \overline{\chi} U^\dagger) \right) \tag{17}$$

where U is the non-linear transforming pseudoscalar Goldstone field, $\bar{\chi}$ the quark mass matrix and tr_f is the trace in flavor space. The pion weak decay constant, f_π^*,

[4] Note that in this formula $\langle \bar{q}(n\beta) q(0) \rangle$ refers to quarks uncoupled to the Polyakov loop while in Eq. (8) it refers to quenched QCD.

at finite temperature in the presence of the Polyakov loop and in the chiral limit is given by

$$f_\pi^{*\,2} = 4M^2\, T\, \mathrm{Tr}_c \sum_{\hat\omega_n} \int \frac{d^3k}{(2\pi)^3} \frac{1}{[\hat\omega_n^2 + k^2 + M^2]^2}\,.$$

The full calculation of the low energy constants at order $\mathcal{O}(p^4)$ as a function of temperature and the Polyakov loop is carried out in Ref. [15]. The main feature is, similarly to $\langle\bar q q\rangle^*$ and f_π^*, a strong suppression $\mathcal{O}(e^{-N_c M\beta})$ at low temperatures, but an enhancement of quark thermal effects close to the chiral-deconfinement phase transition.

6 Conclusions

We see that the coupling of the Polyakov loop to chiral quark models at finite temperature accounts for large gauge invariance and modifies in a non-trivial way the results for physical observables. On the one hand, such a coupling allows to satisfy the requirements of chiral perturbation theory at low temperatures, generating a very strong suppression at low temperatures of quark loop effects. Nonetheless, the onset of deconfinement through a non vanishing value of the Polyakov loop accounts for a chiral phase transition at somewhat similar temperatures as in the original studies where the Polyakov loop was set to one. We expect this feature to hold also in the calculation of other observables. Although these arguments do not justify by themselves the application of these chiral quark-Polyakov models to finite temperature calculations, they do show that they do not contradict basic expectations of QCD at finite temperature.

This work is supported in part by funds provided by the Spanish DGI with grant no. BMF2002-03218, Junta de Andalucía grant no. FM-225 and EURIDICE grant number HPRN-CT-2003-00311.

References

1. D. J. Gross, R. D. Pisarski and L. G. Yaffe, Rev. Mod. Phys. **53**, 43 (1981).
2. N. P. Landsman and C. G. van Weert, Phys. Rept. **145** (1987) 141.
3. B. Svetitsky, Phys. Rept. **132** (1986) 1.
4. L. L. Salcedo, Nucl. Phys. B **549**, 98 (1999)
5. C. Garcia-Recio and L. L. Salcedo, Phys. Rev. D **63**, 045016 (2001)
6. E. Megías, E. Ruiz Arriola and L. L. Salcedo, Phys. Lett. B **563**, 173 (2003)
7. E. Megías, E. Ruiz Arriola and L. L. Salcedo, Phys. Rev. D **69** (2004) 116003
8. E. Ruiz Arriola, Acta Phys. Polon. B **33** (2002) 4443
9. E. Ruiz Arriola and W. Broniowski, Phys. Rev. D **67**, 074021 (2003)
10. J. Gasser and H. Leutwyler, Phys. Lett. B **184**, 83 (1987).
11. W. Florkowski and W. Broniowski, Phys. Lett. B **386**, 62 (1996)
12. A. Gocksch and M. Ogilvie, Phys. Rev. D **31**, 877 (1985).
13. P. N. Meisinger, T. R. Miller and M. C. Ogilvie, Nucl. Phys. Proc. Suppl. **119**, 511 (2003)
14. K. Fukushima, Phys. Lett. B **591** (2004) 277
15. E. Megías, E. Ruiz Arriola and L. L. Salcedo (in preparation)

BLED WORKSHOPS
IN PHYSICS
VOL. 5, NO. 1

Proceedings of the Mini-Workshop
Quark Dynamics *(p. 7)*
Bled, Slovenia, July 12-19, 2004

Application of chiral quark models to high-energy processes*

Wojciech Broniowski[a] and Enrique Ruiz Arriola[b]

[a] The H. Niewodniczański Institute of Nuclear Physics, Polish Academy of Sciences, PL-31342 Cracow, Poland
[b] Departamento de Física Moderna, Universidad de Granada, E-18071 Granada, Spain

Abstract. We discuss the predictions of chiral quark models for basic pion properties entering high-energy processes: generalized parton distributions (GPD's) and unintegrated parton distributions (UPD's). We stress the role of the QCD evolution, necessary to compare the predictions to data.

This is a very brief account of the talk based on Refs. [1–4], where the reader is referred to for the details and references. We discuss the use of low-energy chiral quark models to compute low-energy matrix elements of hadronic operators appearing in high-energy processes, in particular we evaluate the *generalized* and *unintegrated* parton distributions (GPD's and UPD's) of the pion in the Nambu–Jona-Lasinio model and the Spectral Quark Model [4]. We carry on the QCD evolution, necessary when comparing the model predictions to data obtained at much higher scales.

The twist-2 GPD of the pion is defined as

$$H(x,\xi,-\Delta_\perp^2) = \int \frac{dz^-}{4\pi} e^{ixp^+z^-} \langle \pi^+(p')|\bar{q}(0,-\frac{z^-}{2},0)\gamma^+ q(0,\frac{z^-}{2},0)|\pi^+(p)\rangle,$$

where the quark operator $q(z^+,z^-,z_\perp)$ is on the light cone $z^2=0$ and the link operators $P\exp(ig\int_0^z dx^\mu A_\mu)$ are implicitly present to ensure the gauge invariance (as usual we work in the light cone gauge $A_+=0$). A similar definition holds for the gluon distribution. In chiral quark models the evaluation of H at the leading-N_c (one-loop) level is straightforward. For the NJL model with the Pauli-Villars regularization we get

$$H_{\rm NJL}(x,0,-\Delta_\perp^2) = \left[1+\frac{N_c M^2(1-x)|\Delta_\perp|}{4\pi^2 f_\pi^2 s_i}\sum_i c_i \log\left(\frac{s_i+(1-x)|\Delta_\perp|}{s_i-(1-x)|\Delta_\perp|}\right)\right]\theta(x)\theta(1-x),$$

$$s_i = \sqrt{(1-x)^2\Delta_\perp^2+4M^2+4\Lambda_i^2},$$

* Talk delivered by W. Broniowski

where M is the constituent quark mass, Λ_i are the PV regulators, and c_i are suitable constants. For the simplest twice-subtracted case, explored below, one has, for any regulated function f, the operational definition

$$\sum_i c_i f(\Lambda_i^2) = f(0) - f(\Lambda^2) + \Lambda^2 df(\Lambda^2)/d\Lambda^2.$$

We use $M = 280$ MeV and $\Lambda = 871$ MeV, which yields the pion decay constant $f_\pi = 93$ MeV. In the SQM the result is

$$H_{\rm SQM}(x,0,-\Delta_\perp^2) = \frac{m_\rho^2(m_\rho^2-(1-x)^2\Delta_\perp^2)}{(m_\rho^2+(1-x)^2\Delta_\perp^2)^2}\theta(x)\theta(1-x),$$

where m_ρ is the mass of the ρ meson. We check that the pion electromagnetic form factor is

$$F_{\rm SQM}(t) = \int_0^1 dx H_{\rm SQM}(x,0,t) = \frac{m_\rho^2}{m_\rho^2+t},$$

which is the built-in vector-meson dominance principle. For both models $F(0) = 1$ and $H_{\rm SQM}(x,0,0) = \theta(x)\theta(1-x)$.

Our next goal is to compare the results to the data from transverse lattices [5]. We pass to the impact-parameter space via the Fourier-Bessel transformation, as well as carry the LO DGLAP perturbative QCD evolution from the low model scale Q_0=313 MeV [6] up to the scale of the data. The results are shown in Fig. 1. We note that while the results at Q_0 are completely different off the lattice data, when evolved to the scale of 500 MeV, corresponding to the lattice calculations, acquire a great resemblance to the data.

In the second part of this talk we discuss the leading-twist UPD's of the pion, defined as

$$q(x,k_\perp) = \int \frac{dy^- d^2y_\perp}{16\pi^3} e^{-ixp^+y^- + ik_\perp\cdot y_\perp}\langle p \mid \bar\psi(0,y^-,y_\perp)\gamma^+\psi(0)\mid p\rangle,$$

and similarly for the gluon. An elementary one-quark-loop calculation in the NJL model with the PV regularization gives for q and its Fourier-Bessel transform the result

$$q_{\rm NJL}(x,k_\perp,Q_0) = \frac{\Lambda^4 M^2 N_c}{4f_\pi^2\pi^3\left(k_\perp^2+M^2\right)\left(k_\perp^2+\Lambda^2+M^2\right)^2}\theta(x)\theta(1-x)$$

$$F_{\rm NJL}^{\rm NP}(b) = \frac{M^2N_c}{4f_\pi^2\pi^2}\left(2K_0(bM) - 2K_0(b\sqrt{\Lambda^2+M^2}) - \frac{b\Lambda^2K_1(b\sqrt{\Lambda^2+M^2})}{\sqrt{\Lambda^2+M^2}}\right).$$

In SQM we find

$$q_{\rm SQM}(x,k_\perp,Q_0) = \frac{6m_\rho^3}{\pi(k_\perp^2+m_\rho^2/4)^{5/2}}\theta(x)\theta(1-x),$$

$$F_{\rm SQM}^{\rm NP}(b) = \left(1+\frac{bm_\rho}{2}\right)\exp\left(-\frac{m_\rho b}{2}\right)$$

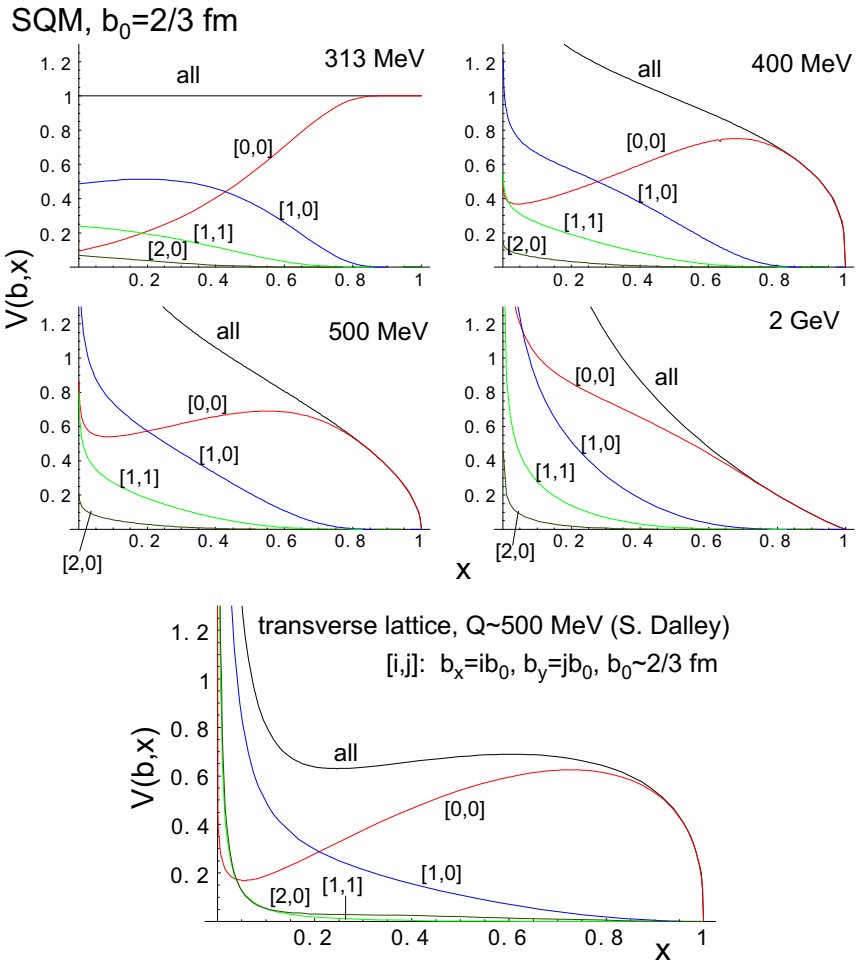

Fig. 1. GPD of the pion in the impact-parameter space plotted as a function of the Bjorken x. Top: model for four momentum scales, from 313 MeV up to 2 GeV. Bottom: transverse lattice [5]. Numbers in brackets label the plaquette [1]. The qualitative agreement to the data is achieved at the scale of about 500 MeV.

(the meaning of b different here, it is the transverse coordinate conjugated to $k_\perp$). The above results are at the low model scale Q_0. Next, we evolve these UPD's from Q_0 to high scales with the Kwieciński equations [2], obtained in the CCFM framework. The results are displayed in Fig. 2.

One may show several qualitative and quantitative results concerning UPD's. At large b they fall off exponentially and at large $k_\perp$ they fall off as a power law. Spreading with increasing Q^2 occurs, with $\langle k_\perp^2 \rangle \sim Q^2 \alpha_S(Q^2)$. Also, asymptotic formulas at limiting cases may be explicitly given [2] which may be useful in checking numerical calculations of CCFM-type cascades [7].

Our basic conclusion is that chiral quark models may be used to provide GPD's and UPD's (also the pion distribution amplitude [3] not presented here) at

the low model scale, Q_0. Upon evolution to higher scales, the agreement with the data (experimental or lattice) is very reasonable.

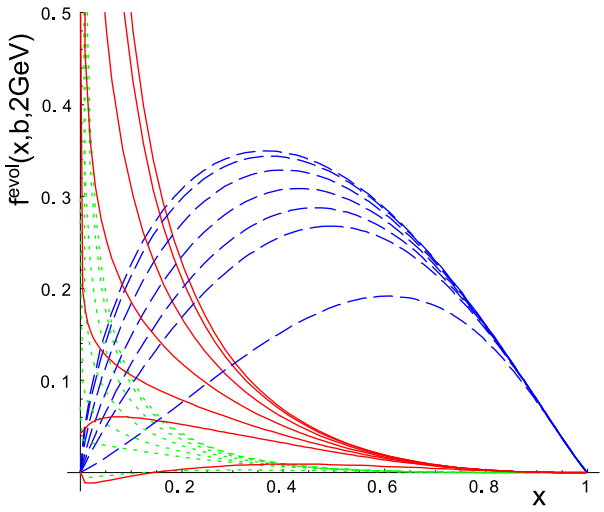

Fig. 2. Valence quarks (dashed lines), sea quarks (dotted lines), and gluons (solid lines), for the transverse coordinate $b = 0, 1, 2, 3, 4, 5$, and 10 fm (bottom to top). Evolution with the Kwieciński equations from the model scale Q_0=313 MeV up to $Q = 2$ GeV has been made.

References

1. W. Broniowski and E. Ruiz Arriola, Phys. Lett. B **574**, 57 (2003) [arXiv:hep-ph/0307198].
2. E. Ruiz Arriola and W. Broniowski, Phys. Rev. D **70**, 034012 (2004) [arXiv:hep-ph/0404008].
3. E. Ruiz Arriola and W. Broniowski, Phys. Rev. D **66**, 094016 (2002) [arXiv:hep-ph/0207266].
4. E. Ruiz Arriola and W. Broniowski, Phys. Rev. D **67**, 074021 (2003) [arXiv:hep-ph/0301202].
5. S. Dalley, Phys. Lett. B **570**, 191 (2003) [arXiv:hep-ph/0306121].
6. E. Ruiz Arriola, lectures given at 42nd Cracow School of Theoretical Physics, *Flavor Dynamics*, Zakopane, Poland, 31 May - 9 Jun 2002, Acta Phys. Polon. B **33** (2002) 4443.
7. H. Jung, Comput. Phys. Commun. **143**, 100 (2002) [arXiv:hep-ph/0109102].

BLED WORKSHOPS
IN PHYSICS
VOL. 5, NO. 1

Proceedings of the Mini-Workshop
Quark Dynamics *(p. 11)*
Bled, Slovenia, July 12-19, 2004

On the Meson-Few-Body Problem From a Few-Nucleon Perspective*

Luciano Canton[a] and Leonid G. Levchuk[b]

[a] Instituto Nazionale di Fisica Nucleare, 35131 Padova, via F. Marzolo, n. 8, Italy
[b] NSC Kharkov Institute of Physics and Technology, 61108 Kharkov, Ukraine

Abstract. The phenomenology of pion production from nucleon-deuteron collisions is analyzed, with reference to the outgoing channel where the three-nucleon system is bound. The available experimental data, from threshold up to the Δ resonance, are compared with calculations using accurate nuclear wavefunctions coming from rigorous solutions of the three-nucleon quantum mechanical equations. The dominant contributions for pion production are obtained through matrix elements involving pion-nucleon rescattering mechanisms in S- and P-waves. S-wave rescattering includes also an isoscalar contribution which is generally suppressed for low-energy pion-nucleon scattering, but becomes enhanced for pion production because the latter implies a different kinematical regime, which involves high-momenta contributions. P-wave rescattering includes also explicitly the Δ degrees of freedom. It is found that the existing data could be described reasonably well with enhanced S-wave rescattering in the isospin-even channel as is described by the Hamilton model. Initial-state interactions (ISI) between the proton and the deuteron have, in general, sizable effects on the spin-averaged and spin-dependent observables. These ISI effects become very important for spin observables involving interference terms amongst the various helicity amplitudes, such as for the nucleon vector analyzing power A_y.

The study of pion production from nucleon-deuteron collisions (this reaction is called also "pionic capture of nucleons on deuterons") represents an interesting topic of research. Potentially, it interconnects low-energy few-nucleon physics with intermediate-energy physics, pion dynamics, etc. With this reaction it is possible to study the $NN \to NN\pi$ inelasticities in the most simple (complex) nuclear environment, the three-nucleon system, where rigorous few-body techniques have been developed to describe adequately the nucleon dynamics. But these reactions can also represent a window, independent and complementary, to the diagrams that presumably contribute to the three-nucleon forces. Traditionally, 3NF's are constructed phenomenologically in low-energy few-nucleon physics to overcome some deficiencies in the three-nucleon and more-nucleon systems, with parameters adjusted *ad hoc* to reproduce some data that could not be reproduced with a given set of conventional 2N potentials. It is most desirable that those diagrams contributing to the 3NF can be studied independently

* Talk delivered by L. Canton

by other experiments, and pion production reactions could be the kind of process that might shed light on these diagrams. Another general aspect that makes pion-capture reactions quite interesting is the dependence of the associated amplitude upon the distribution of the nucleonic axial currents. This makes these processes closely related to neutrino reactions in nuclei, which is another important topic of research in present days.

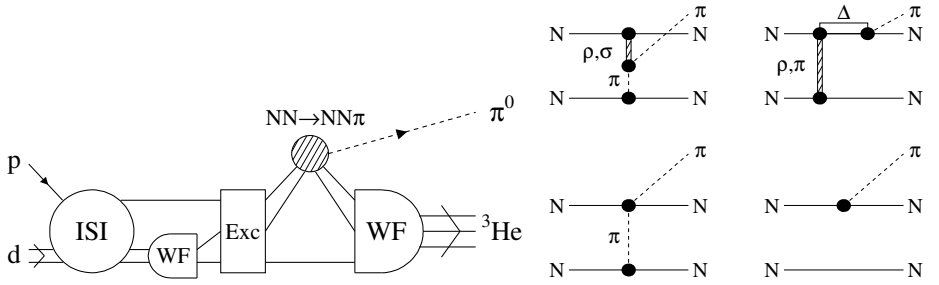

Fig. 1. Diagrammatic representation of the calculation required for determining the pion production amplitude from nucleon-deuteron collisions. *Left*, the overall diagram. *Right*, the elementary production mechanisms.

In Fig.1 the base calculation for pionic capture is illustrated. It involves use of accurate 3N bound-state wavefunctions, calculation of ISI via Faddeev-Alt-Grassberger-Sandhas techniques [1], and an exhorbitant number of multidimensional integrals for the partial-wave evaluation of the elementary pion-production processes. Details and updates for the present calculations can be found in Refs. [2].

The elementary production mechanisms (shown in the r.h.s. of Fig.1) are calculated starting from the phenomenological low-energy interaction Lagrangian, coupling the pion with the nucleon field

$$\mathcal{L}_{\rm int} = \frac{f_{\pi NN}}{m_\pi}\bar\Psi\gamma^\mu\gamma^5\boldsymbol{\tau}\Psi\cdot\partial_\mu\boldsymbol{\Phi} - 4\pi\frac{\lambda_I}{m_\pi^2}\bar\Psi\gamma^\mu\boldsymbol{\tau}\Psi\cdot[\boldsymbol{\Phi}\times\partial_\mu\boldsymbol{\Phi}] - 4\pi\frac{\lambda_O}{m_\pi}\bar\Psi\Psi\,[\boldsymbol{\Phi}\cdot\boldsymbol{\Phi}] \tag{1}$$

and with the Δ field

$$\mathcal{L}^{\Delta}_{\rm int} = -\frac{f_{\pi N\Delta}}{m_\pi}\left(\bar\Psi^\mu_\Delta\mathbf{T}\Psi\cdot\partial_\mu\boldsymbol{\Phi} + \text{h.c.}\right). \tag{2}$$

The calculations herein illustrated have been performed with the following set of parameters: $f^2_{\pi NN}/4\pi = 0.0735$, $f^2_{\pi N\Delta}/4\pi = 0.32$, $\lambda_I = 0.045$ and $\lambda_O = 0.006$. A crucial aspect is represented by the off-shell extrapolations of these parameters in the evaluation of the π-production matrix elements. For the S-waves terms we have (t is the square of the four-momentum transfer of the corresponding exchange particle)

$$\lambda_I^{OFF} = \lambda_I^{ON}\frac{m_\rho^2}{m_\rho^2 - t}\,\frac{\Lambda_\rho^2}{\Lambda_\rho^2 - t} \qquad\qquad \lambda_O^{OFF} = \lambda_O^{ON}\frac{a_{SR} + a_\sigma\frac{m_\sigma^2}{m_\sigma^2 - t}}{a_{SR} + a_\sigma}. \tag{3}$$

The form on the left denotes the isospin-odd contribution in terms of a ρ-exchange model, while on the r.h.s. we describe the isospin-even term as the combined effect of phenomenological short-range (SR) processes and an effective scalar-meson (σ) exchange. The two combined effects act in opposite directions [3]. The form on the right leads to an off-shell enhancement of the probability amplitude for pion production in the scalar-isoscalar channel. The $NN \to NN\pi$ inelasticities have been studied extensively in the case of the simpler reactions $pp \to \pi^+ d$; $pp \to pp\pi^o$; and $pp \to \pi^+ pn$. Reference to earlier works can be found in [4]; a more updated review is Ref. [5]. An interesting element of debate concerns the possible mechanisms responsible for the production yield for the process $pp \to pp\pi^o$ at threshold. This yield has been explained by resorting to two different mechanisms, represented in Fig. 2.

To ascertain which is the kind of mechanism that contribute most likely to the production process remains still an open issue. Studies performed in pion production from nucleon-nucleon collisions have been able to exclude neither of the two mechanisms shown in Fig. 2.

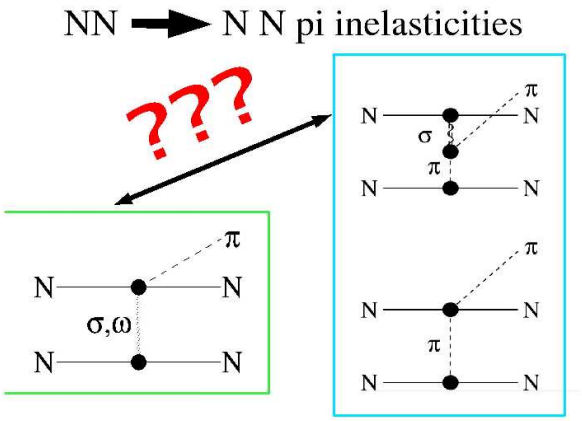

Fig. 2. Alternative mechanisms suggested for the $pp \to pp\pi^o$ reaction at threshold. *Left*, pion coupling to short-range two-body exchange currents, Ref. [6]. *Right*, pion rescattering in the isoscalar channel, Ref. [7].

One hopes that the reactions $pd \to \pi^o\, {}^3He$ and $pd \to \pi^+\, {}^3H$ could help to clarify the question of which is, if any, the correct mechanism that describe the process in the isospin even channel. These three-nucleon-type reactions are extremely complicated, and therefore much more difficult to analyze theoretically. On the other hand, here the interference effects amongst the various mechanisms are much more important than for two-nucleon collisions at threshold and therefore these reactions might represent a more stringent test for the possible mechanisms that describe the process. In the following, I will present results obtained

assuming that the production process in the scalar-isoscalar channel is dominated by the rescattering model (the two mechanisms on the r.h.s of Fig. 2); the mechanism depicted on the l.h.s of the same figure will be possibly analyzed in the future.

The current (spin-averaged) experimental situation has been greatly improved after the addition of recent Cosy data, as exhibited in Fig. 3.

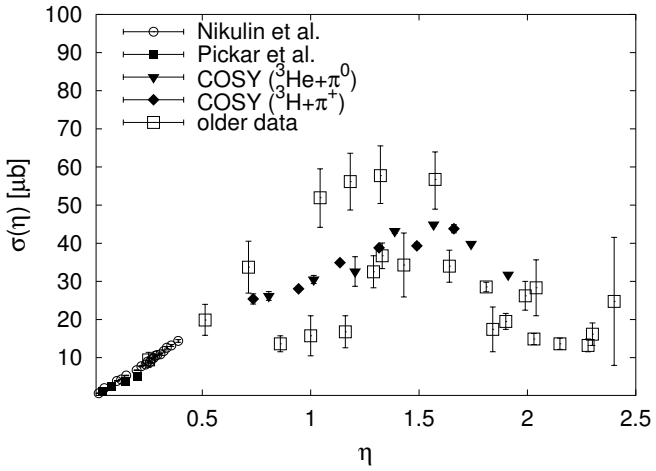

Fig. 3. The current experimental situation for the excitation function, in the energy range from threshold up to the Δ-resonance, after adding recent Cosy data (black diamonds and triangles). Reference to data can be found in [8]. The parameter η represents the pion c.m. momentum in units of pion masses.

The next figure, Fig. 4, shows the excitation function for various plane-wave calculations, using the Bonn-B model for 2N interaction. The dotted line denotes calculations with the standard (nonrelativistic) definition for the πNNN Jacobi momenta. The other two lines refer to the results with replacement of the pion mass by its total energy in this Jacobi momentum set (see details in Ref. [10]). The dotted-dashed line denotes calculations where pion rescattering in the scalar-isoscalar channel is omitted, while the solid line accounts for our full model (which includes the mechanisms on the r.h.s. of Fig. 2).

Fig. 5 shows on the l.h.s. the differential cross-section in collinear kinematics for the $pd \to \pi^o\ ^3He$ process. Calculations are for various 2N potentials. It is seen that ISI have a significant effect on the angular dependence of the differential cross-section, in particular at backward angles. The same figure shows on the r.h.s the dramatic effect that ISI's have on the proton analyzing powers A_y. In the region of interference between s-wave and p-wave mechanisms, which corresponds approximately to $\eta \approx 0.5$, the structure of A_y exhibits a rapid variation in sign, with the appearance of an additional "bump" in the angular distribution. This structure is reproduced by our complete model independently of the selected 2N potentials, once the effects of ISI are taken into account.

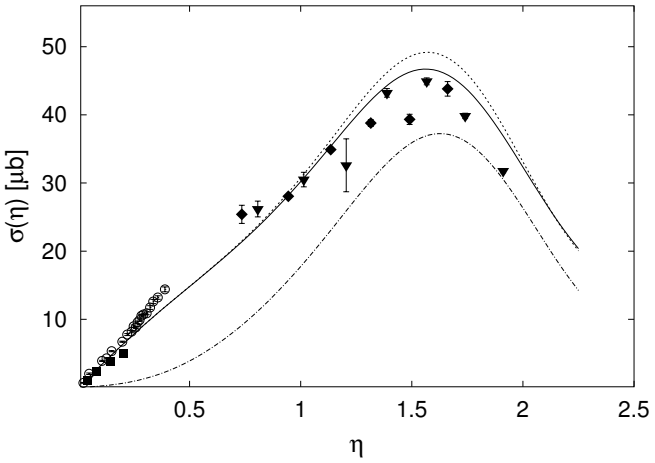

Fig. 4. Excitation function for various plane-wave calculations, using the Bonn-B model for 2N interaction. See text for details on the line notation.

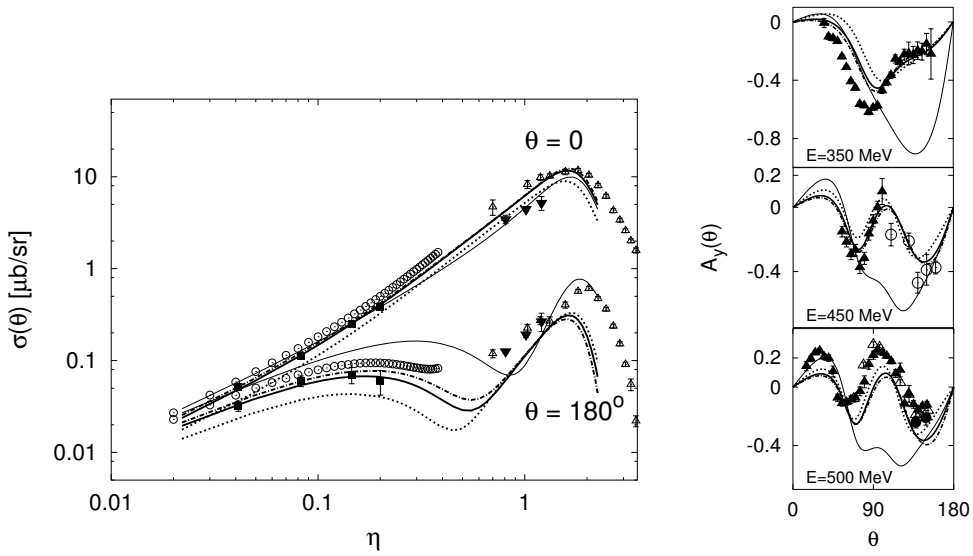

Fig. 5. *(Left)* Differential production cross-section in collinear kinematics. *(Right)* Proton analyzing power in the "interference" region between p-wave and s-wave mechanisms. In all panels, the thin solid line denotes plane-wave calculations with Bonn-B interaction. The thick lines denote ISI calculations for different 2N potentials, dashed (Bonn A), solid (Bonn-B), dotted (Paris).

Another interesting observable that has been analyzed is the deuteron tensor analyzing power T_{20} (Fig. 6). The production reaction acts at threshold as an helicity selector, in that the observed T_{20} is close to its geometrical limit -$\sqrt{2}$. This limit can be obtained in plane-wave calculations with pure isovector πN s-wave rescattering [9]. However, the trend with energy is much better reproduced once the πN rescattering in the scalar-isoscalar channel are also considered. The reproduction improves further once ISI are taken into account [10].

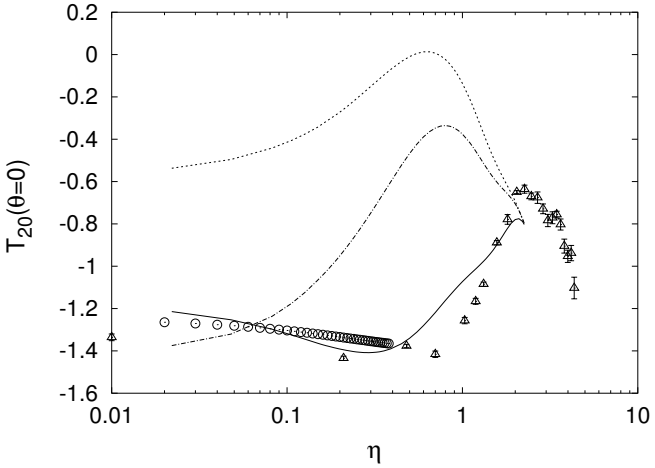

Fig. 6. Deuteron tensor analyzing power T_{20} in (forward) collinear kinematics. All lines refer to plane-wave calculations. The solid line denotes the full model. The dot-dashed line refers to calculations without s-wave πN rescatterings in the scalar-isoscalar channel, the dotted line to calculations deprived also of s-wave rescatterings in the isovector channel.

In conclusion, I have reported on progresses made recently on the pion-3N system, with respect to the pion-production reaction $pd \to \pi^o\ ^3He$. The phenomenology of this reaction is quite complicated, especially if one starts to consider the spin-structure of the process. It is shown that a fair understanding of the process is possible, provided that the variety of elementary production mechanisms used to descibe pion-production from 2N collisions are taken into account, and the nuclear 3-body aspects (bound-states and scattering effects in the initial state) are carefully calculated. Also the interference effects amongst the various production mechanisms are quite important in these processes. This should draw attention to these type of reactions: they could help to clarify the issue of the nature of the pion-production mechanisms for the process $pp \to pp\pi^o$ at threshold.

Acknowledgment I would like to thank the warm hospitality of the organizers of the mini-workshop on quark dynamics in Bled. I express also many thanks to T. Melde, G. Pisent, W. Schadow, A. Shebeko, and J.P. Svenne, for sharing interest and collaborating on many topics that are of relevance for this subject. This work has been co-funded by the Italian MIUR-PRIN project "Fisica Teorica del Nucleo

e dei Sistemi a Molti Corpi". L. Levchuk thanks the University of Padova and the INFN for the support and hospitality.

References

1. E.O. Alt, P. Grassberger, W. Sandhas, Nucl. Phys. **B2**, 167 (1967).
2. L. Canton and W. Schadow, Phys. Rev. C **56**, 1231 (1997); L. Canton *et al.* Phys. Rev. C **57**, 1588 (1998); L. Canton *et al.* Nucl. Phys. **A684**, 417c (2001); L. Canton and W. Schadow, Phys. Rev. C **61**, 064009 (2000); L. Canton and L. Levchuck, submitted for publication.
3. J. Hamilton, *High Energy Physics*, E.H.S. Burhop ed. (Academic, New York, 1967); O.V. Maxwell, W. Weise, and M. Brack, Nucl. Phys. **A348**, 338 (1980).
4. H. Garcilazo and T. Mizutani, *πNN Systems* World Scientific, Singapore (1990).
5. C. Hanart, Phys. Rept. **397**, 155 (2004)
6. T.S-H. Lee and D.O. Riska, Phys. Rev. Lett **70**, 2237 (1993).
7. E. Hernandez and E. Oset, Phys. Lett. **B350** 158, (1995).
8. C. Kerboul *et al.* Phys. Lett. B **181**, 28 (1986); V. Nikulin *et al.* Phys. Rev. C **54**, 1732 (1996); M.A. Pickar *et al.* Phys. Rev. C **46** 397 (1993); M. Betigeri *et al.* Nucl. Phys. **A690** 473 (2001); S. Abdel-Samad *et al.* Phys. Lett. **B553**, 31 (2003).
9. J.F. Germond and C. Wilkin, J. Phys. G **16**, 381 (1990).
10. L. Canton *et al.* in preparation.

BLED WORKSHOPS
IN PHYSICS
VOL. 5, NO. 1

Proceedings of the Mini-Workshop
Quark Dynamics *(p. 18)*
Bled, Slovenia, July 12-19, 2004

Quark matter and quark stars*

M. Fiolhais[a], L. P. Linares[b], M. Malheiro[b], A. Taurines[c]

[a] Departamento de Física and Centro de Física Computacional, Universidade de Coimbra, P-3004-516 Coimbra, Portugal
[b] Instituto de Física, Universidade Federal Fluminense, Av. Litorânea, 24210-310 Niterói, Brazil
[c] Instituto de Física Teórica, Universidade Estadual Paulista, 01405-900 São Paulo, Brazil

Abstract. Strange quark matter is studied in the framework of the Chromodielectric model (CDM), and the corresponding equations of state are used to investigate the structure (mass and radius) of cosmological compact objects. At high densities, the phase of QCD known as "Color Flavour Locked" (CFL) phase, may also be modelled in the CDM through the inclusion of a direct quark-quark correlation (pairing) energy. We studied this phase, obtaining the corresponding equation of state, which we compared with the equations of state of the other phases. The results show that the equations of state obtained in the framework of the CDM are similar to those obtained in the framework of QCD. On the other hand, the CFL phase turns out to be more stable than the normal (beta equilibrium) phase. Work is still in progress regarding the structure of quark stars which are obtained using the equation of state for the CFL phase.

The chromodielectric model is an effective model for the interactions amongst quarks in the low and intermediate energy range [1]. The interactions between the quarks are mediated by meson exchange: the scalar-isoscalar sigma (σ), the pseudoscalar-isovector pion (π), and the scalar, isoscalar, chiral singlet chi (χ), which is the responsible for generating confinement in the model (the χ field is usually viewed as a glueball field). The chromodielectric model is chiral symmetric, a symmetry that is spontaneously broken, leading to a dynamical generation of quark masses which depend on χ^{-1}. The mesons experience self-interactions: a 'mexican-hat' potential for the chiral mesons and, for the confining field, a potential which is usually written in the form [2]

$$U(\chi) = \frac{1}{2} m_\chi^2 \chi^2 \left[1 + \left(\frac{8\eta^4}{\gamma^2} - 2 \right) \left(\frac{\chi}{\gamma m_\chi} \right) + \left(1 - \frac{6\eta^4}{\gamma^2} \right) \left(\frac{\chi}{\gamma m_\chi} \right)^2 \right] , \qquad (1)$$

where m_χ is the χ mass, and γ and η are parameters. It has a global minimum at $\chi = 0$ and a local one at $\chi = \gamma m_\chi$. The height of the local minimum, $U(\gamma m_\chi) = (\eta m_\chi)^4 = B$, is interpreted as a "bag pressure" [3], as in the MIT bag model, and this correspondence is used to fix the model parameters.

* Talk delivered by M. Fiolhais

The chiral CDM has been applied in studies of the baryon structure, in particular, the nucleon and the Delta resonance [4] and the Roper [5]. These states are described as chiral solitons, with three valence quarks dynamically confined to a bag whose radius is approximately 1 fm.

Quark matter has also been studied in the framework of the model [6]. The simplest system which can be considered in this context is the charge neutral u and d infinite quark matter, to which a semiclassical (Thomas-Fermi) formalism can be applied. Such treatment allows us to readily obtain the Equation of State (EOS) for the quark matter.

In a recent study [7], we considered strange quark matter which, in addition to u and d quarks, also contains the strange quark, s. The requirement of (local) charge neutrality and beta equilibrium enforces the need to include electrons into the system. In the semiclassical approximation (quarks described by plane waves, and constant classical meson fields) we found two distinct stable solutions for the same set of model parameters. In both cases, σ remains always close to f_π irrespective of the density. In one solution (solution I in [7]), the χ field stays close to zero, being a slowly increasing function of the density. For such small χ, the quartic potential of the CDM is indistinguishable from $U = \frac{1}{2} m_\chi^2 \chi^2$, thus, in practice, this solution I corresponds to the one obtained and used by Drago et al. [8] in the framework of the simpler quadratic potential [$\gamma \to \infty$ in the potential (1)]. Due to the smallness of the χ field, quark masses are large and the system is in a chiral broken phase. As a consequence of the charge neutrality and beta equilibrium, which are imposed in the variational calculations, a certain number of electrons are required in the system which contains, on the other hand, u and d quarks (in almost the same abundance) and s quark (less abundant than the other flavours).

There is another solution (solution II in [7]) corresponding to a large confining field. This solution cannot exist for quadratic potentials such as the one in [8] and it corresponds to a chiral symmetric phase: the quark masses for the three flavours are all very close to zero, almost independent of the density. The chemical potentials (μ) for each flavour are dominated by the Fermi momentum and one has $\mu_u \simeq \mu_d \simeq \mu_s$. Hence, in this chiral symmetric phase, which pertain to the quartic potentials of the type (1), the abundance of quarks u, d and s are the same and there are no electrons, i.e. $\mu_e \simeq 0$.

Our results in Ref. [7] indicate that strange quark matter at high densities (solution II) is not absolutely stable. However, it is expected that a new phase that is supposed to occur in QCD at very high densities, known as color flavor locked (CFL) phase [9], is likely to be the ground state even if the quark masses are different from each other [10]. This suggests that the strange matter described by our solution II in Ref. [7] may undergo a transition to the CFL phase, whose energy is lowered due to a quark BCS-like pairing interaction.

A recent study described how the CFL phase in dense matter enhances the parameters space for absolute stability of the strange matter [11]. In that study, a phenomenological vacuum energy density or bag constant B is included in the spirit of the MIT bag model. It was shown that, when the gap energy of the QCD Cooper pairs increases, the bag constant can be larger and the strange matter is absolutely stable (i.e., the energy per particle is lower than for the iron).

We performed a similar study in the CDM model including the BCS quark pairing in it and analyze the superconducting color flavor locked phase. The quark pairing interaction is introduced through the inclusion of the extra term $3\Delta^2\mu^2/\pi^2$ in the energy density. The (adjustable) parameter Δ is the paring energy and μ is the (quark) chemical potential. Our goal was to investigate whether the inclusion in the energy density of a negative term of the diquark condensate would maintain the stability of quark matter even for a large potential energy.

The calculation was carried on using the parameters $\gamma = 0.2$ MeV, $\eta = 0.096$ and $m_\chi = 1.7$ GeV for the U(χ) potential. In Fig. 1 we plot the energy per particle as a function of the density ($M = 939$ MeV) to study the stability in the CFL for CDM (solution II in Ref. [7]) and QCD. We present a comparison between the EOS of the CDM + CFL and QCD in the CFL, for $\Delta = 100$ MeV and $\Delta = 0$ (no pairing interaction). The results show that the EOS obtained for the CFL strange matter in the CDM is very similar to the QCD one, suggesting that the CDM has the most relevant features of QCD at high densities. Increasing the quark pairing Δ interaction, the strange quark matter becomes more stable. This result indicates that even for large potential energies of the confining field ($\eta > 0.096$) the CFL strange quark matter may exist as an absolutely stable state.

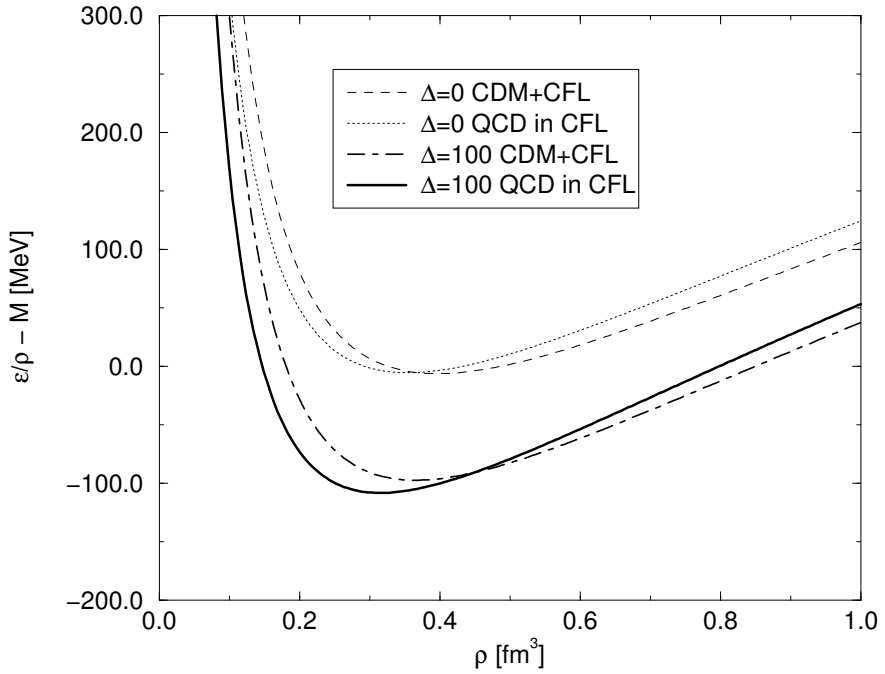

Fig. 1. Stability of the strange quark matter in the CFL phase for CDM (solution II in Ref. [7]) and QCD [11].

This study can be relevant for the structure and formation of compact quark [12,13] and hybrid stars [14]. In Ref. [7] we showed that quark stars with one solar

mass and a radius in the range 6-8 km could be formed if no pairing interaction was included, though they were not absolutely stable. We expect that CFL stars might be absolutely stable and even more compact than strange stars.

References

1. H. B. Nielsen, A. Patkós, *Nucl. Phys. B* **195**, 137 (1982); H. J. Pirner, *Prog. Part. Nucl. Phys.*, **29**, 33 (1992)
2. M. C. Birse, *Prog. Part. Nucl. Phys.*, **25**, 1 (1990)
3. M. Rosina, A. Schuh, H. J. Pirner, *Nucl. Phys.* **A448**, 557 (1986)
4. T. Neuber, M. Fiolhais, K. Goeke, J. N. Urbano, *Nucl. Phys. A* **560**, 909 (1993); A. Drago, M. Fiolhais, U. Tambini, *Nucl. Phys. A* **609**, 488 (1996)
5. P. Alberto, M. Fiolhais, B. Golli, J. Marques, *Phys. Lett. B* **523**, 273 (2001)
6. A. Drago, M. Fiolhais, U. Tambini, *Nucl. Phys. A* **588**, 801 (1995); W. Broniowski, M. Čibej, M. Kutschera, M. Rosina, *Phys. Rev. D* **41**, 285 (1990); J. A. McGovern, M. Birse, *Nucl. Phys. A* **506**, 367 (1990); *Nucl. Phys.* **506**, 392 (1990)
7. M. Malheiro, M. Fiolhais and A. R. Taurines, *J. Phys.* **G29**, 1045 (2003)
8. A. Drago, U. Tambini, M. Hjorth-Jensen, Phys. Lett. B **380**, 13 (1996); Prog. Part. Nucl. Phys. **36**, 407 (1996)
9. M. Alford, K. Rajagopal and F. Wilczek *Nucl. Phys.* **B537**, 433 (1999)
10. M. Alford, J. Berges and K. Rajagopal *Nucl. Phys.* **B558**, 219 (1999)
11. G. Lugones, J. E. Horvath *Phys. Rev.* **D66**, 074017 (2002)
12. G. Lugones, J. E. Horvath *Astronomy and Astrophysics* **403**, 173 (2003)
13. A. Drago, A. Lavagno and G. Pagliara, nucl-th/0401052.
14. P.K. Panda, D.P. Menezes and C. Providência *Phys. Rev.* **C69**, 025207 (2004)

BLED WORKSHOPS
IN PHYSICS
VOL. 5, NO. 1

Proceedings of the Mini-Workshop
Quark Dynamics *(p. 22)*
Bled, Slovenia, July 12-19, 2004

A Time Dependence of the Scale of QCD

H. Fritzsch

Sektion Physik, Ludwig–Maximilians–Universität München, Theresienstrasse 37, 80333 München, Germany

Abstract. From astrophysics there are indications that the finestructure constant α has changed during the past 10 billion years. Within grand unification one can deduce that also the QCD scale has changed. Tests for a time variation of this scale are described. The result of the new experiment in Munich is discussed.

The theory of QCD is very remarkable. It is a theory of very few parameters, i.e. only Λ_c and the quark masses. The latter are related to inputs by the flavor interactions and have nothing to do with the strong interactions. The parameter Λ_c just sets the scale of the strong interactions and is not a real parameter for the strong interaction itself. Thus the QCD–theory, proposed by Gell–Mann and myself in 1972[1], is indeed an exceptional theory, describing lots of complexities in terms of very few parameters, which, as discussed below, might even depend on time.

Usually in physics, especially in particle physics, we deal with the local laws of nature, say the field equations of QCD or the Maxwell equations. But when it comes to the fundamental constants, like the finestructure constant α, we must keep in mind that also questions about the boundary conditions of the universe come up. We do not know, where these constants, like α or α_s or the lepton and quark masses, come from, but it could well be that at least a few of them are products of the Big Bang. If the Bing Bang would be repeated, these constants could easily take different values. But in this case it is clear that the constants could never be calculated.

So in connection to the fundamental constants the question comes up, whether they are really cosmic accidents, or whether they are determined by the dynamics, whether they are changing in time or in space, or whether they are indeed calculable in a hypothetical theory going far above the present Standard Model. Also considerations related to the Anthropic Principle should be made. Life in our universe can exist only if the values of the fundamental constants take on certain values. In a universe in which, for example, the u–quark is heavier than the d-quark, the proton would decay in a neutron, and life would not exist, at least not in a form known to us.

Of course, today α is just the interaction constant, describing e. g. electron–scattering at low energies:

$$\alpha^{-1} = 137.03599976 \; . \tag{1}$$

But it is remarkable. Based on this number, one can calculate all effects in QED to an accuracy of about $1 : 10.000.000$, e. g. the magnetic moment of the electron. Of course, QED is only a part of the Standard Model of today, based on a superposition of QCD and the $SU(2) \times U(1)$ – electroweak theory, and α is just one of at least 18 parameters, entering the Standard Model.

One of the fundamental quantities is the proton mass. I should like to stress that the proton mass is a rather complicated object in the Standard Model. The coupling constant of QCD follows in leading order the equation:

$$\alpha_s\left(Q^2\right) = \frac{2\pi}{b_0} \; \ln\left(\frac{Q}{\Lambda}\right), \quad b_0 = 11 - \frac{2}{3} n_f \; . \tag{2}$$

Here the scale parameter Λ enters, which has been determined to be:

$$\Lambda = 214^{+38}_{-35} \; \text{MeV} \; . \tag{3}$$

Λ is a free parameter of QCD, and all numbers of QCD scale with Λ, at least in the limit where the masses of the quarks are set to zero. But Λ can be expressed in terms of MeV, i. e. it is given in reference to the electron mass, which is outside QCD. The physical parameters like the proton mass are simply proportional to Λ, apart from a small correction due to quark masses. The scale of confinement of the quarks is inversely proportional to Λ.

I should also remind you that Grand Unification imposes that the parameters α_s, α and α_w are not independent. They are related to each other, and related to the unified coupling constant, describing the interaction at the unification scale Λ_{un}.

It is known that the group $SU(5)$ does not describe the observations, since the three coupling constants do not converge precisely. If supersymmetric particles are added at an energy scale of about 1 TeV, a convergence takes place, however[2]. In $SO(10)$, proposed by P. Minkowski and me[3] the situation is different, since in this group the unification is a two–step process, where another mass scale, the mass scale for the righthanded W–boson, enters. If this mass scale is chosen in the right way, the unification can be achieved without supersymmetry.

After these preparations let me come to the question of time dependence. A group of physicists has recently published their evidence that the finestructure constant had a different value billions of years ago[4]. They were investigating the light from about 134 quasars, using the so–called "many multiplet method". They were looking at the fine–structure of atomic lines, originating from elements like Fe, Ni, Mg, Sn, Ag etc.

One particular aspect is that the fine–structure is a rather complex phenomenon, fluctuating in particular also in the sign of the effect. These sign changes have been observed and used in fixing the experimental values of α. The result is:

$$\frac{\Delta\alpha}{\alpha} = (-0.72 \pm 0.18) \cdot 10^{-5} \; . \tag{4}$$

Thus α was slightly larger in the past. If one takes a linear approximation and uses a cosmic lifetime of 14 billion years, the effect is $\dot{\alpha}/\alpha \approx 1.2 \cdot 10^{-15}$ per year.

If α depends on time, the question arises, how this time–variation is generated. Since $\alpha = e^2/\hbar c$, a time variation could come from a time variation of $\hbar$ or c. Both cases are, I think, not very likely. If c depends on time, it would mean, that we have a serious problem with relativity. If $\hbar$ would depend on time, atomic physics runs into a problem. So I think that a time dependence of α simply means that e is becoming time–dependent.

Let me also mention that according to the results of Dyson and Damour[5] there is a rather strong constraint on a time–variation of α, derived from the investigation of the remains of the Oklo reactor in Gabon. If no other parameters change as well, the relative change $(\dot{\alpha}/\alpha)$ per year cannot be more than 10^{-17}, i. e. there is a problem with the astrophysical measurements, unless the rate of change for α has become less during the last 2 billion years. The constraint is derived by looking at the position of a nuclear resonance in Samarium, which cannot have changed much during the last 2 billion years. However, I tend not to take this constraint very seriously. According to the Grand Unification α_s and Λ should have changed as well, and the two effects (change of α and of Λ) might partially cancel each other.

The idea of Grand Unification implies that the gauge group $SU(3)$ of the strong interactions and the gauge group $SU(2) \times U(1)$ of the electroweak sector are subgroups of a simple group, which causes the unification.

Both the groups $SU(5)$ and $SO(10)$ are considered in this way. I like to emphasize that the group $SO(10)$ has the nice property that all leptons and quarks of one generation are described by one representation, the 16–representation. It includes a righthanded neutrino, which does not contribute to the normal weak interaction, but it is essential for the appearance of a mass of the neutrino, which is expected in the $SO(10)$–Theory.

In $SU(5)$ two representations of the group are needed to describe the leptons and quarks of one generation, a 10– and a $(\bar{5})$–representation.

I should also like to emphasize that the gauge couplings α_s, α_w and α meet in the $SU(5)$–theory only, if one assumes that above about 1 TeV supersymmetry is realized. In the $SO(10)$–theory this is not needed. A convergence of the coupling constants can be achieved, since at high energies another energy scale enters, which has to be chosen in a suitable manner.

A change in time of α can be obtained in two different ways. Either the coupling constant α_{un} stays invariant or the unification scale changes. I consider both effects in the $SU(5)$–model with supersymmetry. In this model the relative changes are related:

$$\frac{1}{\alpha}\frac{\dot{\alpha}}{\alpha} = \frac{8}{3}\frac{1}{\alpha_s} - \frac{10}{\pi}\frac{\dot{\Lambda}_{un}}{\Lambda_{un}} \tag{5}$$

One may consider the following scenarios:

1) Λ_G invariant, $\alpha_u = \alpha_u(t)$. This is the case considered in[6] (see also[7]), and one finds

$$\frac{1}{\alpha}\frac{\dot{\alpha}}{\alpha} = \frac{8}{3}\frac{1}{\alpha_s}\frac{\dot{\alpha}_s}{\alpha_s} \tag{6}$$

and

$$\frac{\dot{\Lambda}}{\Lambda} \approx 39 \cdot \frac{\dot{\alpha}}{\alpha} \tag{7}$$

2) α_u invariant, $\Lambda_G = \Lambda_G(t)$. One finds

$$\frac{1}{\alpha}\frac{\dot{\alpha}}{\alpha} = -\frac{1}{2\pi}\left(b_2^S + \frac{5}{3}b_1^S\right)\frac{\dot{\Lambda}_G}{\Lambda_G}, \tag{8}$$

$$\frac{\dot{\Lambda}}{\Lambda} = \left(\frac{b_3^S}{b_3^{SM}}\frac{1}{\alpha}\frac{\dot{\alpha}}{\alpha}\right) \approx -30.8\frac{\dot{\alpha}}{\alpha} \tag{9}$$

3) $\alpha_u = \alpha_u(t)$ and $\Lambda_G = \Lambda_G(t)$. One finds

$$\frac{\dot{\Lambda}}{\Lambda} \cong 46\frac{\dot{\alpha}}{\alpha} + 1.07\frac{\dot{\Lambda}_G}{\Lambda_G}$$

where theoretical uncertainties in the factor $R = (\dot{\Lambda}/\Lambda)/(\dot{\alpha}/\alpha) = 46$ have been discussed in[6]. The actual value of this factor is sensitive to the inclusion of the quark masses and the associated thresholds, just like in the determination of Λ. Furthermore higher order terms in the QCD evolution of α_s will play a role. In [1] it was estimated: $R = 38 \pm 6$.

According to[6] the relative changes of Λ and α are opposite in sign. While α is increasing with a rate of 1.0×10^{-15}/yr, Λ and the nucleon mass are decreasing, e.g. with a rate of 1.9×10^{-14}/yr. The magnetic moments of the proton μ_p as well of nuclei would increase according to

$$\frac{\dot{\mu}_p}{\mu_p} = 30.8\frac{\dot{\alpha}}{\alpha} \approx 3.1 \times 10^{-14}/\text{yr}. \tag{10}$$

The time variation of the ratio M_p/m_e and α discussed here are such that they could by discovered by precise measurements in quantum optics. The wave length of the light emitted in hyperfine transitions, e.g. the ones used in the cesium clocks being proportional to $\alpha^4 m_e/\Lambda$ will vary in time like

$$\frac{\dot{\lambda}_{hf}}{\lambda_{hf}} = 4\frac{\dot{\alpha}}{\alpha} - \frac{\dot{\Lambda}}{\Lambda} \approx 3.5 \times 10^{-14}/\text{yr} \tag{11}$$

taking $\dot{\alpha}/\alpha \approx 1.0 \times 10^{-15}$/yr. The wavelength of the light emitted in atomic transitions varies like α^{-2}:

$$\frac{\dot{\lambda}_{at}}{\lambda_{at}} = -2\frac{\dot{\alpha}}{\alpha}. \tag{12}$$

One has $\dot{\lambda}_{at}/\lambda_{at} \approx -2.0 \times 10^{-15}$/yr. A comparison gives:

$$\frac{\dot{\lambda}_{hf}/\lambda_{hf}}{\dot{\lambda}_{at}/\lambda_{at}} = -\frac{4\dot{\alpha}/\alpha - \dot{\Lambda}/\Lambda}{2\dot{\alpha}/\alpha} \approx -17.4. \tag{13}$$

At present the time unit second is defined as the duration of 6.192.631.770 cycles of microwave light emitted or absorbed by the hyperfine transmission of cesium-133 atoms. If Λ indeed changes, as described above, it would imply that the time flow measured by the cesium clocks does not fully correspond with the time flow defined by atomic transitions.

Recently a high precision experiment was done at the MPQ in Munich, using the precise cesium clock PHARAO from Paris[8].

In this experiment the drift between the year 1999 and 2003 could be measured since in 1999 a similar experiment has been done accidentally. Today the frequency of the 1S–2S–transition is measured to 2466 061 413 187 127 Hz, with an uncertainty of 18 Hz. The drift during the past 43 months is given by 24 Hz, uncertainty about 50 Hz. This implies a change of -0.9 (2.9) 10^{-15} per year.

Thus it is found that the prediction of about 2×10^{-14} per year is presumably not realized. But further tests are going on.

Nevertheless we have to think what might be the reason that no change seems to be there on the level of 10^{-14}. Of course, there is the possibility that the astrophysics result is wrong. Further tests to check this are being prepared. But it could also be that a cancellation takes place. The time change $(\dot{\alpha}_s/\alpha_s)$ receives 2 contributions, one by $(\dot{\alpha}/\alpha)$, but also one by $\left(\dot{\Lambda}_{GUT}/\Lambda_{GUT}\right)$. If both are present, one could have a suppression such that e. g. $\left(\dot{\Lambda}/\Lambda\right)$ is not $30 \cdot (\dot{\alpha}/\alpha)$, but only $3 \times (\dot{\alpha}/\alpha)$. This would imply that in the experiment of Haensch et al. the effect is there at the level of few $\times 10^{-15}$ / year.

Tests to look for such an effect are being prepared. But it will take at least one year, before results are known. It might also be that the astrophysics observations are wrong. Recently new observations were published, indicating a null-effect[9].

I like to thank in particular Prof. Rosina for the arrangement of this nice meeting in the wonderful town of Bled close to the mountains of Slovenija.

References

1. H. Fritzsch and M. Gell–Mann, Proc. XVI Internat Conferences on High Energy Physics, Chicago (1972) Vol. 2.
2. U. Amaldi, W. de Boer and H. Furstenau. Phys.Rev. Lett. 87 (1991) 447.
3. H. Fritzsch and P. Minkowski. Annals of Physics 93 (1975) 193.
4. J.K. Webb et al.: Phys. Rev. Lett. 87 (2001) 091301.
5. T. Damour and F. Dyson. Nucl. Phys. B480 (1996) 37.
6. X. Calmet and H.Fritzsch. arXiv hep-ph/0112110, to appear in Eur. Phys. J. C.
7. F. Langacker, G. Segre and M.J. Strassler. Phys. Lett B528 (2002) 528.
8. T.W. Haensch. Proc. of the Int. Conf. on Laser Spectroscopy (JCOLS 2003), Palm, Cove (Australia).
9. R. Quast, D. Reimers and S. Levshakov. astro–ph/0311280 (2004).

BLED WORKSHOPS
IN PHYSICS
VOL. 5, NO. 1

Proceedings of the Mini-Workshop
Quark Dynamics *(p. 27)*
Bled, Slovenia, July 12-19, 2004

Critical Review of Pentaquarks

L. Ya. Glozman

Institute for Theoretical Physics, University of Graz, Universitätsplatz 5, A-8010 Graz, Austria

Some experimental and theoretical doubts about the $\Theta^+(1540)$ positive results at LEPS, CLAS, COSY-TOF and others are discussed. Negative results at HERA-B, E690, CDF, HYPERCP, PHENIX, ALEPH, DELPHI, BABAR and BELLE are reviewed. If $\Theta^+(1540)$ exists, its production mechanism should be significantly different from the production mechanism of $\Lambda(1520)$ which is well seen in all high statistics and high resolution high energy experiments.

Arguments are given against the Jaffe-Wilczek diquark scheme of the pentaquark antidecuplet.

References

1. L.Ya.Glozman, Phys. Rev. Lett., 92 (2004) 239101

BLED WORKSHOPS
IN PHYSICS
VOL. 5, NO. 1

Proceedings of the Mini-Workshop
Quark Dynamics *(p. 28)*
Bled, Slovenia, July 12-19, 2004

Excited Hadrons on the Lattice

L. Ya. Glozman (for BGR collaboration)

Institute for Theoretical Physics, University of Graz, Universitätsplatz 5, A-8010 Graz, Austria

A new technique is presented how to extract several excited baryon states simultaneously from lattice QCD calculations. The results on $N(939)$, $N^*(1440)$ and $N^*(1710)$ and the negative parity states are pesented.

References

1. T.Burch, et al., Phys. Rev. D70 (2004) 054502.

BLED WORKSHOPS
IN PHYSICS
VOL. 5, NO. 1

Proceedings of the Mini-Workshop
Quark Dynamics *(p. 29)*
Bled, Slovenia, July 12-19, 2004

A heuristic derivation of an effective QCD coupling dominated by gluon condensates*

Dalibor Kekez[a] and Dubravko Klabučar[b]

[a] Rudjer Bošković Institute, P.O.B. 180, 10002 Zagreb, Croatia
[b] Department of Physics, Faculty of Science, Zagreb University Bijenička c. 32, 10000 Zagreb, Croatia

Abstract. We have recently proposed that an effective strong running coupling, which may reproduce the hadronic phenomenology through the Schwinger-Dyson approach in the rainbow-ladder approximation, can originate from the interplay of the dimension 2 gluon condensate $\langle A^2\rangle$ and the dimension 4 gluon condensate $\langle F^2\rangle$. Here we give an alternative, heuristic derivation of this effective running coupling.

1 Introduction

The important role played in QCD by the gauge-invariant, dimension-4 gluon condensate $\langle F^a_{\mu\nu}F^{a\mu\nu}\rangle \equiv \langle F^2\rangle$, has been known for a long time [1]. On the other hand, there was a wide-spread opinion that the dimension-2 gluon condensate $\langle A^a_\mu A^{a\mu}\rangle \equiv \langle A^2\rangle$ cannot have observable consequences, since it is not gauge invariant. Still, $\langle A^2\rangle$ condensate attracted the attention of some researchers well over a decade ago, e.g., in Refs. [2–6]. After it turned out more recently that the Landau-gauge value of $\langle A^2\rangle$ corresponds to a more general gauge-invariant quantity, it attracted a lot of theoretical attention [7–17], to quote just several of many papers offering evidence that this condensate may be important for the nonperturbative regime of Yang-Mills theories. In our Ref. [14], we argued that $\langle A^2\rangle$ condensate may be relevant for the Schwinger-Dyson (SD) approach to QCD. Namely, in order that this approach leads to a successful hadronic phenomenology (which has so far been treated *widely* only in the rainbow-ladder approximation), an enhancement of the effective quark-gluon interaction seems to be needed at intermediate ($Q^2 \sim 0.5$ GeV^2) momenta[1]. Ref. [14] showed that the interplay of the dim.-2 condensate $\langle A^2\rangle$ with the dim.-4 condensate $\langle F^2\rangle$ provides such an enhancement. It also showed that the resulting effective strong running coupling leads to the sufficiently strong dynamical chiral symmetry breaking (DχSB) and successful phenomenology in the light sector of pseudoscalar mesons. In addition, the issue of the parameter dependence of the results was discussed in more detail in Ref. [18]. In the present paper, we give an alternative, heuristic derivation of this effective running coupling.

* Talk delivered by D. Klabučar

[1] Our convention is $k^2 = -Q^2 < 0$ for spacelike momenta k.

2 On SD approach to hadronic phenomenology

In SD approach, the constituent quarks arise through dressing resulting from DχSB in the ("gap") SD equation for the full quark propagators, while mesons are solutions of the Bethe-Salpeter (BS) equation for bound states of these dynamically dressed quarks and antiquarks. Unfortunately, in the system of SD equations, solving for Green's functions of lower order requires also the knowledge of those of Green's functions of higher orders. In other words, the SD equation for a n-point function requires a $(n+1)$-point function, *etc.*, so that an infinite tower of SD equations arises. Since it is impossible to solve such infinite towers of SD equations, it is inevitable at some point to truncate such an infinite system of equations, which should then be patched up by some modeling. Of course, it is essential to use such truncations which preserve important characteristics of the full theory. For the low-energy QCD, the nonperturbative phenomenon of DχSB is the most important one. Phenomenological SD studies have therefore mostly been relying on the *consistently* used rainbow-ladder approximation (RLA). Namely, the generation of DχSB and, consequently, the appearance of light pseudoscalar mesons as (almost-)Goldstone bosons, is well-understood in RLA [19–23]. In practice this means that for interactions between quarks one uses *Ansätze* of the form

$$[K(k)]^{hg}_{ef} = i4\pi\alpha_{\rm eff}(-k^2)\, D^{\rm free}_{\mu\nu}(k)\, [\frac{\lambda^a}{2}\gamma^\mu]_{eg}[\frac{\lambda^a}{2}\gamma^\nu]_{hf}\,, \tag{1}$$

where e, f, g, h schematically represent spinor, color and flavor indices, $\alpha_{\rm eff}(-k^2) = \alpha_{\rm eff}(Q^2)$ denotes an effective running coupling, and $D^{\rm free}_{\mu\nu}(k)$ is the *free* gluon propagator in the gauge in which the aforementioned SD studies have been carried out almost exclusively, namely the Landau gauge:

$$D^{\rm free}_{\mu\nu}(k) = \frac{1}{k^2}(-g_{\mu\nu} + \frac{k_\mu k_\nu}{k^2})\,. \tag{2}$$

The BS equation for the bound-state vertex $\Gamma_{q\bar{q}'}$ of the meson composed of the quark of the flavor q and antiquark of the flavor q', is then

$$[\Gamma_{q\bar{q}'}(k,P)]_{ef} = \int \frac{d^4\ell}{(2\pi)^4}[S_q(\ell+\frac{P}{2})\Gamma_{q\bar{q}'}(\ell,P)S_{q'}(\ell-\frac{P}{2})]_{gh}[K(k-\ell)]^{hg}_{ef}\,. \tag{3}$$

The consistent RLA requires that the same interaction kernel (1) be previously used in the SD equation for the full quark propagator S_q. That is, dressed quark propagators $S_q(k)$ for various flavors q,

$$S_q^{-1}(p) = A_q(p^2)\not{p} - B_q(p^2)\,, \qquad (q = u, d, s, ...)\,, \tag{4}$$

are obtained by solving the gap SD equation

$$S_q^{-1}(p) = \not{p} - \widetilde{m}_q - i4\pi\int\frac{d^4\ell}{(2\pi)^4}\,\alpha_{\rm eff}[-(p-\ell)^2]D^{ab}_{\mu\nu}(p-\ell)_0\,\frac{\lambda^a}{2}\gamma^\mu S_q(\ell)\frac{\lambda^b}{2}\gamma^\nu\,, \tag{5}$$

where $\widetilde{m}_q$ is the bare mass of the quark flavor q breaking the chiral symmetry explicitly. The case $\widetilde{m}_q = 0$ corresponds to the chiral limit where the current quark

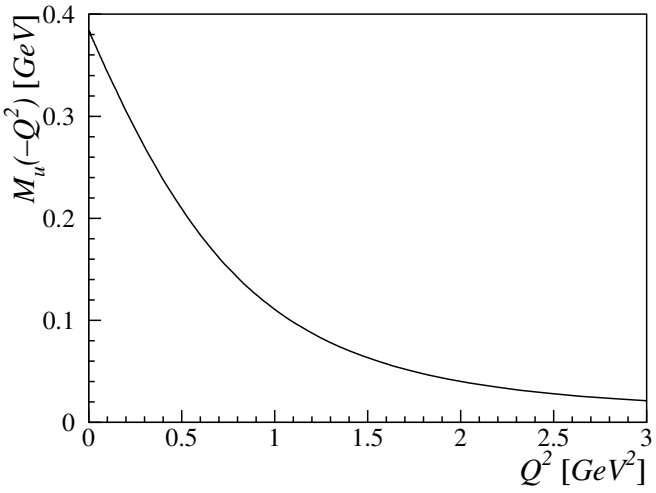

Fig. 1. A typical example of a momentum-dependent dynamically generated constituent quark mass function, which has values of the order of one-third of the nucleon mass at low momenta squared. It is the non-strange ($q = u$) dynamical quark mass of the lightest quark flavor, $M_u(-Q^2)$, calculated using the effective coupling (18) and the input parameters given in Ref. [14] by Eq. (26) there. In the exact chiral limit, the result for $M_u(-Q^2)$ is very similar.

mass $m_q = 0$. In that limit the dynamically generated "momentum-dependent constituent mass function" $M_q(p^2) \equiv B_q(p^2)/A_q(p^2)$ stems exclusively from the *nonperturbative* phenomenon of DχSB. (Of course, for any $\widetilde{m}_q$ which is small with respect to the typical hadronic mass scale ~ 1 GeV, $M_q(p^2)$ stems *largely* from DχSB for values of p^2 below the perturbative domain.) The "constituent quark mass" can be defined as the value of this momentum-dependent constituent mass function at some low $-p^2$, say $p^2 = 0$. The important thing for obtaining a successful hadronic phenomenology, especially in the light-quark sector ($q = u, d, s$), is that DχSB be sufficiently strong; i.e., the gap equation (5) should yield quark propagator solutions $A_q(p^2)$ and $B_q(p^2)$ giving the dressed-quark mass function $M_q(p^2)$ whose values *at low* $-p^2$ are of the order of typical constituent mass values, namely several hundred MeV, as exemplified in Fig. 1.

It turns out that the interaction (1), or, equivalently, $\alpha_{\rm eff}(Q^2)$, which would lead to successful hadronic phenomenology through RLA, must have fairly high integrated strength in the domain of intermediate (around $Q^2 \sim 0.5$ GeV^2) and low momenta. Only then RLA equations (4) and (3) can give acceptable description of hadrons, notably mass spectra and DχSB [20,24]. On the other hand, at *large* spacelike momenta, the running coupling $\alpha_{\rm eff}(Q^2)$ must reduce to $\alpha_{\rm pert}(Q^2)$, the well-known running coupling of perturbative QCD. The question is how to obtain theoretically such an interaction.

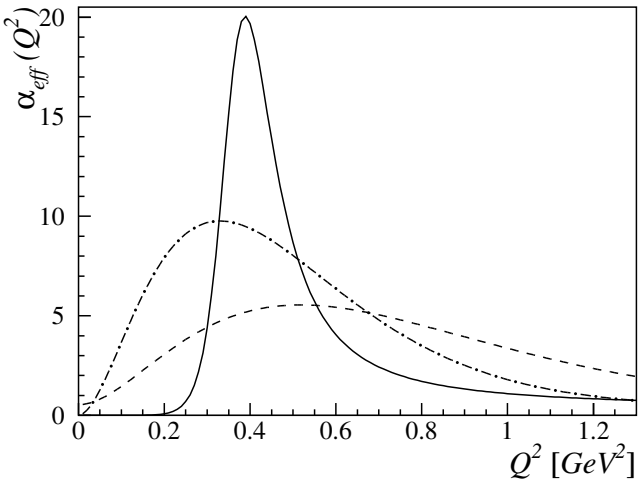

Fig. 2. The effective coupling (18) proposed and analyzed in the present paper is depicted by the solid curve. The two older and also phenomenologically successful effective strong running couplings, namely JM [21] and MRT [23,20] $\alpha_{\rm eff}(Q^2)$, are depicted by, respectively, dashed and dash-dotted curves.

3 Strong coupling enhanced by gluon condensates

We already gave an answer to the above question in our paper [14]. There, we pointed out that such an interaction kernel for SD studies in RLA and the Landau gauge resulted from combining the form the running coupling has in the Landau-gauge SD studies, namely Eq. (6) below [19,25–28], and the ideas on the possible relevance of the dimension 2 gluon condensate $\langle A^2 \rangle$ [7–13,3–6]. In the present paper, we give a simplified and more intuitive derivation thereof as follows.

The definition of the strong running coupling $\alpha_s(Q^2)$ which is appropriate for the SD studies in the Landau gauge [19,25–28] is

$$\alpha_s(Q^2) = \alpha_s(\mu^2)\, Z(Q^2)\, G(Q^2)^2\,, \tag{6}$$

where $\alpha_s(\mu^2) = g^2/4\pi$ and $Z(\mu^2)G(\mu^2)^2 = 1$ at the renormalization point $Q^2 = \mu^2$. The gluon renormalization function $Z(-k^2)$ defines the full gluon propagator $D_{\mu\nu}(k)$ in the Landau gauge:

$$D_{\mu\nu}(k) = Z(-k^2) D^{\rm free}_{\mu\nu}(k) = \frac{Z(-k^2)}{k^2}\,\left(-g_{\mu\nu} + \frac{k_\mu k_\nu}{k^2}\right)\,. \tag{7}$$

Similarly, $G(-k^2)$ is the ghost renormalization function which defines the full ghost propagator:

$$D_G(k) = \frac{G(-k^2)}{k^2}\,. \tag{8}$$

It is sometimes convenient to express the gluon and ghost renormalization functions through the corresponding gluon (A) and ghost (G) polarization functions

$\Pi_G(Q^2)$ and $\Pi_A(Q^2)$:

$$Z(Q^2) = \frac{1}{1+\frac{\Pi_A(Q^2)}{Q^2}} \quad , \quad G(Q^2) = \frac{1}{1+\frac{\Pi_G(Q^2)}{Q^2}} \, . \tag{9}$$

From the recent flurry of papers on $\langle A^2 \rangle$, Refs. [7–10] are particularly relevant for the exposition below, but already a long time ago it was pointed out by, e.g., Refs. [3–6], that in the operator product expansion (OPE) the gluon condensate $\langle A^2 \rangle$ can contribute to QCD propagators. Their [3–6] $\langle A^2 \rangle$-contributions to the OPE-improved gluon (A) and ghost (G) polarization functions were recently confirmed by Kondo [10]. For LG (adopted throughout this paper), number of QCD colors $N_c = 3$ and space-time dimensions $D = 4$, their expressions for the polarizations reduce to

$$\Pi_i(Q^2) = m_i^2 + \mathcal{O}_i(1/Q^2) \, , \qquad (i = A, G) \, , \tag{10}$$

$$m_A^2 = \frac{3}{32} \, g^2 \langle A^2 \rangle = -m_G^2 \, . \tag{11}$$

Here m_A and m_G are, respectively, dynamically generated effective gluon and ghost mass. For $g^2\langle A^2 \rangle$, LG lattice studies of Boucaud *et al.* [7] yield the value 2.76 GeV^2, compatible with the bound resulting from the discussions of Gubarev *et al.* [8,9] on the physical meaning of $\langle A^2 \rangle$ and its possible importance for confinement. Using this value in Eq. (11) yields $m_A = 0.845$ GeV, which will turn out to be a remarkably good initial estimate for $m_{A,G}$.

One should expect that in the contributions $\mathcal{O}_i(1/Q^2)$ in Eq. (10), a prominent role is played by the dimension-4 gluon condensate $\langle F^2 \rangle$, which, contrary to $\langle A^2 \rangle$, is gauge invariant [1]. Refs. [4,5] showed that the OPE contributions of dimension-4 condensates were far more complicated [6] than found previously [3]: not only many kinds of condensates contributed to terms $\propto 1/Q^2$, but for many of them (gauge-dependent gluon, ghost and mixed ones) there has been no assignments of any kind of values yet. Terms $\propto (1/Q^2)^n$ $(n > 1)$ were not considered at all. Thus, at this point, the only practical approach is that the contributions $\mathcal{O}_i(1/Q^2)$ $(i = A, G)$ in Eq. (10) are approximated by the terms $\propto 1/Q^2$ and parametrized, i.e.,

$$\mathcal{O}_A(1/Q^2) \approx \frac{C_A}{Q^2} \, , \qquad \mathcal{O}_G(1/Q^2) \approx \frac{C_G}{Q^2} \, . \tag{12}$$

In Eqs. (12), both C_A and C_G would thus be free parameters to be fixed by phenomenology. Still, we should mention that the effective gluon propagator advocated by Lavelle [29] would indicate $C_A \approx (0.640 \text{ GeV})^4$ for the following reason: for LG and $D = 4$, the contribution which this gluon propagator receives from the so-called "pinch diagrams" vanishes, and its [29] $\mathcal{O}_A(1/Q^2)$ polarization

$$\Pi_A^{\langle F^2 \rangle}(Q^2) = \frac{34 N_c \pi \alpha_s \langle F^2 \rangle}{9(N_c^2 - 1)Q^2} = \frac{(0.640 \text{ GeV})^4}{Q^2} \tag{13}$$

originates entirely from the gluon polarization function in Ref. [4], provided one invokes some fairly plausible assumptions, like using equations of motion, to

eliminate all condensates except $\langle F^2 \rangle$. (The quark condensate $\langle \bar{q} q \rangle$ could also be neglected [29].) Since Ref. [30] indicates that the true value of $\alpha_s \langle F^2 \rangle$ is still rather uncertain, and since Refs. [5,6] make clear that Lavelle's [29] propagator misses some (unknown) three- and four-gluon contributions, we do not attach too much importance to the precise value $C_A = (0.640\ \mathrm{GeV})^4$ [29,1] in Eq. (13), but just use it as an inspired initial estimate. Fortunately, the corresponding variations of C_A still permit good phenomenological fits, since we found in Refs. [14,18] that our results are not very sensitive to C_A.

We do not have a similar estimate for C_G, but one may suppose that it would not differ from C_A by orders of magnitude. We thus try $C_G = C_A = (0.640\ \mathrm{GeV})^4$ as an initial guess. It turns out, *a posteriori*, that this value of C_G leads to a very good fit to phenomenology [14,18].

We can now give a general, although heuristic argument why the contribution (11) of the dimension-2 $\langle A^2 \rangle$ condensate to the gluon and ghost polarizations (10), should indeed lead to the form of $\alpha_{\mathrm{eff}}(Q^2)$ already found in Ref. [14]. As the first step, let us assume that in the gluon and ghost polarization functions, Π_A and Π_G, one can disentangle the perturbative (pert) from nonperturbative (Npert) parts, $\Pi_i = \Pi_i^{\mathrm{pert}} + \Pi_i^{\mathrm{Npert}}$ $(i = A, G)$. At least for high momenta Q^2, it is then possible to approximately factor away the perturbative from nonperturbative contributions; for $i = A$,

$$Z(Q^2) \approx \frac{1}{1 + \frac{\Pi_A^{\mathrm{pert}}(Q^2)}{Q^2}} \, \frac{1}{1 + \frac{\Pi_A^{\mathrm{Npert}}(Q^2)}{Q^2}} \equiv Z^{\mathrm{pert}}(Q^2)\, Z^{\mathrm{Npert}}(Q^2)\,, \tag{14}$$

where we neglect the $\Pi_A^{\mathrm{pert}}(Q^2)\Pi_A^{\mathrm{Npert}}(Q^2)/Q^4$ term. Analogously,

$$G(Q^2) \approx \frac{1}{1 + \frac{\Pi_G^{\mathrm{pert}}(Q^2)}{Q^2}} \, \frac{1}{1 + \frac{\Pi_G^{\mathrm{Npert}}(Q^2)}{Q^2}} \equiv G^{\mathrm{pert}}(Q^2)\, G^{\mathrm{Npert}}(Q^2)\,. \tag{15}$$

For sufficiently high Q^2, the general QCD coupling $\alpha_s(Q^2)$ reduces to the *perturbative* QCD coupling $\alpha_{\mathrm{pert}}(Q^2)$, so that Eq. (6) suggests that $(g^2/4\pi)\, Z^{\mathrm{pert}}(Q^2)\, G^{\mathrm{pert}}(Q^2)^2$ should be identified with $\alpha_{\mathrm{pert}}(Q^2)$.

For high Q^2, we can also assume that nonperturbative parts are given by the OPE-based results of Refs. [3–6,10] [which in our present case boil down to Eqs. (10)-(11)], and by the parametrization (12). Then

$$Z^{\mathrm{Npert}}(Q^2) = \frac{1}{1 + \frac{m_A^2}{Q^2} + \frac{C_A}{Q^4}}\,, \tag{16}$$

$$G^{\mathrm{Npert}}(Q^2) = \frac{1}{1 - \frac{m_A^2}{Q^2} + \frac{C_G}{Q^4}}\,, \tag{17}$$

where m_A is given (11) by the $\langle A^2 \rangle$ condensate.

Obviously, Eqs. (6), (14), (15), (16) and (17) suggest an effective coupling $\alpha_{\mathrm{eff}}(Q^2)$ of the form

$$\alpha_{\mathrm{eff}}(Q^2) = \alpha_{\mathrm{pert}}(Q^2)\, Z^{\mathrm{Npert}}(Q^2)\, G^{\mathrm{Npert}}(Q^2)^2\,. \tag{18}$$

The derivation of the coupling (18) is obviously only heuristic and is far from rigorous. However, we already obtained the same result through a more rigorous derivation in Ref. [14].

Already in Ref. [14], and in more detail also in Ref. [18], we saw how and why the form (18) was sufficiently enhanced at intermediate Q^2 to lead to successful phenomenology when used in quark gap SD equation (5) and bound-state BS equation (3) through Eq. (1), at least in the case when the contribution of the dimension-4 $\langle F^2 \rangle$ condensate to C_A and C_G in Eq. (12), was given by Eq. (13).

Acknowledgment The authors gratefully acknowledge the support of the Croatian Ministry of Science and Technology contracts 0119261 and 0098011.

References

1. M. A. Shifman, A. I. Vainshtein and V. I. Zakharov, Nucl. Phys. B **147**, 385 (1979); *ibid.* 448 (1979).
2. L. S. Celenza and C. M. Shakin, Phys. Rev. D **34**, 1591 (1986).
3. M. J. Lavelle and M. Schaden, Phys. Lett. B **208**, 297 (1988).
4. M. Lavelle and M. Schaden, Phys. Lett. B **246**, 487 (1990).
5. J. Ahlbach, M. Lavelle, M. Schaden and A. Streibl, Phys. Lett. B **275**, 124 (1992).
6. M. Lavelle and M. Oleszczuk, Mod. Phys. Lett. A **7**, 3617 (1992).
7. P. Boucaud, A. Le Yaouanc, J. P. Leroy, J. Micheli, O. Pene and J. Rodriguez-Quintero, Phys. Lett. B **493**, 315 (2000).
8. F. V. Gubarev, L. Stodolsky and V. I. Zakharov, Phys. Rev. Lett. **86**, 2220 (2001).
9. F. V. Gubarev and V. I. Zakharov, Phys. Lett. B **501**, 28 (2001).
10. K. I. Kondo, Phys. Lett. B **514**, 335 (2001).
11. K. I. Kondo, T. Murakami, T. Shinohara and T. Imai, Phys. Rev. D **65**, 085034 (2002).
12. P. Boucaud *et al.*, JHEP **0304**, 005 (2003).
13. D. Dudal and H. Verschelde, J. Phys. A **36**, 8507 (2003).
14. D. Kekez and D. Klabučar, arXiv:hep-ph/0307110.
15. A. A. Slavnov, arXiv:hep-th/0407194.
16. E. Ruiz Arriola, P. O. Bowman and W. Broniowski, arXiv:hep-ph/0408309.
17. X. d. Li and C. M. Shakin, arXiv:nucl-th/0409042.
18. D. Klabučar and D. Kekez, "$\langle A^2 \rangle$-condensate and Dyson-Schwinger approach to mesons", proceedings of Bled Workshops in Physics, Vol. 4, No. 1, pp. 47–56, edited by B. Golli, M. Rosina and S. Širca; published by DMFA - založništvo, Ljubljana 2003, ISSN 1580-4992.
19. R. Alkofer and L. von Smekal, Phys. Rept. **353**, 281 (2001).
20. P. Maris and C. D. Roberts, Int. J. Mod. Phys. E **12**, 297 (2003).
21. P. Jain and H. J. Munczek, Phys. Rev. D **48**, 5403 (1993).
22. P. Maris and C. D. Roberts, Phys. Rev. C **56**, 3369 (1997).
23. P. Maris and P. C. Tandy, Phys. Rev. C **60**, 055214 (1999).
24. C. D. Roberts, arXiv:nucl-th/0304050.
25. R. Alkofer, C. S. Fischer and L. von Smekal, Acta Phys. Slov. **52**, 191 (2002).
26. C. S. Fischer and R. Alkofer, Phys. Rev. D **67**, 094020 (2003).
27. R. Alkofer, C. S. Fischer and L. von Smekal, Prog. Part. Nucl. Phys. **50**, 317 (2003).
28. J. C. R. Bloch, Few Body Syst. **33**, 111 (2003) [arXiv:hep-ph/0303125].
29. M. Lavelle, Phys. Rev. D **44**, 26 (1991).
30. B. L. Ioffe and K. N. Zyablyuk, Eur. Phys. J. C **27**, 229 (2003), and references therein.

BLED WORKSHOPS
IN PHYSICS
VOL. 5, NO. 1

Proceedings of the Mini-Workshop
Quark Dynamics *(p. 36)*
Bled, Slovenia, July 12-19, 2004

Vertex Interactions and Applications

W. H. Klink

Department of Physics and Astronomy University of Iowa, Iowa City, Iowa, USA

Abstract. A relativistic quantum mechanics is formulated in terms of four-momentum operators. The free part of the four-momentum operator is built from irreducible representations of the Poincaré group, while the interacting part comes from integrating a vertex operator over the forward hyperboloid. If the Fock space on which these operators act is truncated, the Poincaré commutation relations no longer hold. But a relativistic few-body theory can still be formulated by using the vertex to define an interacting mass operator. Applications of these ideas are also briefly discussed.

1 Formulation of Relativistic Quantum Mechanics in terms of Vertex Interactions

The foundations of nonrelativistic quantum mechanics can be formulated in terms of representations of the Galilei group, the ten parameter group of transformations connecting different inertial frames. Irreducible representations of the Galilei group provide the Hilbert space for free particles, while the unitary operators representing elements of the group specify the connection between wavefunctions in different inertial frames [1]. The exponential of these unitary operators also generate operators such as the momentum, angular momentum (including spin), position and free energy operators. For example, if $\psi(p)$ is the momentum space wavefunction for a spinless particle of mass m, and $U_v = e^{-imvX}$ is the unitary operator representing a boost, a transformation from one inertial frame to another given by $x \to x + vt$, then the wavefunction in the boosted frame is given by $(U_v\psi)(p) = e^{-imvX}\psi(p) = \psi(p + mv)$, where X is the position operator, which is $i\frac{\partial}{\partial p}$ in a momentum representation.

Few-body quantum mechanics can then be formulated on tensor products of irreducible representation spaces. However, it is simpler to formulate a many-body theory by introducing creation and annihilation operators with the same arguments as one-particle states, and which transform under Galilei transformations as one particle states. Then the free Hamiltonian and momentum operators can be written as

$$H(fr) = \sum \int d^3p \frac{p^2}{2m} a^\dagger(\mathbf{p}m_s)a(\mathbf{p}m_s) \tag{1}$$

$$\mathbf{P}(fr) = \sum \int d^3p \mathbf{p} a^\dagger(\mathbf{p}m_s)a(\mathbf{p}m_s) \tag{2}$$

and must satisfy a number of commutation relations in order to have a Galilei covariant theory. Interactions are introduced by modifying the free Hamiltonian

in such a way that the commutation relations are preserved. For example an n-body kernel must be rotationally and Galilei boost invariant in order to satisfy the commutation relations.

The procedure just outlined can be generalized to relativistic systems. Relativistic transformations are generated by Poincaré transformations, in which a space-time point x is transformed to $x' = \Lambda x + a$, where Λ is a Lorentz transformation, and a a space-time four-vector translation.

Irreducible representation spaces for particles of mass m and spin j are most simply realized as functions over the forward hyperboloid specified by the four-velocity satisfying $v \cdot v = 1$, which is related to the four-momentum by $p = mv$. Then the Hilbert space for a particle of mass m and spin j is $\mathcal{H} = L^2(v) \times V^j$, where V^j is the usual $2j+1$ dimensional spin space[2].

From a relativistic state $|v, \sigma\rangle$, where σ is the relativistic spin projection ranging between $-j$ and j, a many-particle Fock space is generated by creation and annihilation operators satisfying $[a(v,\sigma), a^\dagger(v', \sigma')]_\pm = v_0 \delta^3(v - v')\delta_{\sigma\sigma'}$. To satisfy locality requirements needed for the vertex interactions, it is necessary to also introduce antiparticle creation and annihilation operators satisfying the same commutation relations.

Then the free four-momentum operator can be written as

$$P_\mu(fr) = m \sum \int \frac{d^3v}{v_0} v_\mu (a^\dagger(v,\sigma)a(v,\sigma) + b^\dagger(v,\sigma)b(v,\sigma)); \tag{3}$$

$$[P_\mu(fr), P_\nu(fr)] = 0 \tag{4}$$

$$U_\Lambda P_\mu(fr) U_\Lambda^{-1} = (\Lambda^{-1})^\nu_\mu P_\nu(fr), \tag{5}$$

where the last two equations guarantee the commutation relations of the Poincaré group.

Interactions are generated by vertices with the following properties, the first of which is a locality requirement:

$$[V(x), V(y)] = 0, (x-y)^2 < 0, \tag{6}$$

$$U_a V(x) U_a^{-1} = V(x+a), \tag{7}$$

$$U_\Lambda V(x) U_\Lambda^{-1} = V(\Lambda x); \tag{8}$$

$$P_\mu(I) := \int d^4x \delta(x \cdot x - 1)\theta(x_0) x_\mu V(x), \tag{9}$$

where the interacting four-momentum operator in Eq.(9) is obtained by integrating the vertex operator over the forward hyperboloid.

It then follows that the interacting four-momentum operator satisfies

$$[P_\mu(I), P_\nu(I)] = 0, \tag{10}$$

$$U_\Lambda P_\mu(I) U_\Lambda^{-1} = (\Lambda^{-1})^\nu_\mu P_\nu(I), \tag{11}$$

so that the Poincaré conditions are satisfied for the interacting four-momentum operator[3].

The total four-momentum operator is the sum of free and interacting four-momentum operators and satisfies

$$\begin{aligned}[P_\mu, P_\nu] &= [P_\mu(fr) + P_\mu(I), P_\nu(fr) + P_\nu(I)] \\ &= [P_\mu(fr), P_\nu(I)] - [P_\nu(fr), P_\mu(I)] \\ &= \int d^4x\delta(x\cdot x - 1) \\ &\quad (x_\mu \frac{\partial}{\partial x^\nu} - x_\nu \frac{\partial}{\partial x^\mu})V(x) \\ &= 0.\end{aligned}$$

Vertex operators satisfying the above properties are generally made out of local fields. For the local charged scalar field

$$\Phi(x) = \int \frac{d^3\nu}{\nu_0}(e^{-ip\cdot x}a(\nu) + e^{ip\cdot x}b^\dagger(\nu)), \tag{12}$$

an example of a vertex operator is
$V(x) = \sum a_n D^{\mu_1\cdots\mu_n}\Phi^\dagger(x)D_{\mu_1\ldots\mu_n}\Phi(x)$, where $D_{\mu_1\ldots\mu_n} = \frac{\partial\ldots\partial}{\partial x^{\mu_1}\ldots\partial x^{\mu_n}}$ and the a_n are constant coefficients. The local charged scalar field can readily be generalized to include spin [4] and internal symmetries, including gauge transformations.

2 Application of Vertex Interaction to a Charged Particle in an External Electromagnetic Field

Let $J^\mu(x)$ be the (local) electromagnetic currrent operator for a particle of mass m and spin j. Such an operator can be written as a linear combination of bilinears in creation and annihilation operators and hence is an element of a representation of U(N,N) on Fock space[4]. A vertex can be defined by $V(x) = J^\mu(x)A^{ext}_\mu(x)$ and the four-momentum operator for a particle in an external electromagnetic field is given by

$$P_\mu = P_\mu(fr) + P_\mu(ext),$$

$$P_\mu(ext) = \int d^4x\delta(x\cdot x - 1)x_\mu\theta_{x_0}V(x); \tag{13}$$

$$\Psi_t = e^{-iP_0t}\Psi \tag{14}$$

gives the time evolution of the system. But the exponential of the energy operator is an element of the representation of U(N,N) on Fock space and the action of this representation is known[5]. Hence one can use such a vertex interaction to explicitly calculate particle production from a time independent external electromagnetic field.

3 Bakamjian-Thomas Mass Operators in terms of Vertex Interactions

If the Fock space on which the vertex generated four-momentum operators act is truncated, the components of the four-momentum operator will no longer com-

mute. A procedure for constructing a commuting four-momentum operator is to use the vertex operator to define an interacting mass operator on the truncated Fock space.

To prepare for the construction of interacting mass operators, introduce velocity states, states with simple Lorentz transformation properties. If a Lorentz transformation is applied to a many-particle state, $|p_1,\sigma_1 ... p_n,\sigma_n\rangle = a^\dagger(p_1,\sigma_1)... a^\dagger(p_n,\sigma_n)|0\rangle$, then it is not possible to couple all the momenta and spins together to form spin or orbital angular momentum states, because the Wigner rotations for each momentum state are different. However, velocity states, defined as n-particle states in their overall rest frame boosted to a four-velocity v will have the desired Lorentz transformation properties:

$$|v,\mathbf{k_i},\mu_i\rangle := U_{B(v)}|k_1,\mu_1 ... k_n,\mu_n\rangle \tag{15}$$

$$= \sum |p_1,\sigma_1 ... p_n,\sigma_n\rangle \prod D^{j_i}_{\sigma_i,\mu_i}(R_{W_i}). \tag{16}$$

$$U_\Lambda|v,\mathbf{k_i},\mu_i\rangle = U_\Lambda U_{B(v)}|k_1,\mu_1 ... k_n,\mu_n\rangle$$

$$= U_{B(\Lambda v)} U_{R_W}|k_1,\mu_1 ... k_n,\mu_n\rangle$$

$$= \sum |\Lambda v, R_W \mathbf{k_i},\mu_i'\rangle \prod D^{j_i}_{\mu_i',\mu_i}(R_W). \tag{17}$$

Now all the Wigner rotations in the D functions are the same. Moreover the same Wigner rotation also multiplies the internal momentum vectors, which means that for velocity states, spin and orbital angular momentum can be coupled together exactly as is done nonrelativistically. The relationship between single particle and internal momenta is given by $p_i = B(v)k_i, \sum \mathbf{k_i} = 0$;

From the definition of velocity states it then follows that

$$V_\mu|v,\mathbf{k_i},\mu_i\rangle = v_\mu|v,\mathbf{k_i},\mu_i\rangle, \tag{18}$$

$$M(fr)|v,\mathbf{k_i},\mu_i\rangle = m_f|v,\mathbf{k_i},\mu_i\rangle, \tag{19}$$

$$P_\mu(fr)|v,\mathbf{k_i},\mu_i\rangle = m_f v^\mu|v,\mathbf{k_i},\mu_i\rangle, \tag{20}$$

with $m_f = \sum \sqrt{m_i^2 + \mathbf{k_i}^2}$ the free 'mass' of the n-particle velocity state and $P_\mu(fr) = M(fr)V_\mu$. On velocity states the free four-momentum operator has been written as the product of the four-velocity operator times the free mass operator[6]. Four-momentum operators are written as $P_\mu = MV_\mu$, where the four-velocity operator is defined by $V_\mu := \frac{P_\mu(fr)}{M(fr)}$. The mass operator is the sum of free and interacting mass operators, $M = M(fr) + M(I)$; if the mass operator commutes with the four-velocity operator and Lorentz transformations, then the Poincaré commutation relations, Eqns.(4),(5), are satisfied. Since the four-velocity of the overall system is kinematic, it can be ignored; what remains then is to solve the mass operator eigenvalue equation, $M\Psi = m\Psi$.

Now the vertex operator at the space-time point 0 is a Lorentz scalar. Velocity state matrix elements of $V(0)$ can then be used to generate an interacting mass operator:

$$M(I) := \langle \nu', \mathbf{k}_i', \mu_i' | V(0) | \nu, \mathbf{k}_i, \mu_i \rangle |_{\nu'=\nu} f(\Delta m), \tag{21}$$

where the the initial four velocity equals the final four-velocity; the form factor $f(\Delta m) = f(m_f' - m_f)$ with m_f', m_f given in Eq.(19), guarantees the interacting mass operator is well defined on the truncated Fock space.

From its definition it follows that $M(I)$ is independent of the four-velocity:

$$\begin{aligned} M(I) &= \langle \nu', \mathbf{k}_i', \mu_i' | V(0) | \nu, \mathbf{k}_i, \mu_i \rangle |_{\nu'=\nu} f(\Delta m) \\ &= \langle k_1' \mu_1' ... | U_{B(\nu)}^{-1} V(0) U_{B(\nu)} | k_1 \mu_1 ... \rangle |_{\nu'=\nu} f(\Delta m) \\ &= \langle k_1' \mu_1' ... | V(0) | k_1 \mu_1 ... \rangle |_{\nu'=\nu} f(\Delta m), \end{aligned} \tag{22}$$

and has only off-diagonal matrix elements in the truncated Fock space[6].

4 Application of Vertex Interactions to Strong Decays

Consider a (too) simple model in which negative parity vector mesons $(\rho, \omega ...)$ are considered to be $Q\bar{Q}$ bound states produced by a harmonic oscillator mass operator M_{HO} [7].

Truncate Fock space to the direct sum of $Q\bar{Q}$ and $Q\bar{Q}M$ spaces and couple $Q, \bar{Q}$ to pseudoscalar mesons via the vertex $V(x) = g\bar{\Psi}(x)\gamma_5 \boldsymbol{\lambda_F} \Psi(x) \cdot \boldsymbol{\phi}$. For such a coupled channel problem, the free mass operators are modified to M_{HO} for $Q\bar{Q}$ space and $M_{2Q-M} = \sqrt{M_{HO}^2 + k^2} + \sqrt{m_M^2 + k^2}$ for the $Q\bar{Q}M$ space.

The coupled channel mass operator eigenvalue equation with off-diagonal mass operator given by $K = \langle Q\bar{Q} | V(0) | Q\bar{Q}M \rangle$ is

$$\begin{aligned} M|\Psi\rangle &= m|\Psi\rangle \\ M_{HO}|\Psi_{Q\bar{Q}}\rangle + K|\Psi_{Q\bar{Q}M}\rangle &= m|\Psi_{Q\bar{Q}}\rangle \\ K^\dagger|\Psi_{Q\bar{Q}}\rangle + M_{2Q-M}|\Psi_{Q\bar{Q}M}\rangle &= m|\Psi_{Q\bar{Q}M}\rangle \\ |\Psi_{Q\bar{Q}M}\rangle &= \frac{1}{m - M_{2Q-M}} K^\dagger |\Psi_{Q\bar{Q}}\rangle \end{aligned} \tag{23}$$

$$(M_{HO} + K \frac{1}{m - M_{3Q-M}} K^\dagger)|\Psi_{Q\bar{Q}}\rangle = m|\Psi_{Q\bar{Q}}\rangle, \tag{24}$$

which is a nonlinear eigenvalue equation.

To get the eigenvalues choose a set of values m_a for the m appearing in the propagator and then solve a conventional eigenvalue problem. The resulting eigenvalues will depend parametrically on the chosen values $\lambda_i(m_a)$ and may be complex, above the threshold for meson production. The intersection of the interpolated chosen values with the calculated values give the actual eigenvalues via the equation $m = Re(\lambda_i(m))$. The widths are given by $\Gamma(m_i) = 2|Im(\lambda_i(m_i))|$. Once the two-body wave functions known by solving the above eigenvalue equation, it is possible to get three body wavefunctions from the coupled channel equations.

For this model it is possible to get level shifts and widths from the harmonic oscillator spectrum; however the model is too simple to get good agreement with experiment [7]. In contrast the Graz Goldstone Boson Exchange (GBE) mass operator has eigenvalues that are in good agreement with the experimental mass spectrum [8]; however it is a point spectrum with no widths for excited states. By augmenting this mass operator to a coupled channel mass operator in which meson decays are possible, it should be possible to produce a more realistic baryon spectrum.

The simplest way to do this is to truncate the Fock space to a three quark plus three quark and meson space, in which the vertex is a quark-quark-meson vertex which connects the two spaces.

Consider a mass operator on the direct sum space of the form

$$M = \begin{bmatrix} M_{3Q} & K^\dagger \\ K & M_{3Q-M} \end{bmatrix} \tag{25}$$

where $M_{3Q} = M(fr) + M(conf)$, the sum of free and confinement mass operators, but does not include a hyperfine interaction. Again K is the mass operator generated by the meson-quark vertex,

$$K = \langle \nu, \mathbf{k_i}, \mu_i | V(0) | \nu, \mathbf{k_i'}, \mu_i' \rangle f(\Delta m)$$

where Δm is $m_f - m_f'$ and m_f (respectively m_f') is the mass of the velocity state and $f(\Delta m)$ is a form factor.

The GBE mass operator can be written as $M_{GBE} = M_{3Q} + M_{HY}$ where the last term is the hyperfine mass operator and $M_{3Q-M} = \sqrt{M_{GBE}^2 + k^2} + \sqrt{m_\pi^2 + k^2}$.

Again the coupled channel equation is reduced to one involving only the 3Q space, such that M_{GBE} has another term added to it which accounts for the decays of the excited states:

$$\begin{aligned} M|\Psi\rangle &= m|\Psi\rangle \\ M_{3Q}|\Psi_{3Q}\rangle + K^\dagger|\Psi_{3Q-M}\rangle &= m|\Psi_{3Q}\rangle \\ K|\Psi_{3Q}\rangle + M_{3Q-M}|\Psi_{3Q-M}\rangle &= m|\Psi_{3Q-M}\rangle \\ |\Psi_{3Q-M}\rangle &= \frac{1}{m - M_{3Q-M}} V|\Psi_{3Q}\rangle \\ (M_{3Q} + K^\dagger \frac{1}{m - M_{3Q-M}} K)|\Psi_{3Q}\rangle &= m|\Psi_{3Q}\rangle \\ M_{GBE}|\Psi_{3Q}\rangle + (K^\dagger(\frac{1}{m - M_{3Q-M}})K - M_{HY})|\Psi_{3Q}\rangle &= m|\Psi_{3Q}\rangle \end{aligned} \tag{26}$$

In addition to M_{GBE}, Eq.(26) has an additional mass operator which gives the coupled channel contribution. With this additional term it should be possible to use perturbation theory to compute widths and level shifts.

These and other applications [9] show the utility of a coupled channel approach to few-body systems, in which the interactions are generated by vertices arising from quantum field theory.

References

1. J. Levy-Leblond, Jour. Math. Phys. 4 (1963) 776; W. Klink, R. Warren, Jour. Math. Phys. 11 (1970) 1155.
2. W. H. Klink, Ann. Phys. 213 (1992) 31.
3. W. H. Klink, Phys. Rev. C58 (1998) 3587.
4. W. H. Klink, Nucl. Phys. A 716 (2003) 136.
5. Mark G. Davidson, Pac. J. Math. 129 (1987) 33.
6. W. H. Klink, Nucl. Phys. A 716 (2003) 158.
7. A. Krassnigg, W. Schweiger, W. Klink, Phys. Rev. C67 (2003)064003.
8. L. Ya. Glozman, W. Plessas, K. Vargas, and R. F. Wagenbrunn, Phys. Rev. C57 (1998) 3406; C58 (094030) 1998.
9. M. Lechner, W. Schweiger, and W. Klink, Proceedings of the 17th IUPAP Conference on Few-Body Problems in Physics, W. Gloeckle, W. Tornow editors, Elsevier, Amsterdam (2004) pg. S258, gives a preliminary account of using vertex interactions to compute positronium bound states.

BLED WORKSHOPS
IN PHYSICS
VOL. 5, NO. 1

Proceedings of the Mini-Workshop
Quark Dynamics *(p. 43)*
Bled, Slovenia, July 12-19, 2004

Strong Decays of Baryons*

T. Melde[a], L. Canton[b], W. Plessas[a], and R. F. Wagenbrunn[a]

[a] Theoretical Physics, Institute for Physics, University of Graz, Universitätsplatz 5, A-8010 Graz, Austria
[b] INFN Sezione di Padova and Dipartimento di Fisica, Via Marzolo 8, Padova, Italy

Abstract. A Poincaré-invariant description of mesonic baryon resonance decays is presented following the point form of relativistic quantum mechanics. In this contribution we focus on pionic decay modes. It is found that the theoretical results in general underestimate the experimental ones considerably. Furthermore, the problem of a nontrivial normalization factor appearing in the definition of the decay operator is investigated. The present results for decay widths suggest a normalization factor that is consistent with the choice adopted for the current operator in the studies of electroweak nucleon form factors.

1 Introduction

Constituent quark models (CQMs) provide an effective tool to describe the essential hadronic properties of low-energy quantum chromodynamics. Recently, in addition to the traditional CQM, whose hyperfine interaction derives from one-gluon exchange (OGE) [1], alternative types of CQMs have been suggested such as the ones based on instanton-induced (II) forces [2,3] or Goldstone-boson-exchange (GBE) dynamics [4]. In particular, the GBE CQM aims to include the effective degrees of freedom of low-energy QCD, as they are suggested by the spontaneous breaking of chiral symmetry (SBχS).

Over the years, a number of valuable insights in strong decays of baryon resonances have been gained by various groups, e.g., in refs. [5–9]. Nonetheless, one has still not yet arrived at a satisfactory explanation especially of the N and Δ resonance decays. This situation is rather disappointing from the theoretical side, especially in view of the large amount of experimental data accumulated over the past years [10].

Here, we study the mesonic decays of baryon resonances along relativistic, i.e. Poincaré-invariant, quantum mechanics [11]. This approach is a-priori distinct from a field-theoretic treatment. It assumes a finite number of degrees of freedom (particles) and relies on a relativistically invariant mass operator with the interactions included according to the Bakamjian-Thomas construction [12] thereby fulfilling all the required symmetries of special relativity. We assume a decay operator in the point-form spectator approximation (PFSA) with a pseudovector coupling. The PFSA has already been applied to the calculation of electromagnetic and axial form factors of the nucleons [13–15] and electric radii as well as

* Talk delivered by T. Melde

magnetic moments of all octet and decuplet baryon ground states [16]. In all cases the experimental data are described suprisingly well within this approach.

Covariant results for the strong decays of N and Δ resonances have already been presented in ref. [17] for the relativistic GBE and OGE CQMs. They show a dramatically different behaviour as compared to previous non-relativistic calculations [18,19]. Specifically, it turns out that the theoretical results, in general, underestimate the experimental ones considerably. This behaviour has also been observed in the relativistic calculation based on the Bethe-Salpeter equation using instanton-induced dynamics [20]. Up till now all relativistic approaches face the problem of defining appropriate decay operators. Usually one has resorted to simplified versions such as the spectator model.

2 Theory

Generally, the decay width Γ of a resonance is defined by the expression

$$\Gamma = 2\pi\rho_f \left|F\left(i \to f\right)\right|^2 , \tag{1}$$

where $F\left(i \to f\right)$ is the transition amplitude and ρ_f is the phase-space factor. In eq. (1) one has to average over the initial and to sum over the final spin-isospin projections. Previous calculations, based on nonrelativistic approximations of the transition amplitude encountered an ambiguity in the proper definition of the phase-space factor [7,21,22]. Here, we present a Poincaré-invariant definition of the transition amplitude, thereby resolving this ambiguity. In particular, we adhere to the point-form of relativistic quantum mechanics [11], because in this case the generators of the Lorentz transformations remain purely kinematic and the theory is manifestly covariant [23]. The interactions are introduced into the (invariant) mass operator following the Bakamjian-Thomas construction [12]. The transition amplitude for the decays is defined in a covariant manner, under overall momentum conservation ($P'_\mu - P_\mu = Q_{\pi,\mu}$), by

$$F\left(i \to f\right) = \langle P, J, \Sigma | \, \hat{\mathcal{D}}_\alpha \, | P', J', \Sigma' \rangle \ . \tag{2}$$

Here $\langle P, J, \Sigma|$ and $|P', J', \Sigma'\rangle$ are the eigenstates of the decaying resonance and the nucleon ground state, respectively. Inserting the appropriate identities leads to the reduced matrix element

$$\begin{aligned} F\left(i \to f\right) \sim & \sum_{\sigma_i,\sigma'_i} \sum_{\mu_i,\mu'_i} \int d^3k_2 \, d^3k_3 \, d^3k'_2 \, d^3k'_3 \\ & \Psi^\star_{MJ\Sigma}\left(\mathbf{k}_1, \mathbf{k}_2, \mathbf{k}_3; \mu_1, \mu_2, \mu_3\right) \Psi_{M'J'\Sigma'}\left(\mathbf{k}'_1, \mathbf{k}'_2, \mathbf{k}'_3; \mu'_1, \mu'_2, \mu'_3\right) \\ & \prod_{\sigma_i} D^{\frac{1}{2}\star}_{\sigma_i\mu_i}\left[R_W\left(k_i, B\left(v_{in}\right)\right)\right] \\ & \langle p_1, p_2, p_3; \sigma_1, \sigma_2, \sigma_3 | \, \hat{\mathcal{D}}_\alpha \, | p'_1, p'_2, p'_3; \sigma'_1, \sigma'_2, \sigma'_3 \rangle \\ & \prod_{\sigma'_i} D^{\frac{1}{2}}_{\sigma'_i\mu'_i}\left[R_W\left(k'_i, B\left(v_f\right)\right)\right] , \end{aligned} \tag{3}$$

where the rest-frame baryon wave functions $\Psi^{\star}_{MJ\Sigma}$ and $\Psi_{M'J'\Sigma'}$ stem from the velocity-state representations of the baryon states $\langle P, J, \Sigma|$ and $|P', J', \Sigma'\rangle$, respectively. These wave functions depend on the quark momenta $\mathbf{k}_i$ for which $\sum_i \mathbf{k}_i = \mathbf{0}$. They are related to the individual quark momenta by the Lorentz boost relations $p_i = B(v)\, k_i$. The main challenge lies in the definition of a consistent and reasonable momentum-space representation of the decay operator $\hat{\mathcal{D}}_\alpha$. Here, we adopt the PFSA and proceed in analogy to previous studies of the electroweak nucleon structure [13–15] but use a pseudovector coupling at the quark-pion vertex:

$$\begin{aligned}\langle p_1, p_2, p_3; \sigma_1, \sigma_2, \sigma_3|\, \hat{\mathcal{D}}_\alpha\, |p_1', p_2', p_3'; \sigma_1', \sigma_2', \sigma_3'\rangle \\ = \sqrt{\frac{M^3 M'^3}{(\sum \omega_i)^3 \,(\sum \omega_i')^3}}\, 3ig_{qq\pi}\bar{u}(p_1, \sigma_1)\,\gamma^5\gamma^\mu \boldsymbol{\lambda}^F u(p_1', \sigma_1') \\ 2p_2'^0\delta(\mathbf{p}_2 - \mathbf{p}_2')\, 2p_3'^0\delta(\mathbf{p}_3 - \mathbf{p}_3')\,\delta_{\sigma_2\sigma_2'}\delta_{\sigma_3\sigma_3'} Q_{\pi,\mu}. \quad (4)\end{aligned}$$

The overall momentum conservation, $P'_\mu - P_\mu = Q_{\pi,\mu}$, together with the two spectator conditions define the relation between all incoming and outgoing quark momenta. In particular, the momenta of the active quark are related by $\mathbf{p}_1 - \mathbf{p}_1' = \tilde{\mathbf{Q}}$, where $\tilde{\mathbf{Q}}$ is completely determined. Thus the momentum transferred to the active quark is different from the momentum transfer to the baryon as a whole. This is a consequence of translational invariance which thereby introduces effective many-body contributions into the above definition of the spectator-model decay operator. Furthermore, in eq. (4) there appears an overall normalization factor

$$\mathcal{N} = \sqrt{\frac{M^3 M'^3}{(\sum \omega_i)^3\,(\sum \omega_i')^3}}. \quad (5)$$

Through the ω_i and the on-mass-shell condition of the quarks it depends on the individual quark momenta. This choice of $\mathcal{N}$ is consistent with the one used in the definition of the electromagnetic and axial currents in the PFSA calculations of the nucleon electroweak form factors by the Graz-Pavia collaboration [13–15]. It guarantees for the correct proton charge. However, it is not a unique choice. Any other normalization factor of the asymmetric form

$$\mathcal{N}(y) = \left(\frac{M^3}{(\sum \omega_i)^3}\right)^y \left(\frac{M'^3}{(\sum \omega_i')^3}\right)^{1-y} \quad (6)$$

would do the same. In order to study the effects of these further choices we investigate the dependence of the decay widths on the parameter range $0 \le y \le 1$.

3 Results

The decay widths of the PFSA calculation with the decay operator given in eq. (4), with the symmetric normalization factor, are shown in table 1 for the GBE and OGE CQMs. It is immediately seen that only the N^*_{1535} and N^*_{1710} predictions are

Table 1. PFSA predictions for π decay widths of the relativistic GBE [4] and OGE [9] CQMs in comparison to the Bethe-Salpeter results of the II CQM [20] and experimental data [24]. In the last three columns the theoretical results are expressed as percentage fractions of the (best-estimate) experimental values in order to be compared to the measured $\Delta\pi$ branching ratios.

Decays	Experiment	Rel. CQM			$\Delta\pi$	% of Exp. Width		
$\to N\pi$		GBE	OGE	II	branching ratio	GBE	OGE	II
$N^\star_{1440}$	$(227 \pm 18)^{+70}_{-59}$	33	53	38	$20-30\%$	14	24	17
$N^\star_{1520}$	$(66 \pm 6)^{+\ 9}_{-\ 5}$	17	16	38	$15-25\%$	26	24	58
$N^\star_{1535}$	$(67 \pm 15)^{+28}_{-17}$	90	119	33	$< 1\%$	134	178	49
$N^\star_{1650}$	$(109 \pm 26)^{+36}_{-\ 3}$	29	41	3	$1-7\%$	27	38	3
$N^\star_{1675}$	$(68 \pm 8)^{+14}_{-\ 4}$	5.4	6.6	4	$50-60\%$	8	10	6
$N^\star_{1700}$	$(10 \pm 5)^{+\ 3}_{-\ 3}$	0.8	1.2	0.1	$> 50\%$	8	12	1
$N^\star_{1710}$	$(15 \pm 5)^{+30}_{-\ 5}$	5.5	7.7	n/a	$15-40\%$	37	51	n/a
Δ_{1232}	$(119 \pm 1)^{+\ 5}_{-\ 5}$	37	32	62	–	31	27	52
Δ_{1600}	$(61 \pm 26)^{+26}_{-10}$	0.07	1.8	n/a	$40-70\%$	≈ 0	3	n/a
Δ_{1620}	$(38 \pm 8)^{+\ 8}_{-\ 6}$	11	15	4	$30-60\%$	29	39	11
Δ_{1700}	$(45 \pm 15)^{+20}_{-10}$	2.3	2.3	2	$30-60\%$	5	5	4

within the experimental range. All other decay widths are underestimated, some of them considerably. In this regard, it is noteworthy that in the case of the N^*_{1535} the $\Delta\pi$ branching ratio is exceptionally small ($< 1\%$). Therefore we found it interesting to look at the results with a view to the measured $\Delta\pi$ branching ratios. In fact, one can observe a striking relation between these branching ratios and the sizes of the theoretical decay widths, expressed as percentage fractions of the experimental values in the last three columns of table 1: The larger the $\Delta\pi$ branching ratio of a resonance, the bigger the underestimation of the (best-estimate) experimental value. This observation hints to a possible systematic problem in the description of mesonic decay widths within (relativistic) CQMs. It calls for a more complete treatment of baryon resonances with a more realistic coupling to decay channels. In fig. 1 we demonstrate the dependence of the PFSA predictions (for the case of the GBE CQM) on the possible asymmetric choice of the normalization factor $\mathcal{N}$ (see eq. (6)). In the range $0 \leq y \leq 1$ all decay widths grow rapidly with increasing y. In this way one could enhance the theoretical predictions considerably. However, if one wants neither one of the decay widths to exceed its experimental range, one is limited to a value of $y \leq 0.5$. Any y lower than 0.5 would lead to decay widths much too small in most cases. Consequently, a symmetric normalization factor as in eq. (4) seems to be the preferred and most reasonable choice also in the context of hadronic decay widths.

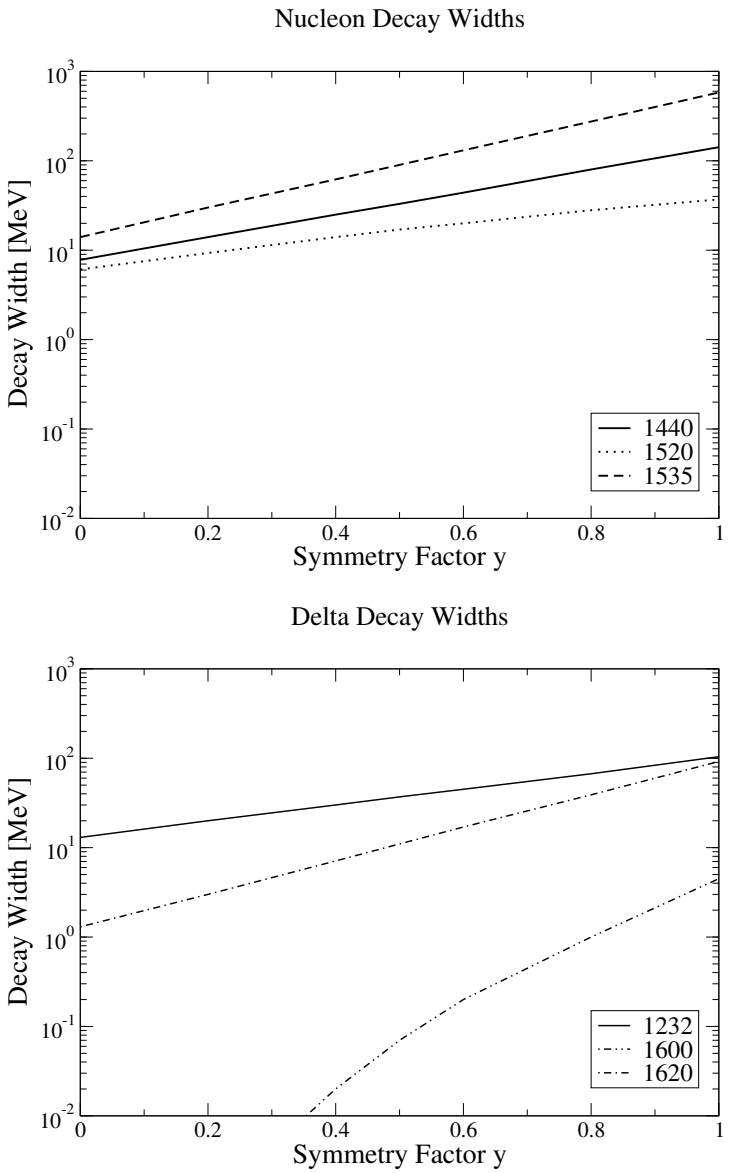

Fig. 1. Dependence of some resonance decay widths on the choice of the normalization factor after eq. (6).

4 Summary

We have presented a Poincaré-invariant description of strong baryon resonance decays in point form within relativistic CQMs. Covariant predictions have been given for π decay widths. They are considerably different from previous nonrelativistic results or results with relativistic corrections included. The covariant results calculated with a spectator-model decay operator show a uniform trend. In almost all cases the corresponding theoretical predictions underestimate the ex-

perimental data considerably. This is true in the framework of Poincaré-invariant quantum mechanics (here in point form) as well as in the Bethe-Salpeter approach [20]. Indications have been given that for a particular resonance the size of the underestimation is related to the magnitude of the $\Delta\pi$ branching ratio. This hints to a systematic defect in the description of the decay widths.

The investigation of different possible choices for a normalization factor in the spectator-model decay operator has led to the suggestion that the symmetric choice is the most natural one. It is also consistent with the same (symmetric) choice that had been adopted before for the spectator-model current in the study of the electroweak nucleon form factors.

This work was supported by the Austrian Science Fund (Project P16945). T.M. would like to thank the INFN and the Physics Department of the University of Padova for their hospitality, and MIUR-PRIN for financial support

References

1. S. Capstick and N. Isgur, Phys. Rev. D **34**, 2809 (1986).
2. U. Loering, K. Kretzschmar, B. C. Metsch, and H. R. Petry, Eur. Phys. J. **A10**, 309 (2001).
3. U. Loering, B. C. Metsch, and H. R. Petry, Eur. Phys. J. **A10**, 395 (2001).
4. L. Y. Glozman, W. Plessas, K. Varga, and R. F. Wagenbrunn, Phys. Rev. D **58**, 094030 (1998).
5. F. Stancu and P. Stassart, Phys. Rev. D **39**, 343 (1989).
6. S. Capstick and W. Roberts, Phys. Rev. D **47**, 1994 (1993).
7. P. Geiger and E. S. Swanson, Phys. Rev. D **50**, 6855 (1994).
8. E. S. Ackleh, T. Barnes, and E. S. Swanson, Phys. Rev. D **54**, 6811 (1996).
9. L. Theussl, R. F. Wagenbrunn, B. Desplanques, and W. Plessas, Eur. Phys. J. **A12**, 91 (2001).
10. S. A. Dytman, and E. S. Swanson (Eds.): NSTAR 2002 (Proc. of the Workshop on the Physics of Excited Nucleons, Pittsburgh, Pennsylvania, 2002). Singapore: World Scientific 2003.
11. B. D. Keister and W. N. Polyzou, Adv. Nucl. Phys. **20**, 225 (1991).
12. B. Bakamjian and L. Thomas, Phys. Rev. **92**, 1300 (1953).
13. R. F. Wagenbrunn *et al.*, Phys. Lett. **B511**, 33 (2001).
14. L. Y. Glozman *et al.*, Phys. Lett. **B516**, 183 (2001).
15. S. Boffi *et al.*, Eur. Phys. J. **A14**, 17 (2002).
16. K. Berger, R. F. Wagenbrunn, and W. Plessas, nucl-th/0407009 (2004).
17. T. Melde, W. Plessas, and R. F. Wagenbrunn, Few-Body Syst. Suppl. **14**, 37 (2003).
18. A. Krassnigg *et al.*, Few Body Syst. Suppl. **10**, 391 (1999).
19. W. Plessas *et al.*, Few Body Syst. Suppl. **11**, 29 (1999).
20. B. Metsch, hep-ph/0403118 (2004).
21. S. Kumano and V. R. Pandharipande, Phys. Rev. D **38**, 146 (1988).
22. R. Kokoski and N. Isgur, Phys. Rev. D **35**, 907 (1987).
23. W. H. Klink, Phys. Rev. C **58**, 3587 (1998).
24. S. Eidelman *et al.*, Phys. Lett. **B592**, 1 (2004).

BLED WORKSHOPS
IN PHYSICS
VOL. 5, NO. 1

Proceedings of the Mini-Workshop
Quark Dynamics *(p. 49)*
Bled, Slovenia, July 12-19, 2004

Relativistic Treatment of Baryon Reactions

W. Plessas

Theoretical Physics, Institute for Physics, University of Graz, Universitätsplatz 5, A-8010 Graz, Austria

Abstract. We give a survey of the performance of modern relativistic constituent quark models in the description of baryon properties and reactions. In particular, we address baryon spectroscopy, elastic electromagnetic and axial nucleon form factors, electric radii and magnetic moments of the octet and decuplet baryon ground states, electromagnetic transitions, as well as mesonic baryon resonance decays. Directions for further improvements of constituent quark models are indicated.

1 Relativistic Constituent Quark Models

Constituent quark models (CQMs) represent a powerful tool in modern hadronic physics. They serve as an effective description of hadron properties at low and intermediate energies. CQMs have undergone a vivid development over the past few years. Notably, one has found that CQMs must take into account the relevant properties of quantum chromodynamics (QCD) in the nonperturbative regime and have to fulfill the requirements of a relativistic theory. In order to arrive at a reasonable description of hadron phenomena, CQMs should meet the symmetry requirements of both (low-energy) QCD and special relativity.

From the outset, CQMs rely on a finite number of degrees of freedom. One assumes a few-quark system, $\{Q\bar{Q}\}$ or $\{QQQ\}$ etc., with certain internal interactions and solves the corresponding dynamical equations. The theory should be covariant. Thus, it is most natural to resort to a Poincaré-invariant relativistic quantum theory. Such an approach is well defined and it can be solved rigorously, at least for confined two- and three-quark systems. In particular, one solves the eigenvalue problem of the invariant mass operator for a given CQM, obtains the eigenenergies and eigenstates, and can go ahead to calculate reactions involving the corresponding hadron states. If one uses relativistic operators and carries out the necessary Lorentz transformations exactly, one will arrive at covariant predictions for the observables in question. The latter task is most efficiently achieved in the point-form version of relativistic quantum mechanics (RQM), since in this case the generators of Lorentz boosts remain purely kinematical.

It should be noted that for a CQM to be considered as 'relativistic' it is not necessary that the inherent dynamics is derived in a relativistic manner, e.g., from a quantum field theory. It suffices that the mutual interactions between the constituents of a given system meet the requirements of Poincaré invariance. One

could even introduce phenomenologically motivated interactions into the Hamiltonian (or equivalently into the mass operator). Once such an interacting Hamiltonian fulfills the commutator relations of the Poincaré algebra, all the symmetries of a Lorentz-covariant theory can be implemented.

Recently, we have seen interesting new results for baryons especially from the relativistic CQMs that rely on one-gluon-exchange (OGE), Goldstone-boson-exchange (GBE), and instanton-induced (II) effective interactions between confined constituent quarks. In this paper, we concentrate on the GBE CQM by the Graz group [1], a relativistic version [2] of the Bhaduri-Cohler-Nogami (BCN) OGE CQM [3], and the II CQM by the Bonn group [4]. The first two are constructed in the framework of RQM, while the last one is formulated in the Bethe-Salpeter approach. Incidentally, the main differences lie in the hyperfine interactions, while the (linear) confinement potential is very similar in all cases; its strength is practically compatible with the string tension of QCD. As a result, the local extensions of the corresponding $\{QQQ\}$ states are also commensurable. They are much narrower than in nonrelativistic CQMs, which use a confinement potential with an unreasonably weak strength.

2 Baryon Spectroscopy

The detailed light and strange baryon spectra of the GBE, OGE, and II CQMs can be found in the original papers [1,9,2]. A critical discussion of the qualitative differences between the GBE and OGE hyperfine interactions is presented in ref. [5]. For a critique of some erroneous and misleading results in the literature see also ref. [6]. In the comparison of the GBE, OGE, and II CQMs some relevant observations are to be made specifically with regard to the N and Λ spectra as exemplified in Figure 1.

Only the GBE CQM can provide for the correct level orderings of positive- and negative-parity excitations in the N spectrum. The $\frac{1}{2}^+ N(1440)$ Roper resonance cannot be brought down below the $\frac{1}{2}^- N(1535)$ resonance by the OGE and II CQMs (as long as the correct N-Δ splitting is maintained). The success of the GBE CQM is due to its particular spin-flavor dependence in the hyperfine interaction. It is also favourable for reproducing simultaneously the right level ordering in the Λ spectrum (which is opposite to the nucleon case). However, all CQMs fail to describe the lowest excitation in the Λ spectrum, the $\frac{1}{2}^- \Lambda(1405)$ resonance, at the right energy. Most probably this is due to the limitation to $\{QQQ\}$ configurations only. Here, an intriguing shortcoming of the present CQMs becomes evident with respect to a realistic description of baryon resonances, namely, the missing coupling to decay channels. The same conclusion can be drawn from studies of inelastic electromagnetic reactions and mesonic resonance decays (cf. also the discussion below).

3 Elastic Electroweak Nucleon and Baryon Structure

An immediate application of any CQM for baryons is the calculation of elastic electromagnetic and axial nucleon form factors. It provides a stringent test of the

quality of the nucleon wave functions. All of the relativistic CQMs considered here have been studied in this respect. A (partial) comparison is presented in Figure 2. The covariant predictions of the GBE CQM for electromagnetic and weak nucleon form factors calculated in point-form spectator approximation (PFSA) are published in refs. [8,14,15]. The electric radii and magnetic moments of the octet and decuplet ground states are presented in ref. [11]. In all cases a remarkable good agreement of the direct predictions of the GBE CQM with the existing experimental data is found. The PFSA calculation is most favourable for reaching a consistent explanation of the electroweak nucleon structure at low momentum transfers. The good quality of the results, being covariant and practically current-conserving, is not yet fully understood in detail. Large differences of the theoretical predictions are found with the nonrelativistic impulse approximation (NRIA) [8,14–16]; see also Figure 3 below. It has become evident that a nonrelativistic theory does not work for the nucleon form factors. This is even true with regard to the electric radii and magnetic moments, i.e. with observables in the limit of zero momentum transfer.

The comparison of the GBE and OGE CQMs, both calculated in PFSA, tells us that there is no big influence from the type of the nucleon wave function [12]. As soon as the nucleon wave function is realistic, especially with the right spatial extension and the correct (mixed symmetry) spatial components contained, the nucleon form factors will be predicted quite reasonably if the relativistic effects are properly taken into account. At least the influences of different dynamics in the CQM are much smaller than relativistic effects. Only if an oversimplified wave function is employed, such as a completely symmetric $SU(6)$ one, like in the case of confinement only, the description evidently falls short (cf., e.g., the corresponding results for the neutron electric form factor shown in Figure 2). In general, the PFSA predictions are also rather similar to the results obtained for

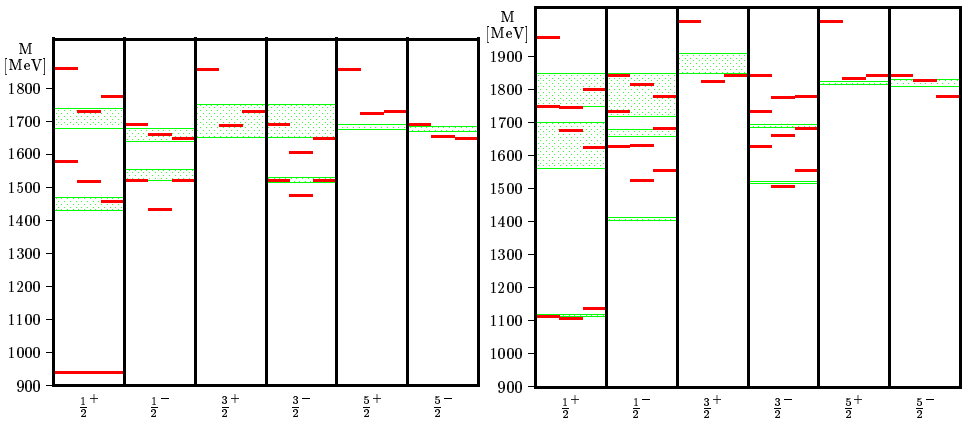

Fig. 1. Nucleon (left) and Λ (right) excitation spectra of three different types of relativistic CQMs. In each column the left horizontal line represents the results of the BCN OGE CQM, as parametrised in [2], the middle one of the II CQM (version A) [4], and the right one of the GBE CQM [1]. The shadowed boxes give the experimental data with their uncertainties after the latest compilation of the PDG [7].

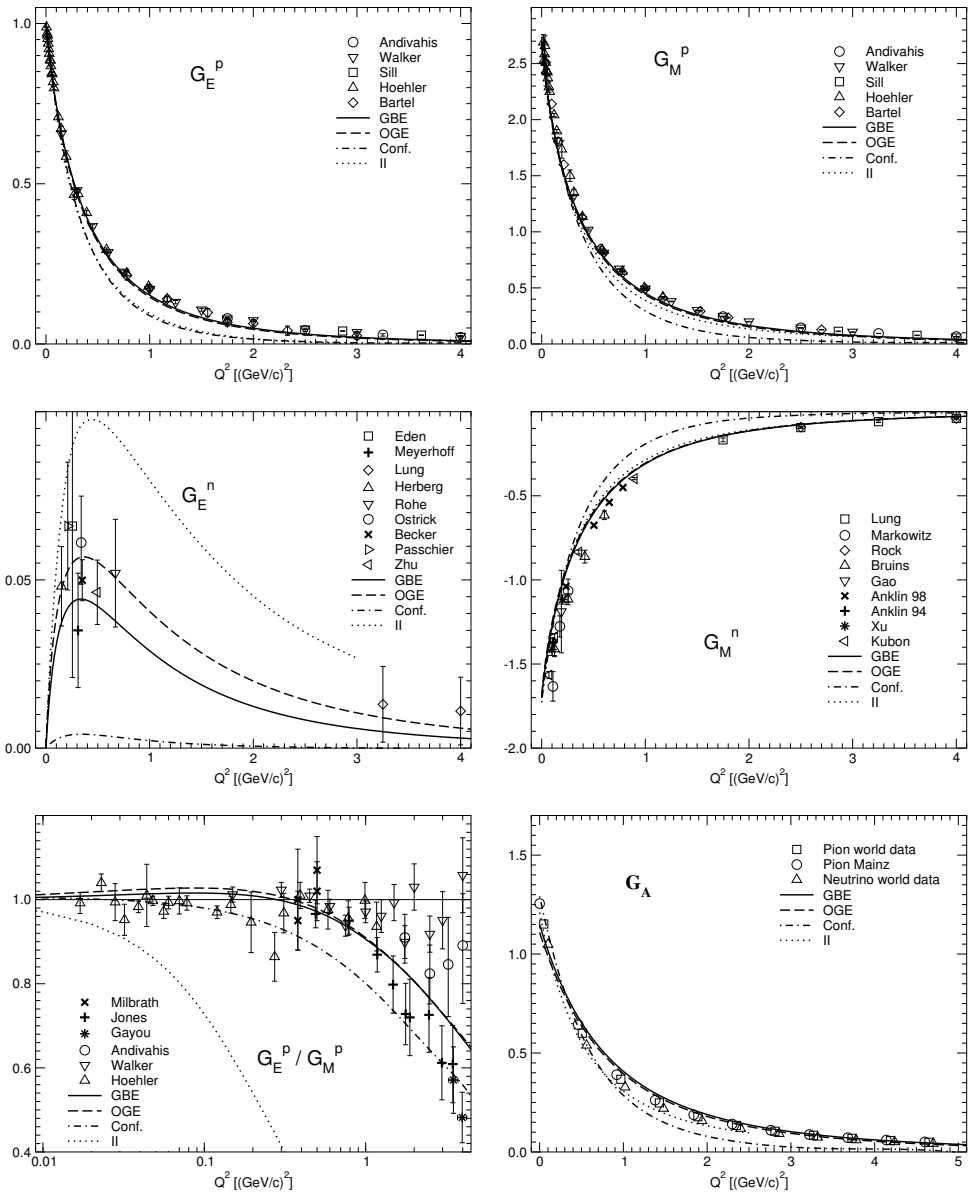

Fig. 2. Predictions of different CQMs for the nucleon electromagnetic and axial form factors. The solid and dashed lines represent the PFSA results for the GBE CQM [1] and the BCN OGE CQM [2], respectively; the dash-dotted lines refer to the case with confinement only. The dotted lines show the results of the II CQM [4] within the Bethe-Salpeter approach after ref. [13].

the II CQM following the Bethe-Salpeter approach [13]. This observation is remarkable in view of the differences in the dynamics of the CQMs and the distinct frameworks of the calculations. One may interpret these findings in such a way that for the nucleon ground states any degrees of freedom other than $\{QQQ\}$ are presumably unimportant (at least in the low-momentum-transfer range considered here) and the relativistic current in the spectator approximation is working quite well. If the relativistic boost effects are properly included in the calculation of the matrix elements of elastic form factors and covariant results are thus obtained, a rather consistent explanation of all experimental data becomes possible. The boost effects are taken into account accurately in the point-form calculations; the same is claimed for the Bethe-Salpeter approach [13].

In order to elucidate the peculiarities of the PFSA further, the Graz group has recently undertaken analogous calculations of the nucleon electromagnetic form factors in instant-form spectator approximation (IFSA). The comparison is given in Figure 3 for the case of the GBE CQM. It is seen that the IFSA predictions obtained with the same wave functions as in the case of the PFSA, without introducing any additional parameters, can by no means explain the experimental data. In some way the IFSA results even resemble the ones from the NRIA. In addition to this obvious shortcomings in the comparison with phenomenology, the IFSA must be rejected because it does not account for the correct boost effects and it is not covariant (frame-independent). In instant form the generators of the boosts are a-priori interaction-dependent. Instead, in all IFSA calculations so far, like in the one of Figure 3, free boost transformations have been employed. We consider this as a notorious problem of approximative instant-form approaches. The IFSA results shown in Figure 3 were calculated in the Breit frame. They would be different in another reference system, such as the laboratory frame. Clearly, one cannot rely on such results. Contrary to that the PFSA is manifestly covariant and the corresponding predictions are frame-independent.

The point-form approach works remarkably well in the case of elastic nucleon form factors; the same is true with regard to electric radii and magnetic moments of all octet and decuplet baryon ground states (as far as we can compare to existing experiments) [11]. Still, one has to bear in mind that the PFSA calculation is approximative and incomplete. In particular, explicit many-body currents are still missing. On the other hand, one meets Lorentz covariance and seemingly also the continuity equation is fulfilled to a good extent. The latter property has been tested by calculating the matrix element of the third component of the current operator $\hat{j}^3(q)$. This matrix element must vanish exactly in the Breit frame if the current is conserved. Indeed, the numerical values we obtain are extremely small. In the range of momentum transfers considered here, the magnitude of the matrix element of $\hat{j}^3(q)$ remains lesser than 1 % of the zeroth component $\hat{j}^0(q)$ (from which the electric form factor is deduced).

4 Electromagnetic Transition Form Factors

The next step is testing the relativistic CQMs in $\gamma N \rightarrow N^*$ reactions. First results in this regard have been gained recently for the GBE CQM in PFSA [14]. In

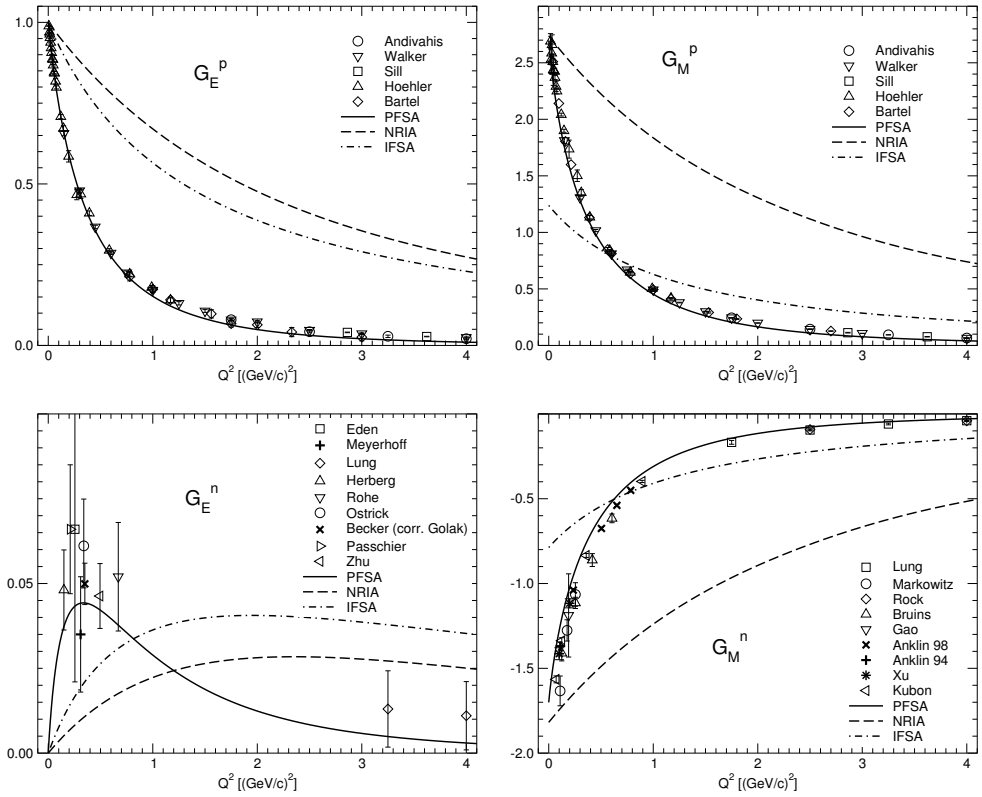

Fig. 3. Comparison of proton and neutron electromagnetic form factors of the GBE CQM [1] calculated in PFSA and IFSA as well as in NRIA.

Figure 4 covariant predictions for helicity amplitudes of γ-induced transitions to several N^* resonances are shown. They were calculated in a manner completely analogous to the elastic nucleon form factors. Data are still scarce and have relatively large uncertainties. In case of the neutron there are only data at $Q^2 = 0$. The theoretical predictions appear reasonable even though one finds deviations from the experimental data that are bigger than in the elastic case. We do not yet know the definite reasons for the discrepancies. One may suspect that the description of the resonances in a CQM with $\{QQQ\}$ configurations only is not realistic enough, as soon as resonances are involved. Further investigations in this field are urgently needed.

5 Mesonic Decays of Baryon Resonances

Another wide field for applications of CQMs are the decays of baryon resonances. Preliminary relativistic predictions for widths of pionic decays of N^* and Δ^* resonances were already presented in ref. [16]. In that work one produced first covari-

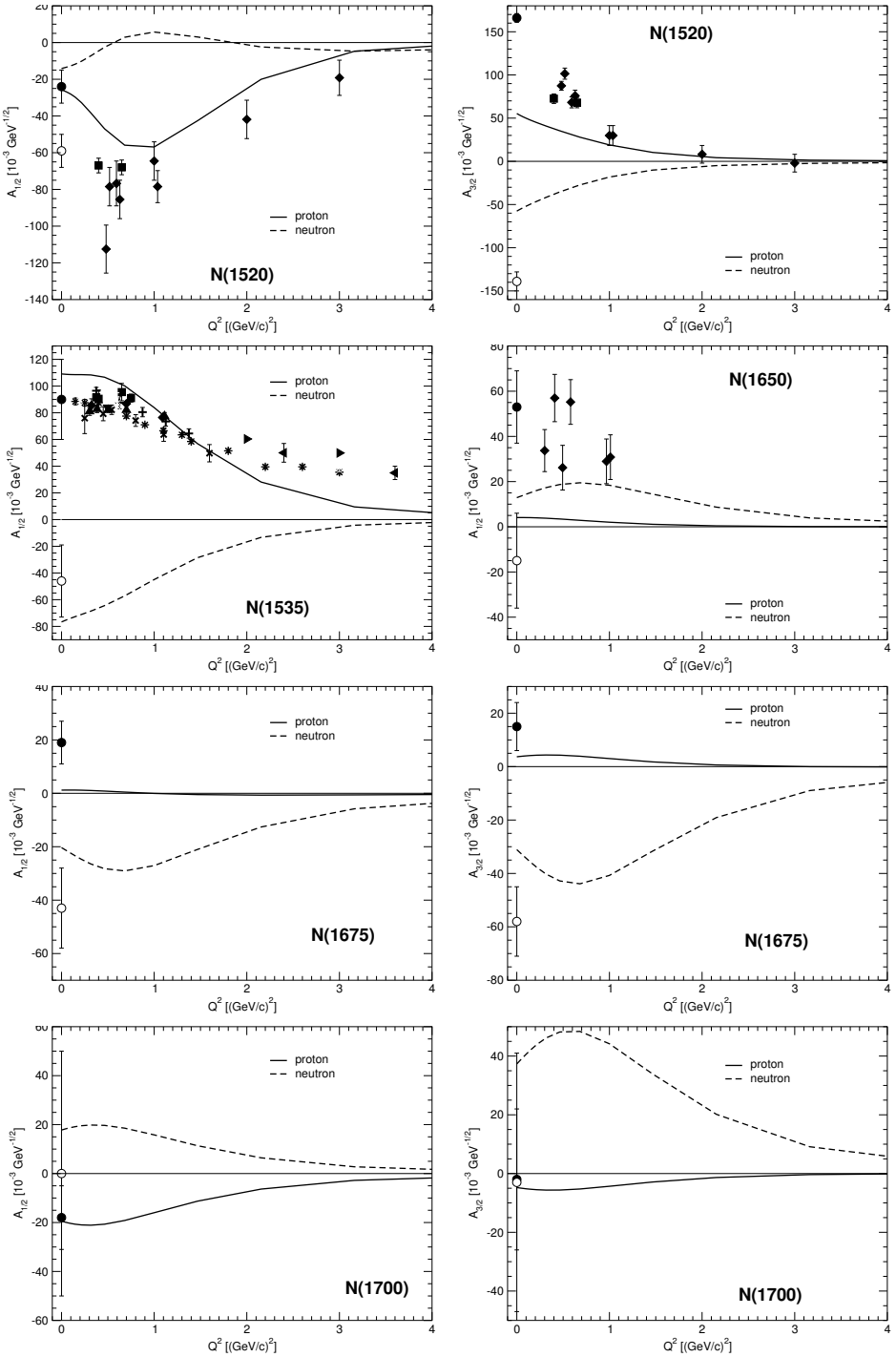

Fig. 4. PFSA predictions of the GBE CQM [1] for helicity amplitudes of $\gamma N \rightarrow N^*$ transitions. The data at $Q^2 = 0$ are from the PDG [7] for the proton (solid circles) and the neutron (open circles). The proton data at $Q^2 > 0$ are taken from the review [15] and references cited therein.

ant results with the GBE and OGE CQMs using a spectator model decay operator in point form (PFSA). The relativistic PFSA results were found to be quite distinct from previous results of nonrelativistic calculations or calculations with relativistic corrections. Almost all decay widths turned out to be (much) too small. Only in two cases, namely in $N(1535)$ and $N(1710)$, the magnitude of the experimental value for the π-decay width is reached.

In the meantime the calculations have been improved and further investigations have been undertaken, such as the calculation of η-decay modes [17]. Also the Bonn group has calculated decay widths with the II CQM in the Bethe-Salpeter approach [18]. They found results that are again quite similar to the ones obtained for the GBE CQM in PFSA. In particular, they confirmed the general trend of the decay widths resulting too small. Obviously an important ingredient is missing in the present description. Once more we are hinted to the necessity of taking into account the coupling to the decay channels and including explicit mesonic degrees of freedom. For a further and more detailed discussion of these aspects see T. Melde's contribution to this Workshop [19].

Acknowledgment The results discussed in this paper rely on essential contributions by my colleagues K. Berger, L. Glozman, T. Melde, and especially R. Wagenbrunn (Graz) as well as on collaborations with W. Klink (Iowa), S. Boffi, and M. Radici (Pavia). This work was supported by the Austrian Science Fund (Project P16945).

References

1. L. Y. Glozman, W. Plessas, K. Varga, and R. F. Wagenbrunn, Phys. Rev. D **58**, 094030 (1998).
2. L. Theussl, R. F. Wagenbrunn, B. Desplanques, and W. Plessas, Eur. Phys. J. **A12**, 91 (2001).
3. R. K. Bhaduri, L. E. Cohler, and Y. Nogami, Nuovo Cim. **A65**, 376 (1981).
4. U. Loering, K. Kretzschmar, B. C. Metsch, and H. R. Petry, Eur. Phys. J. **A10**, 309 (2001); ibid., 395 (2001).
5. L. Ya. Glozman, Z. Papp, W. Plessas, K. Varga, and R. F. Wagenbrunn, Phys. Rev. C **57**, 3406 (1998).
6. W. Plessas, Few-Body Syst. Suppl. **15**, 139 (2003).
7. S. Eidelman et al., Phys. Lett. **B592**, 1 (2004).
8. R. F. Wagenbrunn, S. Boffi, W. Klink, W. Plessas, and M. Radici, Phys. Lett. **B511**, 33 (2001).
9. L. Y. Glozman, M. Radici, R.F. Wagenbrunn, S. Boffi, W. Klink, and W. Plessas, Phys. Lett. **B516**, 183 (2001).
10. S. Boffi, L.Y. Glozman, W. Klink, W. Plessas, M. Radici, and R.F. Wagenbrunn, Eur. Phys. J. **A14**, 17 (2002).
11. K. Berger, R. F. Wagenbrunn, and W. Plessas, arXiv:nucl-th/0407009 (2004), to appear in Phys. Rev. D.
12. R. F. Wagenbrunn, S. Boffi, L. Y. Glozman, W. Klink, W. Plessas, and M. Radici, Few Body Syst. Suppl. **14**, 411 (2003).
13. D. Merten, U. Loering, K. Kretzschmar, B. Metsch, and H.R. Petry, Eur. Phys. J. **A14**, 477 (2002).

14. R.F. Wagenbrunn, Contribution to the 19th European Conference on Few-Body Problems, Groningen, 2004, to appear in the proceedings.
15. V. D. Burkert and T. S. H. Lee, arXiv:nucl-ex/0407020, to appear in Int. J. Mod. Phys. E.
16. T. Melde, W. Plessas, and R. F. Wagenbrunn, Few-Body Syst. Suppl. **14**, 37 (2003).
17. T. Melde, W. Plessas and R. F. Wagenbrunn, Contribution to the N*2004 Workshop, Grenoble, 2004, to appear in the proceedings; arXiv:hep-ph/0406023.
18. B. Metsch, arXiv:hep-ph/0403118 (2004).
19. T. Melde, L. Canton, W. Plessas, and R. F. Wagenbrunn, Contribution to this Workshop; arXiv:hep-ph/0410274.

BLED WORKSHOPS
IN PHYSICS
VOL. 5, NO. 1

Proceedings of the Mini-Workshop
Quark Dynamics *(p. 58)*
Bled, Slovenia, July 12-19, 2004

The Double-Charm Hyperons and Their Interactions

Dan-Olof Riska

Helsinki Institute of Physics and Department of Physical Sciences, 00014 University of Helsinki, Finland

Abstract. The main interaction of the ground states of the double-charm hyperons form is due to their light quarks and can be derived from the corresponding nucleon-nucleon interaction by rescaling of the interaction to take into account the difference between interaction strengths for pairs of light flavor quarks and pairs of triplets of light flavor quarks. Nucleons and double-charm (and double-beauty hyperons) are very likely to form bound states in the triplet state.

1 The double-charm hyperons

Several double-charm hyperons, the lowest one of which is the ground state multiplet with the Ξ_{cc} at 3.46 GeV have been found[1]. The corresponding (probably) spin 3/2 multiplet has been found at 3.52 GeV. The ground state multiplet Ξ_{cc}^{+}, Ξ_{cc}^{++} of the double-charm hyperons forms a spin 1/2 isospin 1/2 multiplet, with the valence quark configuration dcc and ucc [2].

2 Models for the double-charm hyperons

The energy of the ground state multiplet is in the range $\sim$ 3.5 GeV, suggested by early model calculations [2,3]. The Skyrme model slightly underpredicted (40 MeV) the value of the empirically found splitting 60 MeV between the spin 1/2 ground state and the spin 3/2 excited state while the extant lattice value of this splitting is somewhat large value (90 MeV) [4].

3 Hyperfine splitting structure

The discovery of the ground state multiplets of the doubly charmed hyperons allows an overall view of the mass and flavor dependence of the ground state baryon splittings (Table 1). These do not vary smoothly with baryon mass, as heavy quark symmetry would suggest. As an example the splitting in the Ξ spectrum is larger than that in the Σ spectrum, and the ground state splitting is similar in the single and double-charm hyperons.

The splittings may be described by the schematic phenomenological flavor and spin dependent hyperfine interaction model [5]:

$$V = -\sum_{i<j}\left[C\sum_{a=1}^{3} + C_S\sum_{a=4}^{8} + C_C\sum_{a=9}^{12} + C_{SC}\sum_{a=13}^{14}\right]\lambda_i^a\lambda_j^a\,\boldsymbol{\sigma}^i\cdot\boldsymbol{\sigma}^j\,. \qquad (1)$$

quark content	baryons	model	splitting
uud	$\Delta(1232) - N$	$12C - 2C_S$	293
uds	$\Sigma(1385) - \Sigma$	$10C_S$	190
uss	$\Xi(1530) - \Xi$	$10C_S$	210
uus	$\Sigma_c(2520) - \Sigma_c$	$6C$	65
usc	$\Xi_c(2645) - \Xi_c{}'$	$3C_C + 3C_S$	71
ucc	$\Xi_{cc}(3520) - \Xi_{cc}$	$6C_C$	60

Table 1. The ground state splittings in MeV of the baryons

This interaction provides a fair description of the known baryon spectrum. It may be interpreted as an "effective" description of the pion and two-pion (C = 28 MeV), K, K^*, η (C_S = 19 MeV), D and D^* (C_C = 10 MeV and D_s and D_s^* (C_{CS} = 10 MeV) exchange interactions between the quarks of appropriate flavor. With this interaction the empirical splitting 60 MeV between the $\Xi_{cc}(3520)$ and the Ξ_{cc} obtains.

4 The interactions of the double-charm hyperons

The main color-neutral strong interaction between double-charm hyperons is that between their light flavor quark components. This may be inferred from the nucleon-nucleon interaction, by multiplication of the components of the nucleon-nucleon interaction by appropriate coefficients, which relate the interaction strength between pairs of light flavor quarks to that between such triplets. The interaction between the charm quark pairs in different hadrons is weaker than that between light flavor quarks in different hadrons, as the latter either arises from the short range interaction that is mediated by the exchange of charmonia or the color van der Waals interaction. The weaker strong interaction between double-charm hyperons is partially compensated by their larger mass in comparison to nucleons.

The nucleon-nucleon interaction may be expressed in terms of rotational invariants of spin and isospin as well as momenta and angular momenta. The quark model scaling factors between the matrix elements of the spin-isospin invariants for Ξ_{cc} and nucleon states may be derived from the quark model matrix elements of light flavor quark operators [6]:

$$\langle \Xi_{cc}|1|\Xi_{cc}\rangle = \frac{1}{3}\langle N|1|N\rangle\,,\ \ \langle \Xi_{cc}|\sum_q \sigma_a^q|\Xi_{cc}\rangle = -\frac{1}{3}\langle N|\sum_q \sigma_a^q|N\rangle\,,$$
$$\langle \Xi_{cc}|\sum_q \tau_a^q|\Xi_{cc}\rangle = \langle N|\sum_q \tau_a^q|N\rangle\,,\ \ \langle \Xi_{cc}|\sum_q \sigma_a^q\tau_b^q|\Xi_{cc}\rangle = -\frac{1}{5}\langle N|\sum_q \sigma_a^q\tau_b^q|N\rangle\,. \tag{2}$$

The interaction between two double-charm hyperons that arises from the interaction between the light flavor quarks may be determined from realistic nucleon-nucleon interaction models as eg. the models in refs. [7–9]. From these the corresponding interactions between double-charm hyperons may be derived by application of the appropriate downscaling of the strengths of the corresponding interaction components.

With the quark model scaling factors two of the three rescaled nucleon-nucleon interactions models yield that deuteron-like bound states of double-charm hyperons, with binding energies in the range $87 - 457$ MeV.

In Table 2 contains the calculated binding energies obtained for the deuteron-like states of double-charm hyperons. The difference between these values gives an estimate of the theoretical uncertainty that derives from the different short range behavior of the nucleon-nucleon interaction models.

Two-baryon states formed of double-charm hyperons can couple to states with a single charm and a triple-charm Ω_{CCC} by quark rearrangement. If the latter states have lower energy the former are metastable rather than bound. This depends on the size of the binding energy as compared to the mass difference: $\Delta^c \equiv M_{ccc}+M_{cll}-2M_{ccl}$, where l represents a light quark. For some quark models the inequality $\Delta^c < 0$ holds and for those $\Delta \approx [130 - 158]$ MeV [10]. Adoption of those values imply that the double charm hyperons form bound states with the AV18 potential, but only metastable states with the Nijm II potential.

Double-Charm hyperons	
Potential	Binding Energy (MeV)
AV18	-457 (-28)
Paris	$-$
Nijm II	-87
Double-Beauty double-charm hyperons	
AV18	-603 (-183)
Paris	-0
Nijm II	-102
Double-Beauty hyperons	
AV18	-782 (-439)
Paris	-2
Nijm II	-123 (-20)

Table 2. Binding energies for the $\Xi_{cc}^{++} - \Xi_{cc}^{+}$ and $\Xi_{bb}^{0} - \Xi_{bb}^{-}$ systems obtained with Argonne V18 [7], AV18, Nijmegen II [8] and Paris [9] potentials. The value in brackets corresponds to a second bound state (from [6]).

The origin of the large binding energy given by the AV18 interaction model is its large squared spin-orbit interaction, which acts in the D−state. In the large N_c limit the angular momentum dependent interaction components are proportional to one power of $1/N_c$ for each power of the angular momentum **L**. As the baryon mass scales as N_c that would suggest that an additional factor of m_N/m_H, where m_N is the nucleon and m_H the heavy hyperon mass respectively, should be associated with the each power of **L** in the scaling relations [11,12]. Inclusion of such a factor would suppress the role of the angular momentum dependent interaction operators, and would reduce the calculated binding energies obtained with the AV18 interaction.

The interaction between the ground state multiplets of double-beauty should be similar to that of the double charm hyperons, as the main interaction is that between their light flavor quarks. Their binding energy will however be larger than that of double-charm hyperons in view of their larger mass. This is shown in Table 2 where the binding energy of two double-beauty hyperons is calculated with the assumption that their mass is: $M_{bbu} = M_{bbd} \approx 2m_b \approx 2 \times 4500$ MeV.

Metastability is in this case is determined by a similar inequality, as in the case of the charmed hyperon case: $\Delta^b \equiv M_{bbb} + M_{bll} - 2M_{bbl} < 0$, where its estimated value ranges $[348 - 372]$ MeV [10]. Therefore he result obtained with the AV18 potential is a bound state, while that obtained with the Nijm II potential is a metastable state.

Deuteron-like bound states of nucleons and double-heavy hyperons: $N-\Xi_{cc}$ and $N-\Xi_{bb}$ are also very likely. The AV18 potential gives bound states at -388 MeV and -494 MeV for the $N-\Xi_{cc}$ and $N-\Xi_{bb}$ systems respectively. The Nijm II potential gives bound states at -35 MeV and -76 MeV for the $N-\Xi_{cc}$ and $N-\Xi_{bb}$ systems respectively.

Acknowledgment This talk is based on collaboration with Bruno Juliá-Díaz. Research supported in part by the Academy of Finland under grant 54038.

References

1. M. Mattson et al., Phys. Rev. Lett. **89** (2002) 112001; M. Moinester et al., hep-ex/0212029; A. Ocherashvili et al., hep-ex/04506033.
2. S. Fleck and J. M. Richard, Prog. Theor. Phys. **82** (1989) 760.
3. M. Rho, D. O. Riska and N. N. Scoccola, Z. Phys. **A 341** (1992) 343.
4. J. M. Flynn, JHEP 0307, 066 (2003)
5. F.Coester, K. Dannbom and D. O. Riska, Nucl. Phys. **A 634** (1998) 335
6. B. Juliá-Díaz and D. O. Riska, nucl-th/0405061
7. R. B. Wiringa, V. G. J. Stoks and R. Schiavilla, Phys. Rev. **C 51** (1995) 38.
8. V. G. J. Stoks et al., Phys. Rev. **C 49** (1994) 2950.
9. M. Lacombe et al., Phys. Rev. **C 21** (1980) 861.
10. J. M. Richard, Phys. Rept. **212** (1992) 1; B. Silvestre-Brac, Few Body Syst. **20** (1996) 1.
11. D. B. Kaplan and A. V. Manohar, Phys. Rev. **C56** (1997) 76.
12. D. O. Riska, Nucl. Phys. **A710** (2002) 99.

BLED WORKSHOPS
IN PHYSICS
VOL. 5, NO. 1

Proceedings of the Mini-Workshop
Quark Dynamics *(p. 62)*
Bled, Slovenia, July 12-19, 2004

Calculation of electroproduction amplitudes in the K-matrix formalism*

B. Golli[a,b], P. Alberto[c,e], L. Amoreira[d,e], M. Fiolhais[c,e], and S. Širca[f,b]

[a] Faculty of Education, University of Ljubljana, 1000 Ljubljana, Slovenia
[b] J. Stefan Institute, 1000 Ljubljana, Slovenia
[c] Department of Physics, University of Coimbra, 3004-516 Coimbra, Portugal
[d] Department of Physics, University of Beira Interior, 6201-001 Covilhã, Portugal
[e] Centre for Computational Physics, University of Coimbra, 3004-516 Coimbra, Portugal
[f] Faculty of Mathematics and Physics, University of Ljubljana, 1000 Ljubljana, Slovenia

Abstract. The K-matrix approach is applied to the calculation of the multipole amplitudes M_{1+}, E_{1+}, and S_{1+} in the Δ channel within the Cloudy Bag Model. The separation of the amplitudes into the resonant part and the background is presented and discussed.

1 Introduction

In our previous work [1] (see also [2]) we presented a method to calculate pion electroproduction amplitudes in the framework of chiral quark models. We derived the expressions for the transition K-matrix and the T-matrix and showed how to separate the resonant part from the background. In the present work we apply this method to the calculation of amplitudes M_{1+}, E_{1+}, and S_{1+} in the $\Delta(1232)$ channel.

We use the Cloudy Bag Model as a simple example of a chiral quark model. In spite of the known limitations of the model we show that it is possible to reproduce these amplitudes sufficiently well in a broad energy range. We explain how to isolate the resonant parts of the amplitudes and show that these parts are in good agreement with the results extracted from the experiment.

2 Electro-production amplitudes and cross-sections

In electro-production, the incoming virtual photon with four-momentum $(\omega_\gamma, \mathbf{k}_\gamma)$, $\omega_\gamma^2 - \mathbf{k}_\gamma^2 = -Q^2$, and polarization μ interacts with the nucleon with the third components of spin m_s and isospin m_t; the final state consists of the scattered pion with four-momentum $(\omega_0, \mathbf{k}_0)$ and the third component of isospin t and the nucleon with good m_s' and m_t'. In the c.m. frame the nucleon momentum is opposite to that of the photon (pion). If the z-axis is oriented in the direction of the incoming photon, the K-matrix for this process can be written as

$$K_{\gamma\pi} = -\pi\langle\Psi^P(m_s, m_t; \mathbf{k}_0, t)|H_\gamma|N(m_s', m_t'); \mathbf{k}_\gamma, \mu\rangle \ . \qquad (1)$$

* Talk delivered by B. Golli

Here Ψ^P is a *principal-value* state (see e.g. [3]) while $|N(m_s', m_t'); \mathbf{k}_\gamma, \mu\rangle$ stands for the asymptotic (free) states representing the nucleon and the photon. The principal value state can be written in the form[1]:

$$|\Psi^P\rangle = \sqrt{\frac{\omega_0}{k_0}} \left\{ a_t^\dagger(\mathbf{k}_0)|N(m_s, m_t)\rangle + \int d\mathbf{k} \, \frac{\chi(k_0, k)}{\omega_k - \omega_0} a_t^\dagger(\mathbf{k})|N(m_s, m_t)\rangle + c_R|R\rangle \right\} , \tag{2}$$

where $a_t^\dagger(\mathbf{k})$ is the pion creation operator, $|N\rangle$ is the nucleon state, and $|R\rangle$ is a (possible) resonant state with excited internal degrees of freedom (e.g. quarks and/or mesons). The amplitude describing the scattered pion, $\chi(k_0, k)$, is related to the phase shift. The state (2) is normalized as

$$\langle \Psi_\alpha^P(E)|\Psi_\beta^P(E')\rangle = (1 + K^2)_{\alpha\alpha} \, \delta(E - E')\delta_{\alpha\beta} , \tag{3}$$

where E is the total energy of the system K is the K-matrix for pion scattering, and α, β label different channels. The normalization (3) is not practical in numerical calculations because the factor in front of the δ function diverges as E approaches the resonant energy. It is more convenient to work with the state normalized simply to $\delta(E - E')$ at the resonance:

$$|\Psi_R\rangle = K_{\pi\pi}^{-1}|\Psi^P\rangle . \tag{4}$$

We now expand Ψ^P (or equivalently Ψ_R) in (1) in states with good total angular momentum J and isospin T:

$$\begin{aligned} K_{\gamma\pi} = K_{\pi\pi}\sqrt{\omega_\gamma k_\gamma} \sum_{lm} \langle \Psi_R J, T, M_J M_T; k_0, l|[H_\gamma \, , a_\mu^\dagger(\mathbf{k}_\gamma)]|N(m_s', m_t')\rangle \\ \times Y_{lm}(\vartheta, \varphi) C^{JM_J}_{\frac{1}{2}m_s lm} C^{TM_T}_{\frac{1}{2}m_t 1t} + \dots , \end{aligned} \tag{5}$$

where ϑ is the angle between the scattered pion and the incident photon, $a_\mu^\dagger(\mathbf{k}_\gamma)$ is the creation operator for the photon, the factor $\sqrt{\omega_\gamma k_\gamma}$ ensures the proper normalization of the photon asymptotic state, and C's are the Clebsh-Gordan coefficients. Since we are usually interested in one particular channel with given J and T we have denoted by $\dots$ other channels not taken into account.

The T-matrix is obtained as

$$T_{\gamma\pi} = K_{\gamma\pi}(1 + iT_{\pi\pi}) , \tag{6}$$

yielding a similar expression as (5) in which $K_{\pi\pi}$ is replaced by $T_{\pi\pi}$. The appearance of $K_{\pi\pi}$ ($T_{\pi\pi}$) in front of the (real) transition amplitude means that the phase shift of the transition K or T-matrix is that of the meson scattering – an explicit manifestation of the Watson theorem. In fact, in the above derivations, we have tacitly assumed that "switching on" the electro-magnetic interaction H_γ does not change the strong scattering amplitudes, i.e. the principal-value state (2) remains unchanged.

[1] Here the normalization of the principal value state (see (3)) and consequently the definition of the K-matrix is changed slightly with respect to the ones used in [1].

To obtain the electro-production amplitudes in the Δ-channel, we keep only the p-wave pions and the $J = T = \frac{3}{2}$ component of the final state in (5); we furthermore neglect nucleon recoil and the effect of the two-pion decay channel. The pertinent electro-production amplitudes are related to the matrix elements of the T-matrix, by

$$M_{1+}^{(3/2)} = T_{\pi\pi}\sqrt{\frac{3}{16k_0k_\gamma}}\,\frac{1}{\pi}\,\left[-\frac{1}{2\sqrt{3}}\,(3K_{3/2}+\sqrt{3}K_{1/2})\right] \tag{7}$$

and

$$E_{1+}^{(3/2)} = T_{\pi\pi}\sqrt{\frac{3}{16k_0k_\gamma}}\,\frac{1}{\pi}\,\frac{1}{2\sqrt{3}}\,(K_{3/2}-\sqrt{3}K_{1/2})\,. \tag{8}$$

Here we have introduced the analogues of the familiar helicity amplitudes:

$$K_\lambda = \sqrt{\omega_\gamma k_\gamma}\,\langle\Psi_R(M_J=\lambda)|\frac{e_0}{\sqrt{2\omega_\gamma}}\int d\mathbf{r}\,\boldsymbol{\varepsilon}_\mu\cdot\mathbf{j}(\mathbf{r})e^{i\mathbf{k}_\gamma\cdot\mathbf{r}}|N(m_s'=\lambda-\mu)\rangle\,, \tag{9}$$

where $\mathbf{j}(\mathbf{r})$ is the vector part of the electro-magnetic current. The differential cross section then reads

$$\frac{d\sigma_T}{d\Omega} = \frac{k_0}{k_\gamma}\left\{\frac{1}{2}\,|M_{1+}|^2(5-3\cos^2\vartheta)+\frac{9}{2}\,|E_{1+}|^2(1+\cos^2\vartheta)\right.$$
$$\left.+\,3\mathrm{Re}M_{1+}^*E_{1+}(1-3\cos^2\vartheta)\right\}\,.$$

The longitudinal amplitude is

$$L_{1+}^{(3/2)} = T_{\pi\pi}\sqrt{\frac{3\omega_\gamma}{32\pi^2k_0}}\,\langle\tilde{\Psi}(M_J=\tfrac{1}{2})|\frac{e_0}{\sqrt{2\omega_\gamma}}\int d\mathbf{r}\,\boldsymbol{\varepsilon}_0\cdot\mathbf{j}(\mathbf{r})e^{i\mathbf{k}_\gamma\cdot\mathbf{r}}|N(m_s'=\tfrac{1}{2})\rangle\,, \tag{10}$$

with

$$\frac{d\sigma_L}{d\Omega} = \frac{k_0}{k_\gamma}\,|L_{1+}|^2\left\{4+12\cos^2\vartheta\right\}\,. \tag{11}$$

3 Calculation of the K-matrix in chiral quark models

We consider quark models in which the p-wave pions couple to the three-quark core. Assuming a pseudo-scalar interaction, the pion part of the Hamiltonian is

$$H_\pi = \int dk\sum_{mt}\left\{\omega_k\,a_{mt}^\dagger(k)a_{mt}(k)+\left[V_{mt}(k)a_{mt}(k)+V_{mt}(k)^\dagger\,a_{mt}^\dagger(k)\right]\right\}\,, \tag{12}$$

where $a_{mt}^\dagger(k)$ is the creation operator for a p-wave pion with the third components of spin m and isospin t, and $V_{mt}(k) = -V(k)\sum_{i=1}^3\sigma_m{}^i\tau_t{}^i$ represents the general form of the pion source in which the function $V(k)$ depends on the particular model. In the Cloudy Bag Model, $V(k)$ reads

$$V(k) = \frac{k^2}{\sqrt{12\pi^2\omega_k}}\,\frac{\omega_{MIT}^0}{\omega_{MIT}^0-1}\,\frac{j_1(kR)}{2f_\pi kR}\,, \tag{13}$$

where $\omega_{MIT}^0 = 2.0428$. The free parameters are the bag radius R and the energy splitting between the bare nucleon and the bare delta which is adjusted such that the experimental position of the resonance is reproduced.

Neglecting recoil, $\omega_\gamma = \omega_0 = E - E_N$, the trial state takes the form

$$|\Psi\rangle = \sqrt{\frac{\omega_0}{k_0}} \left\{ \left[a^\dagger_{mt}(k_0)|\Phi_N\rangle \right]^{\frac{3}{2}\frac{3}{2}} + \int dk\, \frac{\chi(k,k_0)}{\omega_k - \omega_0} \left[a^\dagger_{mt}(k)|\Phi^E_N\rangle \right]^{\frac{3}{2}\frac{3}{2}} + c^E_\Delta |\Phi_\Delta\rangle \right\} . \tag{14}$$

Here Φ_Δ denotes the resonant state representing the bare delta (i.e. three quarks in s-state coupled to $J = T = \frac{3}{2}$) and a cloud of up to two pions around the bare nucleon and delta.

The pion profiles in Φ_N and Φ_Δ can be most easily determined from the following relations that hold for Hamiltonians of the type (12):

$$a_{mt}(k)|A\rangle = -\frac{V^\dagger_{mt}(k)}{\omega_k + H - E_A}|A\rangle \tag{15}$$

and

$$a_{mt}(k)a_{m't'}(k')|A\rangle = \frac{V^\dagger_{mt}(k)}{\omega_k + \omega'_k + H - E_A}\ \frac{V^\dagger_{m't'}(k')}{\omega'_k + H - E_A}|A\rangle + [k \leftrightarrow k'] , \tag{16}$$

where $|A\rangle$ is an eigenstate of H; in our case either $|\Phi_N\rangle$ or $|\Psi\rangle$.

From (14) we have calculated the P33 phase shift as well as the multipole amplitudes for the electroproduction. In order to reproduce the experimental phase shift (see Fig. 1) we had to reduce the value of the pion decay constant appearing in (13) from the experimental value 93 MeV to $83\,\text{MeV} > f_\pi > 78\,\text{MeV}$ for $0.9\,\text{fm} < R < 1.1\,\text{fm}$, respectively.

As seen from Figs. 2 the experimental values for the electroproduction amplitudes are underestimated. The reason lies in a too weak $\gamma N\Delta$ vertex, which is a known feature of the Cloudy Bag Model. Taking a smaller R and reducing further the value of f_π [4] enhances the contribution of the pion cloud, and thus increases the strength of the $\gamma N\Delta$ vertex. Yet this mechanism does not help to improve the agreement: increasing the strength of the quark-pion interaction leads to a larger width of the resonance, and since $\sqrt{\Gamma}$ appears (implicitly) in the denominator of the amplitudes (9) and (10), the net effect is such that the magnitude of the $\text{Im}\, M_{1+}$ in the vicinity of the resonance *decreases*.

4 Extracting the resonance

In some models, the delta resonance is described as a particle with a finite lifetime and an energy corresponding to the pole of the T-matrix in the complex energy plane. The properties of such a particle can not be directly related to the measured amplitudes since the amplitude include also non-resonant processes. In this section we show how to relate the results obtained in the K-matrix approach to those of the above mentioned models.

The resonant part of the amplitudes is usually assumed to have a Breit-Wigner shape with a constant width (see Eq. (18)) below). In order to identify

the part in the total amplitude that possesses this type of behavior we write the pertinent K-matrix in the form proposed in [5]:

$$K_{\pi\pi} = \frac{C}{E_\Delta - E} + D\,, \tag{17}$$

with two constant coefficients C and D. Using these two parameters and the experimental value for E_Δ we obtain an excellent fit to the calculated phase shift (see Fig. 1). The corresponding T-matrix can be cast in the form, suggested by Wilbois et al. in the speed-plot analysis (Eqs. (71)-(76) of [6]):

$$T_{\pi\pi} = \frac{K_{\pi\pi}}{1 - iK_{\pi\pi}} = e^{2i\delta_b}\,\frac{\Gamma_\Delta^T/2}{M_\Delta - E - i\Gamma_\Delta^T/2} + \sin\delta_b e^{i\delta_b}\,. \tag{18}$$

The parameters of the T-matrix can be easily deduced from (17) and are given in Table 1. Since we started from a real K-matrix, the resulting T-matrix automatically obeys unitarity, which is an important merit of our approach.

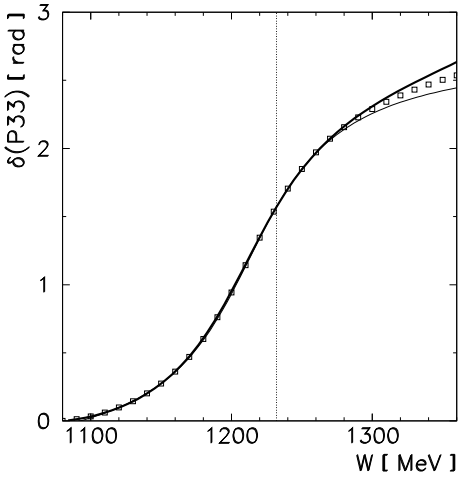

Fig. 1. The phase shift in the P33 channel as a function of the invariant mass. The data points are the single-energy values of the SM02K (2GeV) solution of the SAID πN partial-wave analysis [7]. The thick line represents the calculated phase shift, while the thin line is the two-parameter fit to the calculated values. The agreement is worse only above 1300 MeV where the two-pion channel becomes relevant and our approach is not valid anymore.

In a similar way we can split the K-matrix for the electroproduction in the resonant and the background part:

$$K_{\gamma\pi} = \frac{A}{E_\Delta - E} + B\,. \tag{19}$$

The parameters A and B for each multipole can be determined by fitting the calculated amplitudes using the form implied by (7) and (8):

$$\mathcal{M} = \frac{1}{\sqrt{k_0 k_\gamma}}\,\frac{K_{\gamma\pi}}{1 - iK_{\pi\pi}}\,, \tag{20}$$

where $\mathcal{M}$ is ether $M_{1+}^{(3/2)}$ or $E_{1+}^{(3/2)}$. Alternatively, one can use a simplified form:

$$\mathcal{M} = \frac{K_{\gamma\pi}}{1 - iK_{\pi\pi}}\,, \tag{21}$$

which is more frequently used in the experimental analysis, e.g. in [8] and in the SP-analysis of [6]; the form (20) being used in the MSP analysis of [6]. The resulting parameters are listed in Table 1.

Table 1. Resonance pole parameters extracted from the computed phase shifts and electro-production amplitudes using the form (21). Parameter C is the resonance width divided by 2, D is the tangent of the background phase shift, and M_Δ and Γ_Δ^T are parameters of the T-matrix (see (18)). Experimental values are the recent PDG values [9] and from [6].

R	f_π	C	D	M_Δ	Γ_Δ^T	A(M1)	B(M1)	A(E2)	B(E2)
[fm]	[MeV]	[MeV]		[MeV]	[MeV]		$[10^{-3}/m_\pi]$		$[10^{-3}/m_\pi]$
1.1	78	57	−0.39	1213	49	0.0123	−2.57	−0.000235	−1.19
1.0	81	56	−0.40	1213	48	0.0117	−3.53	−0.000236	−1.09
0.9	83	56	−0.41	1212	48	0.0115	−4.00	−0.000221	−1.00
Experiment		60	−0.435	1210	50				

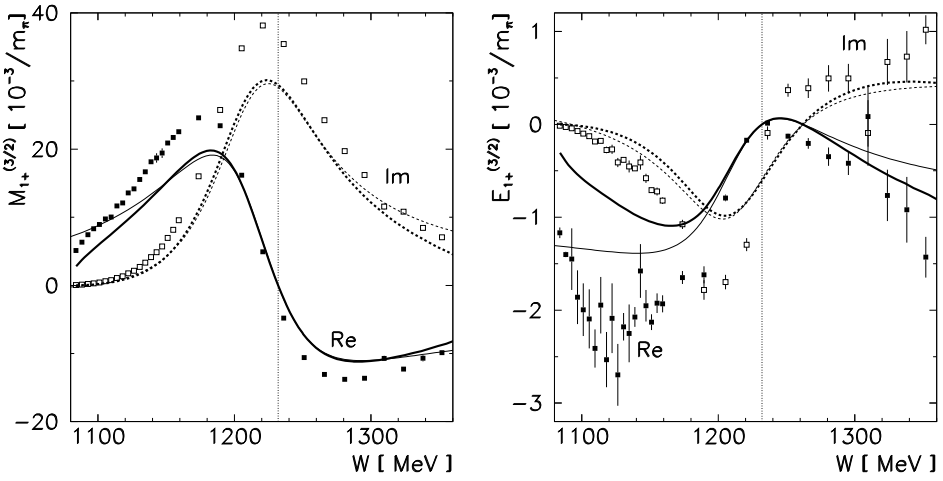

Fig. 2. The $M_{1+}^{(3/2)}$ and the $E_{1+}^{(3/2)}$ electro-production amplitude in the CBM by using $R = 1.0$ fm and $f_\pi = 81$ MeV. The data points in the figures are the single-energy values of the SM02K (2 GeV) solution of the SAID πN partial-wave analysis [7]. The thick lines represent the calculated amplitudes for $R = 1.0$ fm and $f_\pi = 81$ MeV, while the thin lines are the fits to the calculated values using the parameters from Table 1.

From our results it is possible to extract the resonance parameters at the pole of the T-matrix, based on the separation of the amplitude into the resonant and

background parts, using the parameterization [6,8]

$$T = T_R + T_B\,, \qquad T_R = \frac{r\Gamma_\Delta^T e^{i\phi}}{M_\Delta - E - i\Gamma_\Delta^T/2}\,. \tag{22}$$

Using (20), the parameters r, ϕ, and T_B can be expressed in terms of A, B, C, and D. The moduli and phases for the transverse multipoles are shown in Table 2 together with the EMR ratio. While the magnitudes are underestimated, the ratio as well as the phases are much better reproduced.

Table 2. Resonance pole parameters extracted from the computed $E_{1+}^{(3/2)}$ and $M_{1+}^{(3/2)}$ multipoles using the form (21) and parameters in Table 1, compared to various determinations from data. The moduli r are in units of $10^{-3}/m_\pi$. R_Δ is the EMR ratio at the pole of the T-matrix.

R [fm]$/f_\pi$ [MeV]	r_E	ϕ_E	r_M	ϕ_M	R_Δ
1.1 / 78	0.75	$-154°$	16	$-25°$	$-0.031 - 0.037\,i$
1.0 / 81	0.72	$-158°$	15	$-28°$	$-0.030 - 0.037\,i$
0.9 / 83	0.67	$-159°$	14	$-31°$	$-0.029 - 0.037\,i$
Ref. [8]	1.23	$-154.7°$	21.2	$-27.5°$	$-0.035 - 0.046\,i$
Ref. [6] (SP)	1.23	$-156°$	19.9	$-26.0°$	$-0.040 - 0.047\,i$
Ref. [10], Fit 1	1.22	$-149.7°$	22.2	$-27.4°$	$-0.029 - 0.046\,i$
Ref. [11], Fit A	1.38	$-158°$	20.9	$-31°$	$-0.040 - 0.053\,i$

Table 3. Same as Table 2 except that the parameterization (20) is used.

R [fm]$/f_\pi$ [MeV]	r_E	ϕ_E	r_M	ϕ_M	R_Δ
1.1 / 78	0.74	$-157°$	16	$-34°$	$-0.026 - 0.038\,i$
1.0 / 81	0.68	$-160°$	15	$-37°$	$-0.025 - 0.037\,i$
0.9 / 83	0.62	$-162°$	14	$-40°$	$-0.023 - 0.037\,i$
Ref. [6] (MSP)	1.12	$-162°$	20.7	$-36.5°$	$-0.032 - 0.044\,i$

5 Discussion

We have presented a method to calculate directly the K-matrices of resonant electro-production processes in the framework of chiral quark models.

The identification of the resonant part and the background is unambiguous in the K-matrix formalism. In the T-matrix formalism, this separation is based on

the assumption that the position and the width of the resonance do not depend on the invariant energy and is intimately connected to our picture of a resonance as a short-lived particle. While such an assumption cannot be justified in a microscopic model, it is surprising how well it reproduces the experimental results in a broad range of energies. (The agreement at low and high energies in Fig. 2 can be improved by assuming that the background part is energy-dependent.)

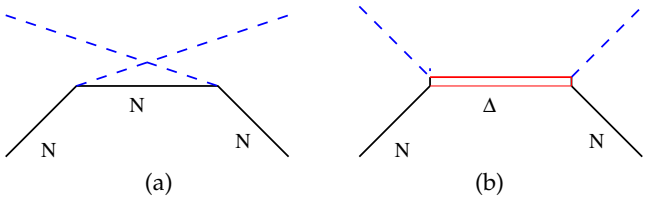

Fig. 3. Two processes dominating the P33 channel

Neither the resonant part nor the background are related to a specific process, such as those depicted in Fig 3. Naively, one would expect that graph (b) corresponds to the resonant part and graph (a) to the background. Yet they both contribute to the resonant part as well as to the background; note that the process (a) alone can lead to the resonance in this channel for sufficiently strong πN coupling and has the opposite sign with respect to the background contribution in the whole energy range.

Let us conclude by noting that a good microscopic model should be able to reproduce the *total* amplitude and not just the resonant part, since, as seen from Tables 2 and 3, the extracted values from the experiment are too unreliable to serve as benchmarks.

References

1. B. Golli, in: B. Golli, M. Rosina, S. Širca (eds.), *Proceedings of the Mini-Workshop "Effective Quark-Quark Interaction*, July 7–14, 2003, Bled, Slovenia, p. 83.
2. P. Alberto, L. Amoreira, M. Fiolhais, B. Golli, S. Širca, submitted to Phys. Lett. B, hep-ph/0409246.
3. R. G. Newton, *Scattering Theory of Waves and Particles*, Dover Publications, New York 1982.
4. K. Bermuth, D. Drechsel, L. Tiator, J. B. Seaborn, Phys. Rev. D **37** (1988) 89.
5. R. M. Davidson, N.C. Mukhopadhyay, Phys. Rev. D **42** (1990) 20.
6. Th. Wilbois, P. Wilhelm, H. Arenhövel, Phys. Rev. C **57** (1998) 295.
7. R. A. Arndt, W. J. Briscoe, R. L. Workman, I. I. Strakovsky, SAID Partial-Wave Analysis, `http://gwdac.phys.gwu.edu/`.
8. O. Hanstein, D. Drechsel, L. Tiator, Phys. Lett. B **385** (1996) 45.
9. S. Eidelman et al., Phys. Lett. B **592** (2004) 1.
10. R. M. Davidson et al., Phys. Rev. C **59** (1999) 1059; the average of VPI and RPI analysis results is listed.
11. R. Workman, R. A. Arndt, Phys. Rev. C **59** (1999) 1810.

BLED WORKSHOPS
IN PHYSICS
VOL. 5, NO. 1

Proceedings of the Mini-Workshop
Quark Dynamics *(p. 70)*
Bled, Slovenia, July 12-19, 2004

Molecular binding of $T_{cc} = DD^*$ tetraquark ⋆

Damijan Janc[a] and Mitja Rosina[a,b]

[b] J. Stefan Institute, 1000 Ljubljana, Slovenia
[a] Faculty of Mathematics and Physics, University of Ljubljana, 1000 Ljubljana, Slovenia

Abstract. We present the results of detailed calculations with Bhaduri and AL1 potential for the $T_{cc} = DD^*$ tetraquark. We show that it has a molecular structure, which can transform, under the influence of an additional three-body force, into a Λ_b-like system where the role of the b quark is played by the heavy cc diquark.

Nonrelativistic potential models have proven to be quite a successful tool for understanding the meson and baryon sector. It is challenging to extend them from one-hadron to two hadron systems, such as the double heavy tetraquarks. Probably the most intriguing tetraquark in this class is the $T_{cc} = DD^*$ tetraquark. The results obtained with different potential models are very contradictive, from unbound [1,2] to deeply bound states [3,4]. If one demands, however, that the model used in the calculations must reproduce accurately the meson as well as baryon sector, then we believe that the dependence of the results on the model should not be so strong. Actually, the results should only be sensitive to the details of the interaction, which are not of the great importance for the meson or baryon sector, such as for example the colour dependent three-body force.

We present the results obtained with two one-gluon-exchange potentials, the Bhaduri [5] and Grenoble AL1 [6] potential. For a long time it was supposed that T_{cc} is unbound with these two potentials, according to seemingly accurate calculations [2,7]. We expanded the tetraquark wavefunction in 140 Gaussians of optimized widths for three sets of Jacobi coordinates to obtain 0.1 MeV accuracy (Fig.1) and show [8,9], however, that with both, the Bhaduri and the Grenoble AL1 potentials, T_{cc} is bound below the DD^* threshold by 0.6 and 2.7 MeV, respectively.

It is essential to use a large enough model space to accommodate the *molecular structure*, in contradistinction to T_{bb} which has an *atomic structure* similar to Λ_b. Both types of configurations are schematically illustrated in Fig.2. If the basis is too small the T_{cc} tetraquark without additional interactions remains unbound. This had happened in [10], where the same basis functions were used as here, but the final basis was spanned with only 40 functions, since so extremely weak binding was not expected. From Fig.1 we see that at least 80 basis function are needed to obtain the energy of the DD^* system lower than the threshold.

⋆ Talk delivered by D. Janc.

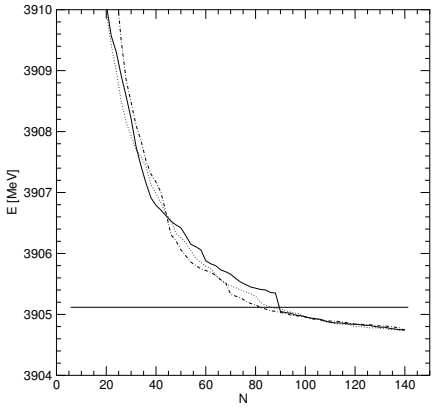

Fig. 1. Energy of the T_{cc} tetraquark with Bhaduri potential as a function of the number of the basis states for three different runs. The $D + D^*$ threshold is also shown. Since the initial parameters are chosen randomly, the convergence is similar as with the stochastic variational approach.

In Fig.3a we plot the probability densities ρ_{QQ} between heavy quarks in T_{bb} and T_{cc} as a function of the interquark distance r_{QQ}:

$$\rho_{QQ}(r) = \langle\psi|\delta(r - r_{QQ})|\psi\rangle.$$

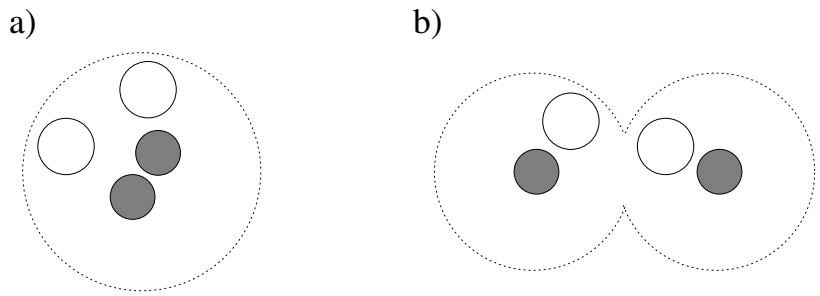

Fig. 2. Schematic illustration of the two light antiquarks (empty circles) and two heavy quarks (dashed circles) in **a):** atomic configuration as we can find it in the T_{bb} tetraquark and in **b):** molecular configuration characteristic for the T_{cc} tetraquark.

There are also other mechanisms to help binding: 3-body forces (which are more effective for 4 particles than for 3 particles – baryons) and pion exchange (pions are almost real when exchanged between D and D^* mesons). The form of the three-body interaction which we introduced into the tetraquark is

$$V^{3b}_{qq\bar{q}}(\mathbf{r}_i, \mathbf{r}_j, \mathbf{r}_k) = -\frac{1}{8} d^{abc} \lambda^a_i \lambda^b_j \lambda^{c*}_k U_0 \exp[-(r^2_{ij} + r^2_{jk} + r^2_{ki})/r^2_0],$$
$$V^{3b}_{q\bar{q}\bar{q}}(\mathbf{r}_i, \mathbf{r}_j, \mathbf{r}_k) = \frac{1}{8} d^{abc} \lambda^a_i \lambda^{b*}_j \lambda^{c*}_k U_0 \exp[-(r^2_{ij} + r^2_{jk} + r^2_{ki})/r^2_0].$$

Here r_{ij} is the distance between i-th and j-th (anti)quark, and similarly for r_{jk} and r_{ki}. λ_a are the Gell-Mann colour matrices and d^{abc} are the SU(3) structure constants ($\{\lambda^a, \lambda^b\} = 2d^{abc}\lambda^c$).

It should be noted that in the baryon sector such a colour structure is irrelevant since there is only one colour singlet state and thus the colour factor

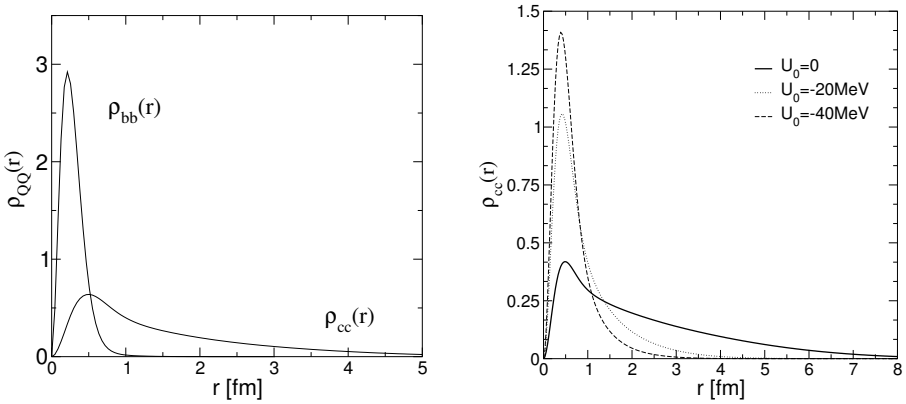

Fig. 3. (a): T_{bb} shows atomic structure while T_{cc} is molecular, $r = r_{bb}$ or r_{cc}; (b): The effect of three-body interaction on the structure of T_{cc} for 3 different strengths.

is just a constant which can be included into the strength of the potential. In tetraquarks the situation is different since there are two colour singlet states: $\bar{3}_{12}3_{34}$ and $6_{12}\bar{6}_{34}$ (or $1_{13}1_{24}$ and $8_{13}8_{24}$ after recoupling). The three-body force operates differently on these two states [11,12] and one can anticipate that in the case of the weak binding it can produce large changes in the structure of the tetraquark. This cannot be otherwise produced simply by reparameterization of the two-body potential, so the weakly bound tetraquarks are a very important laboratory for studying the effect of such an interaction.

It is well known that the constituent quark models with the colour $\lambda \cdot \lambda$ structure give rise to the long-range van der Waals forces [13–15], which can have dramatic effect especially for weakly bound systems with the molecular structure, such as the T_{cc} tetraquark. This interaction appears due to the colour polarization of two mesons in the colour singlet state and is an artefact of the potential approach. It is not present in the full QCD where quark-anriquark pair creation from the confining filed energy would produce an exponential cut-off of this residual interaction. The radial dependence has in the case of the linear confining interaction the structure

$$V(r)_{v.d.Waals} = \mathcal{O}(r^{d-4}) = \mathcal{O}(r^{-3})$$

We now check the effect of this spurious interaction in the T_{cc} tetraquark. In Fig. 4 we present useful quantity, which we call effective potential density

$$\nu_{ij}(r) = \langle\psi|V_{ij}(r_{ij})\delta(r - r_{ij})|\psi\rangle = V_{ij}(r)\rho_{ij}(r). \quad (1)$$

In Fig. 4b one can see that this effect is indeed present at large separations ($r > 2$ fm) but is extremely small. Integrating this attractive tail of the potential, we obtain a contribute less than 100 keV to the binding of the system. On the other hand, more interesting feature of the effective potential shown in Fig. 4 is the repulsive force between quarks at the medium distance between quarks (1.5 fm$> r > 2$ fm). The maximal value of potential barrier is $V_{ij}(r \sim 1.5\,\text{fm}) = \nu_{ij}/\rho_{ij} = 1$ MeV. This then allows that also resonant states can appear in the model which are not possible in a simple potential well.

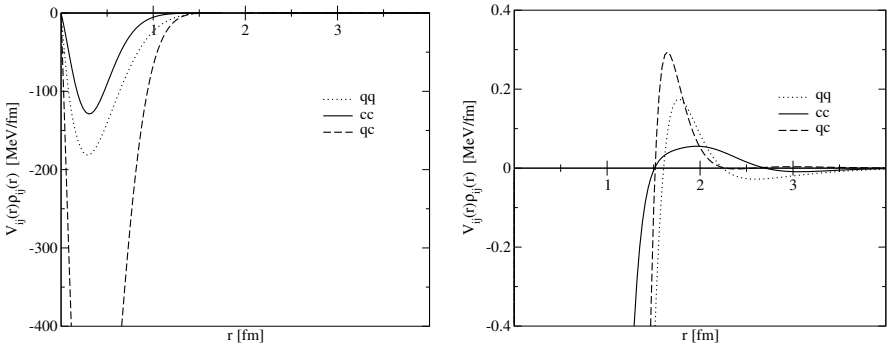

Fig. 4. Left: Potential densities v_{ij} between (anti)quarks as calculated from Eq. 1 for Bhaduri potential. Right: Enlarged section of the left-hand side figure, where van der Waals attraction and medium-range repulsion can be seen.

References

1. Manohar A. V., Wise M. B.: Nucl.Phys. **B399**, 17 (1993).
2. Silvestre-Brac B., Semay C.: Z. Phys. **C57**, 273 (1993).
3. Vijande J., Fernandez F., Valcarce A., Silvestre-Brac B.: Eur. Phys. J. **A19**, 383 (2004).
4. Pepin S., Stancu Fl., Genovese M., Richard J.M.: Phys. Lett. **B393**, 119 (1997).
5. Bhaduri R. K., Cohler L. E., Nogami Y.: Nuovo Cim. **A65**, 376 (1981).
6. Silvestre-Brac B.: Few-Body Systems **20**, 1 (1996).
7. Semay C. Silvestre-Brac B.: Z. Phys. **C61**, 271 (1994).
8. Janc D., Rosina M.: hep-ph/0405208.
9. Del Fabbro A., Janc D., Rosina M., Treleani D.: hep-ph/0408258.
10. Janc D., Rosina M.: *Bled Workshops in Physics* **4**, No.1, 89 (2003).
11. Dmitrasinovic V.: Phys. Lett. **B499**, 135 (2001).
12. Dmitrasinovic V.: Phys. Rev. **D67**, 114007 (2003).
13. Weinstein J., Isgur N.: Phys. Rev. **D27**, 588 (1983).
14. Greenberg O.W., Lipkin H.J.: Nuc. Phys. **A370**, 349 (1981).
15. Feinberg G., Sucher J.: Phys. Rev. **D20**, 1717 (1979).

BLED WORKSHOPS
IN PHYSICS
VOL. 5, NO. 1

Proceedings of the Mini-Workshop
Quark Dynamics *(p. 74)*
Bled, Slovenia, July 12-19, 2004

New ideas about production and detection of cc-tetraquarks ⋆

Mitja Rosina[a,b] and Damijan Janc[a]

[b] J. Stefan Institute, 1000 Ljubljana, Slovenia
[a] Faculty of Mathematics and Physics, University of Ljubljana, 1000 Ljubljana, Slovenia

Abstract. We estimate the rate of double charm production in B-factories Belle and BaBar, in hadronic machines with fixed targets RHIC and SELEX, and in high energy colliders Tevatron and LHC. For detection we propose the branching ratio between pionic and gamma decay.

1 Introduction

We have shown that the molecule-like configuration of the DD^* dimeson (also called tetraquark) enables weak binding even in the case of the Bhaduri or Grenoble AL1 interaction (-0.7 or -2.6 MeV, respectively) [1,2]. The surprise that the cc-tetraquark is likely to be bound against the $D + D^*$ decay strongly motivates experimental exploration. To encourage future experimental analyses, we estimate the production rate on several present and future machines, and propose an experimental signature for detection.

2 Production

Regarding the **production of** T_{cc}, we consider a three-step process:
(i) production of two $c\bar{c}$ pairs,
(ii) formation of a diquark $c + c \to cc$,
(iii) dressing of the diquark $cc \to ccq$, $q = u, d, s$ (90 %), or $cc \to cc\bar{u}\bar{d}$ (10 %).
Here are some provocative guesses: [3]

- SELEX [4] has seen 50 candidates for $ccq \Longrightarrow$ the corresponding hypothetical 5 T_{cc} are to few to be recognized at present.
- Belle reported prompt J/ψ production in e^+e^- annihilation at $\sqrt{s}$ = 10.6 GeV and found that the most of the observed J/ψ production is due to the double $c\bar{c}$ production $\sigma(e^+e^- \to J/\psi c\bar{c})/\sigma(e^+e^- \to J/\psi X) = 0.59$ which correspond to 2000 events from their 46.2 fb^{-1} data sample $\Longrightarrow$ promising for the T_{cc} production! Similar rate is also expected for BaBar.

⋆ Talk delivered by M. Rosina.

- High energy colliders (RHIC (p-p), RHIC (p-Au); Tevatron, LHCb, LHC--ALICE) might produce sufficient double charm by double two-gluon fusion [5–8,3]
  $(g+g)+(g+g) \to (c+\bar{c})+(c+\bar{c})$. Our estimate for the T_{cc} cross section are 4, 750; 21, 27, 58 nb, respectively.

In most machines, the rate seems promising to start the hunt!

3 Detection

The main problem with detection of the weakly bound T_{cc} tetraquark is how to distinguish the pion or photon emitted by the decay of the free D^* meson from the one emitted by the D^* meson bound inside the tetraquark. We can exploit the fact that the phase space for $D^* \to D + \pi$ decay is very small. Therefore we propose as a signature the branching ratio between radiative and pionic decay. In addition, the analysis using the Dalitz plot can help to distinguish whether the pion was emitted from a bound state, resonance state of $D + D^*$ or from free D^* meson.

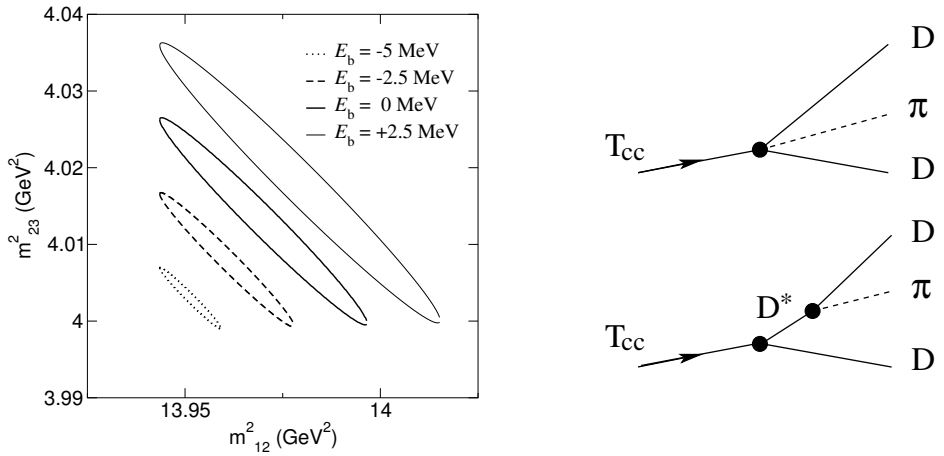

Fig. 1. Left: Dalitz plot for the $T_{cc} \to DD\pi$ decay, E is binding energy of T_{cc}, 3 is pion; Right: The two graphs contributing in the case of resonance $E > 0$

References

1. These Proceedings
2. D. Janc and M. Rosina, hep-ph/0405208, submitted to *Few-Body Systems*.
3. D. Janc and M. Rosina, hep-ph/0408258, submitted to *Phys. Rev. D*.
4. M. Mattson et al. (SELEX Collaboration), *Phys. Rev. Lett.* **89**, 112001 (2002); J. S. Russ (on behalf of the SELEX Collaboration), hep-ex/0209075
5. A. Del Fabbro and D. Treleani, *Phys. Rev.* **D61**, 077502 (2000); *Phys. Rev.* **D63**, 057901 (2001); *Nucl. Phys. B* **92**, 130 (2001).

6. M. Rosina, D. Janc, D. Treleani, and A Del Fabbro, *Bled Workshops in Physics* **3**, No.3, 63 (2002).
7. D. Janc, M. Rosina, D. Treleani, and A. Del Fabbro, Few-Body Systems Suppl. 14 (2003) 25.
8. A. Del Fabbro and D. Treleani, *Bled Workshops in Physics* **4**, No.1, 75 (2003).

BLED WORKSHOPS
IN PHYSICS
VOL. 5, NO. 1

Proceedings of the Mini-Workshop
Quark Dynamics *(p. 77)*
Bled, Slovenia, July 12-19, 2004

Recent results on Δ resonance production at MIT-Bates, MAMI, and JLab (Hall A)

S. Širca[a,b]

[a] Faculty of Mathematics and Physics, University of Ljubljana, 1000 Ljubljana, Slovenia
[b] Jožef Stefan Institute, 1000 Ljubljana, Slovenia

Abstract. Electro-production of mesons on nucleons is the optimal tool to investigate the dynamics of nucleon resonance excitation. In the past years, tremendous advances have been made based on new instrumental capabilities of modern electron beam facilities, in particular by measuring polarization observables. Some of the recent results on Δ resonance production from three major coincidence electron-scattering collaborations are presented.

1 The facilities

Modern electron-scattering facilities possess distinct instrumental features which allow for a mutually complementary kinematic coverage, exploitation of various polarization degrees of freedom (e.g. through measurement of double-polarization observables), and different controls of systematic uncertainties.

The MIT-Bates facility has two collaborations: the Out-of-Plane Spectrometer System (OOPS) and the Bates Large-Acceptance Spectrometer Toroid (BLAST). Both utilize $\sim 1\,\mathrm{GeV}$ polarized electron beams of the Bates linac, in extraction (quasi-CW) or storage mode, respectively. OOPS has recently stopped taking data and is now in the process of data analysis. It operated four relatively light-weight spectrometer modules that can be positioned almost independently about the momentum transfer direction, and out of the electron scattering plane, to detect protons and charged pions [1]; this ensures an excellent control of systematics. BLAST is a large-acceptance toroidal magnetic spectrometer [2] that has only recently started taking production data, with a capability of simultaneous detection of charged and neutral particles in large momentum and angular ranges, with a moderate energy resolution. Its key feature are the gaseous, isotopically pure, vector-polarized hydrogen, and vector- and tensor-polarized deuterium internal targets. In a high-luminosity environment of the MIT-Bates storage ring, excellent figures of merit are achievable, which enable us to access double-polarization observables in a number of physical channels.

The A1 Collaboration at the MAMI-B accelerator makes use of the high-polarization, $\sim 0.9\,\mathrm{GeV}$ CW beam in conjunction with either target (high-polarization $^3\vec{\mathrm{He}}$) or recoil polarimetry (focal-plane polarimeter), and a setup of three high-resolution spectrometers [3] (one of them can be positioned out of plane).

In addition, individual dedicated spectrometers or non-magnetic detector systems are installed periodically for measurements of specific reaction channels. The accelerator is presently being upgraded to the energy of 1.5 GeV, and one of the spectrometers is being added to the setup to accommodate the higher particle momenta.

The Hall A Collaboration at Jefferson Lab operates two high-resolution magnetic spectrometers and auxiliary detector systems, making use of the high-polarization CW beam of energies up to 6 GeV. Both target polarization ($^3\vec{\mathrm{He}}$ with similar operational parameters as at A1) and recoil polarimetry (focal-plane polarimeter with optimizable secondary-scattering configuration) are possible. The large kinematic freedom given by the high beam energies allows us to explore the nucleon resonance production at relatively high Q^2, with invariant energies W extending beyond ~ 2 GeV.

2 Pion-cloud effects at low Q^2

One of the key goals of the experiments devoted to the $N \to \Delta$ transition is to determine the electric (E2) and Coulomb (C2) quadrupole transition amplitudes. These are much smaller than the leading magnetic dipole amplitude (M1), and indicate that the nucleon and/or the Δ deviate from spherical symmetry. In models involving explicit pion degrees of freedom, large contributions to M1 and dominant contributions to E2 and C2 can be attributed, schematically, to the pion cloud surrounding the bare quark core (or pion loop effects). The motivation behind the recent $N \to \Delta$ program at MIT-Bates and MAMI is therefore to map out the M1, E2, and C2 multipoles in the region of low $Q^2 \simeq 0.1\,(\mathrm{GeV/c})^2$ where pion-cloud effects are expected to play the most important role.

The electric quadrupole amplitude E2 is accessible through a particular combination of the partial cross-sections

$$\begin{aligned}\sigma_{0\pi}(\theta_\pi^\star) &= \sigma_0(\theta_\pi^\star) + \sigma_{TT}(\theta_\pi^\star) - \sigma_0(180^\circ) \\ &\sim 2\,(\cos\theta_\pi^\star + 1)\,\mathrm{Re}\,[E_{0+}^* M_{1+}] - 12\,\sin^2\theta_\pi^\star\,\mathrm{Re}\,[E_{1+}^* M_{1+}]\,,\end{aligned}$$

where $\theta_\pi^\star$ is the center-of-mass emission angle of the pion and $\sigma_0 = \sigma_T + \varepsilon\sigma_L$. It is clear that $\sigma_{0\pi}$ exhibits a large sensitivity to $EMR \sim \mathrm{Re}\,[E_{1+}^* M_{1+}]$. However, backgrounds like the electric dipole amplitude E_{0+} in the $\mathrm{Re}\,[E_{0+}^* M_{1+}]$ interference, as well as higher partial waves ($l \geq 2$), need to be obtained from a model in order to extract the EMR.

Similarly, the quadrupole amplitude C2 is accessed through LT-terms in the cross-section which contain interferences of the scalar quadrupole S_{1+} with the dominant magnetic dipole M_{1+}:

$$\sigma_{LT}(\theta_\pi^\star) \sim \sin\theta_\pi^\star\,\mathrm{Re}\,[S_{0+}^* M_{1+}] - 6\,\cos\theta_\pi^\star\,\sin\theta_\pi^\star\,\mathrm{Re}\,[S_{1+}^* M_{1+}]\,,$$

$$\sigma_{LT'}(\theta_\pi^\star) \sim -\sin\theta_\pi^\star\,\mathrm{Im}\,[(-6\cos\theta_\pi^\star\,S_{1+} + S_{0+})^* M_{1+}]\,.$$

The σ_{LT} is primarily sensitive to $CMR \sim \mathrm{Re}\,[S_{1+}^* M_{1+}]$ while $\sigma_{LT'}$, accessible only with a polarized beam and out-of-plane detection, probes $\mathrm{Im}\,[S_{1+}^* M_{1+}]$. (This is important as the relative phases between the multipoles need to be fixed.)

The analysis of all existing OOPS data at $Q^2 = 0.127\,(\mathrm{GeV/c})^2$, including the latest runs with the CW beam at MIT-Bates [5], yield

$$\mathrm{EMR} = (-2.3 \pm 0.3_{\mathrm{stat+sys}} \pm 0.6_{\mathrm{model}})\,\% ,$$
$$\mathrm{CMR} = (-6.1 \pm 0.2_{\mathrm{stat+sys}} \pm 0.5_{\mathrm{model}})\,\% .$$

At this moment, these are the most accurately known EMR and CMR values at any finite value of Q^2. (Note that the E2 multipole and EMR are more difficult to isolate in electro-production than C2 and CMR because the transverse responses are dominated by $|M_{1+}|^2$ which is absent in the longitudinal sector.) The extracted CMR is in agreement with the older OOPS extractions, with the Mainz determination from recoil polarimetry at $Q^2 = 0.121\,(\mathrm{GeV/c})^2$ which resulted in $\mathrm{CMR} = (-6.4 \pm 0.7_{\mathrm{stat}} \pm 0.8_{\mathrm{sys}})\,\%$ [6], as well as with the CLAS data in a broader Q^2-range [7]. (New preliminary results for EMR and CMR from CLAS exist at Q^2 up to $6\,(\mathrm{GeV/c})^2$ and have been reported at various meetings in 2004.)

In addition to the extractions of EMR and CMR at low Q^2, the present data sets will be used to try to answer several open questions arising from previous experiments at MIT-Bates and MAMI (see contribution of S. Širca to the 2003 Proceedings [8]). When final results in σ_{LT}, $\sigma_{\mathrm{LT'}}$, and other partial cross-sections from OOPS and MAMI become available, they will help constrain the models of pion electro-production [9–11]. In particular the observables involving polarized beams in conjunction with either polarized targets or recoil polarimetry, represent severe tests of the models. Preliminary results on $\sigma_{\mathrm{LT'}}$ from the MAMI runs in 2003 are shown in Fig. 1.

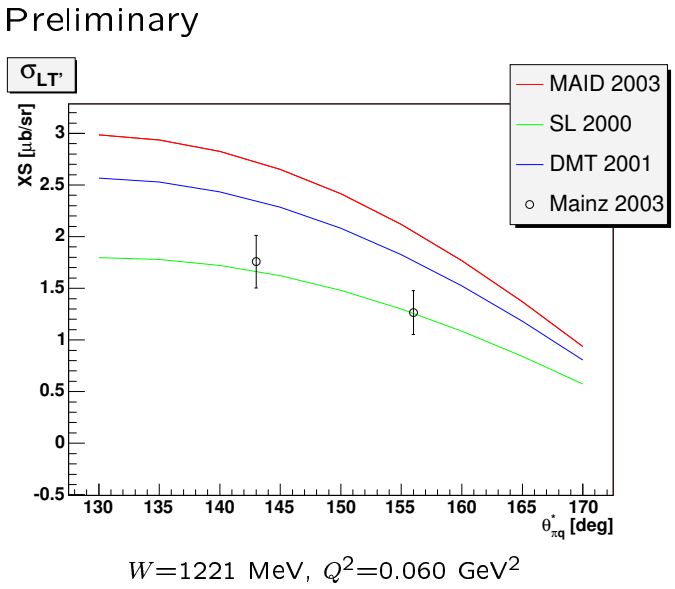

Fig. 1. Preliminary results on $\sigma_{\mathrm{LT'}} \sim \mathrm{Im}\,[S^*_{1+} M_{1+}]$ from MAMI, compared to three state-of-the-art model calculations [9–11].

3 Multipole decompositions at high Q^2

To minimize the model dependence of the extracted multipole amplitudes, a measurement with a sufficient number of independent observables is needed. The $N \rightarrow \Delta$ transition cross-section in the case of a polarized beam, unpolarized target, and recoil polarimetry, can be decomposed into 18 independent structure functions, each one of which contains different forms of multipole bilinears. Through a partial-wave analysis of the measured angular distributions of the structure functions, all relevant multipoles can be extracted from the data in a model-independent way. By measuring the angular distributions of 16 independent structure functions in broad angular ranges, the Hall A experiment E91-011 has succeeded in delivering Re and Im parts of all $l = 0, 1$ multipoles in the vicinity of $Q^2 = 1.0\,(\mathrm{GeV/c})^2$ and $W = 1232\,\mathrm{MeV}$. The residual model-dependence is due to the higher partial waves ($l \geq 2$) which were constrained by MAID.

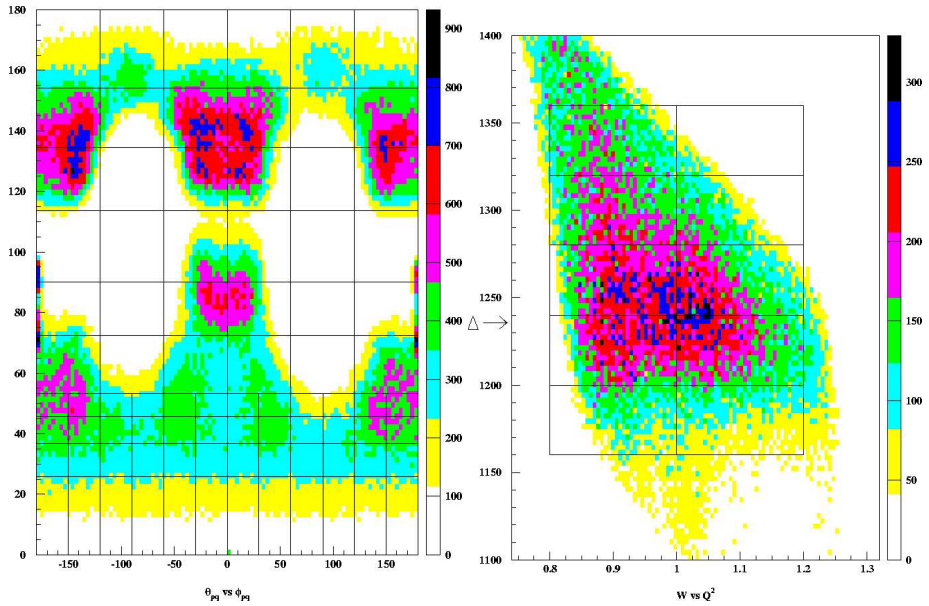

Fig. 2. Kinematical coverage in the E91-011 experiment, with indicated binning for the polarization analysis. Left: angular acceptance in recoil nucleon center-of-mass angles; Right: acceptance in W and Q^2.

Recoil polarimetry in the $p\pi^0$ channel is indeed the most powerful and hence the preferred method to cleanly disentangle individual multipoles; however, this goal could be achieved because of the strong kinematic focusing of the proton emission cone into the spectrometer acceptance at relatively high Q^2. In this way, a substantial angular coverage was achieved (see Fig. 2). The measured structure functions at $W = (1.23 \pm 0.02)\,\mathrm{GeV}$ and $Q^2 = (1.0 \pm 0.2)\,(\mathrm{GeV/c})^2$ are shown in Fig. 3. The final analysis which will result in the individual multipoles, as well as the EMR and the CMR is almost complete, and will be reported soon.

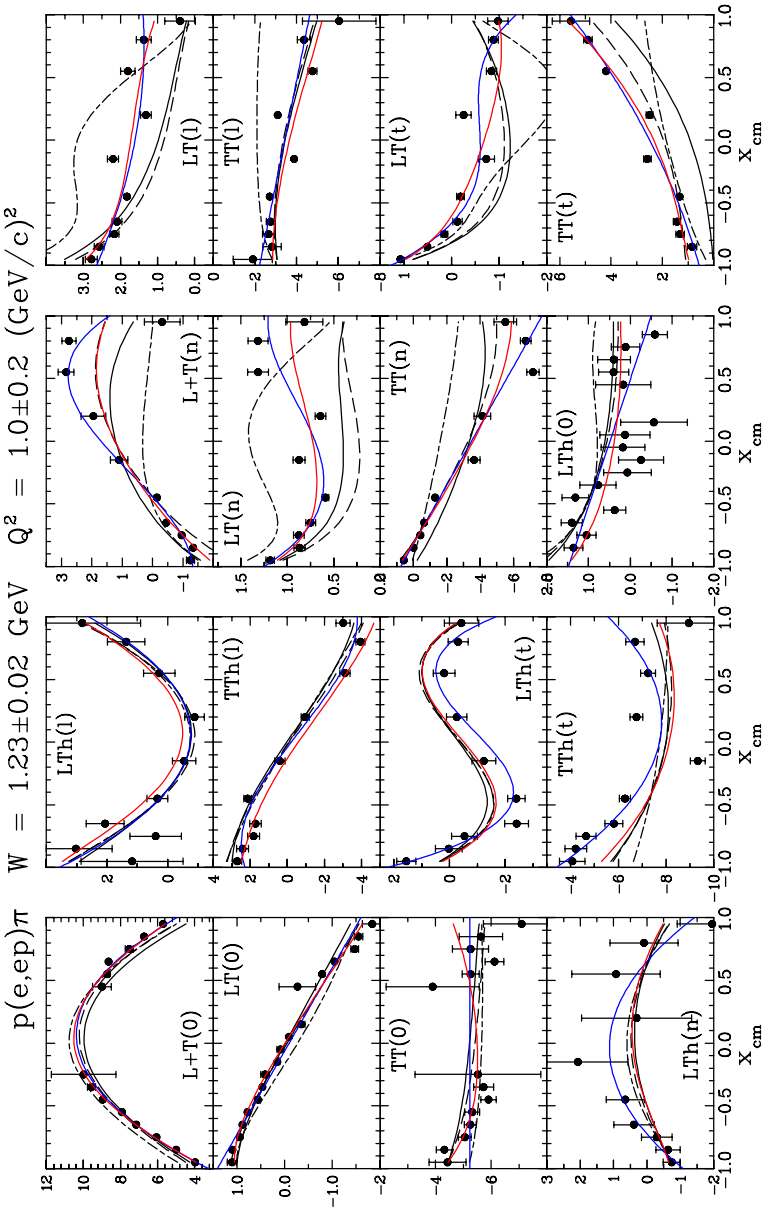

Fig. 3. Preliminary E91-011 results for the polarized structure functions in $p(\vec{e}, e'\vec{p})\pi^0$ at $W = (1.23 \pm 0.02)$ GeV and $Q^2 = (1.0 \pm 0.2)$ $(GeV/c)^2$, compared to the pion electroproduction models, and different multipole fits.

4 Work in progress and outlook

The analysis of the data taken with the OOPS spectrometer system at $Q^2 = 0.127\,(\mathrm{GeV/c})^2$ is underway both in the $p\pi^0$ and the $n\pi^+$ channels, at the resonance ($W = 1232\,\mathrm{MeV}$) and below it ($W = 1175\,\mathrm{MeV}$). Selected unpolarized responses have measured which allow for a precise extraction of the EMR and CMR ratios with a relatively small model dependence. By measuring two channels, a first step towards the isospin decomposition of the amplitudes will have been made.

Preliminary responses in the $p\pi^0$ channel from A1 at MAMI are already available, while the full analysis is expected to be complete soon. We expect it to yield five unpolarized responses and the EMR and CMR ratios at $Q^2 = 0.06$ and $0.2\,(\mathrm{GeV/c})^2$, where the effects of the pion cloud appear to be most prominent. The measurement of σ'_{LT} alone, with respect to the older A1 [12] and the latest CLAS (JLab) [13] data set, will represent an important constraint on the state-of-the-art models, in particular by constraining the $l = 0$ background amplitudes. (In σ'_{LT}, the discrepancies between the theories in the $l = 0$ partial waves arise predominantly through the $\mathrm{Im}\,[M^*_{1+}S_{0+}]$ interference.)

The data analysis of the $N \to \Delta$ experiment in Hall A has been concluded and is being prepared for publication. The focal-plane polarimetry approach used in this experiment can be straightforwardly extended to the energy region of the Roper resonance; an experiment proposal is presently being considered. However, the cross-sections in the second resonance region are far smaller than in the Δ region, and the sensitivities to the resonant Roper multipoles appear to be largest at small Q^2 where the kinematic focusing is too weak to allow for a full partial-wave decomposition.

References

1. Z.-L. Zhou, S. Širca et al., Nucl. Instr. and Meth. A **487** (2002) 365.
2. R. Alarcon, Prog. Part. Nucl. Phys. **44** (2000) 253.
3. K. I. Blomqvist et al., Nucl. Instr. and Meth. A **403** (1998) 263.
4. J. Alcorn et al., Nucl. Instr. and Meth. A **522** (2004) 294.
5. N. F. Sparveris et al., submitted to Phys. Rev. Lett., `arXiv:nucl-ex/0408003`.
6. Th. Pospischil et al. (A1 Collaboration), Phys. Rev. Lett. **86** (2001) 2959.
7. K. Joo et al., Phys. Rev. Lett. **88** (2002) 122001.
8. S. Širca, in: B. Golli, M. Rosina, S. Širca (eds.), *Proceedings of the Mini-Workshop "Effective Quark-Quark Interaction*, July 7–14, 2003, Bled, Slovenia, p. 107.
9. D. Drechsel, O. Hanstein, S. S. Kamalov, L. Tiator, Nucl. Phys. A **645** (1999) 145.
10. T. Sato, T.-S.H. Lee, Phys. Rev. C **63** (2001) 055201.
11. S. S. Kamalov, S. Yang, Phys. Rev. Lett. **83** (1999) 4494.
12. P. Bartsch et al. (A1 Collaboration), Phys. Rev. Lett. **88** (2002) 142001.
13. K. Joo et al., Phys. Rev. C **68** (2003) 032201(R).

BLED WORKSHOPS
IN PHYSICS
VOL. 5, NO. 1

Proceedings of the Mini-Workshop
Quark Dynamics *(p. 83)*
Bled, Slovenia, July 12-19, 2004

Search for Pentaquarks at HERA-B

Tomi Živko

for the HERA-B Collaboration

Abstract. A search for Θ^+ and $\Xi_{3/2}$ pentaquarks has been performed in channels $p\,K^0_S$ and $\Xi\,\pi$ in proton - nucleus interactions at mid-rapidity and $\sqrt{s} = 41.6$ GeV/c^2 . No evidence for pentaquarks has been found in analyzed channels. Upper limits have been set on pentaquark production cross sections.

Experimental evidence for a new hadron state at 1540 MeV/c^2 decaying to $n\,K^+$ was presented by experiment LEPS [1] in 2003. The particle was named $\Theta^+(1540)$. Due to a quark picture of neutron and K^+, the hadron Θ^+ must contain at least four quarks and one antiquark. After that, several other collaborations reported evidence for a peak in the invariant mass spectrum of $n\,K^+$ or $p\,K^0_S$. The $p\,K^0_S$ peak was regarded as evidence for $\Theta^+ \to pK^0_S$ on the grounds "no narrow $\Sigma^{\star+}$ is known around 1.5 GeV/c^2 ". Currently, there are 12 experiments that have claimed evidence for decays $\Theta^+ \to nK^+$ or $\Theta^+ \to pK^0_S$. The measured mass lies in the range 1521 - 1555 MeV/c^2 . There is a peculiarity that $p\,K^0_S$ experiments report smaller value of mass than $n\,K^+$ ones. The measured widths have all been consistent with the experimental resolution which is typically 20 MeV/c^2 . The presented peaks have statistical significance of about 5 σ. In theoretical models Θ^+ is a member of an antidecuplet which also contains isospin 3/2 family $\Xi_{3/2}$ of doubly strange pentaquarks. Evidence for doubly charged and neutral member of the family was observed in $\Xi\,\pi$ decay channels at mass of 1862 MeV/c^2 by NA49 [2]. The statistical significance of $\Xi_{3/2}$ peak is also about 5 σ. Up to now, this has been the only evidence for $\Xi_{3/2}$. From the other side, the number of high statistics experiments reporting negative search results for Θ^+ and $\Xi_{3/2}$ is growing. Direct comparison of positive and negative search results is not possible because the experiments are not of the same type. However, the negative search results reported much larger yield of common particles like $\Lambda(1520)$ and $\Xi(1530)^0$, thus proving their ability to search for possible pentaquark signals in channels $p\,K^0_S$ and $\Xi\,\pi$. This short survey of experimental situation suggests that existence of pentaquarks is not proven beyond reasonable doubt. The search for Θ^+ and $\Xi_{3/2}$ was done also at HERA-B. The main features of the analysis are presented here, while details can be found elsewhere [3].

HERA-B is a fixed target experiment at the 920 GeV proton storage ring of DESY. It is a forward magnetic spectrometer with a high resolution vertexing and tracking system and good particle identification. The detector has good

acceptance in the mid-rapidity region. The informations from the silicon vertex detector, the main tracker system, ring imaging Cherenkov (RICH) counter and the electromagnetic calorimeter (ECAL) were used in this analysis. The present study was performed on a sample of about 200 millions of minimum bias events that were taken at $\sqrt{s} = 41.6$ GeV/c^2 using carbon, titanium and tungsten targets. Strange particles are frequent in proton - nucleus interactions at this energy, and HERA-B has reconstructed a large number of $K^0_S \to \pi^+\pi^-$, $\Lambda \to p\pi^-$ and $\bar{\Lambda} \to \bar{p}\pi^+$ decays. A clean sample of Ξ hyperons was obtained in decay modes $\Xi^- \to \Lambda\pi^-$ and $\bar{\Xi}^+ \to \bar{\Lambda}\pi^+$. Background in all fore mentioned channels was efficiently reduced using decay topology, so there was no need for particle identification. Table 1 summarizes the statistics of relevant signals together with the measured mass resolutions. All measured masses are within 1 MeV/c^2 compatible with the table values.

Signal	C target	all targets	σ [MeV/c^2]
K^0_S	2.2M	4.9M	4.9
Λ [$\bar{\Lambda}$]	440k[210k]	1.1M[520k]	1.6
Λ (1520) [$\bar{\Lambda}$(1520)]	1.9k[1.1k]	5.1k[2.3k]	2.3
Ξ^- [$\bar{\Xi}^+$]	4.7k [3.4k]	11.8k [8.2k]	2.6
$\Xi(1530)^0$ [$\bar{\Xi}(1530)^0$]	610 [380]	1.4k [940]	2.9

Table 1. Statistics and experimental mass resolution (σ) for relevant particles are given for carbon target and for all targets.

HERA-B does not have capabilities for the identification of neutrons. Therefore, the search for Θ^+ was performed in the decay channel $p\,K^0_S$. Protons were identified requiring the proton likelihood from the RICH to be larger than 0.95. Probability that a particle which is not proton passes this cut is below 1%. Both particles, proton and K^0_S had to point to the main vertex. K^0_S candidates had to lie in $\pm 3\sigma$ mass window around the table mass. A clean K^0_S sample remained after removing particles whose mass was consistent with Λ or $\bar{\Lambda}$. The invariant mass spectrum of selected $p\,K^0_S$ pairs is shown for p+C data in Fig. 1a. The shape of background was obtained by event mixing technique and is represented by a full line. MC studies show that the mass resolution in the presented mass region is in 2.6 - 6.1 MeV/c^2 range. At the Θ^+ mass, the resolution is 3.9 MeV/c^2. We determined the upper limit on the number of signal events in the invariant mass plot as a function the signal mass. The resulting nuclear cross section as a function of the signal mass is presented in Fig. 1b (full line).

Assuming $A^{0.7}$ dependence of the nuclear cross section on the atomic number, we obtained the upper limit on $Br \times d\sigma/dy|_{y=0} < 3.7$ μb/nucleon in the mid-rapidity region for Θ^+ mass of 1530 MeV/c^2. The upper limit varies from 3 to 22 μb in the mass region 1521 - 1555 MeV/c^2. The upper limits obtained using data from all targets are similar. We also tried with other search strategies,

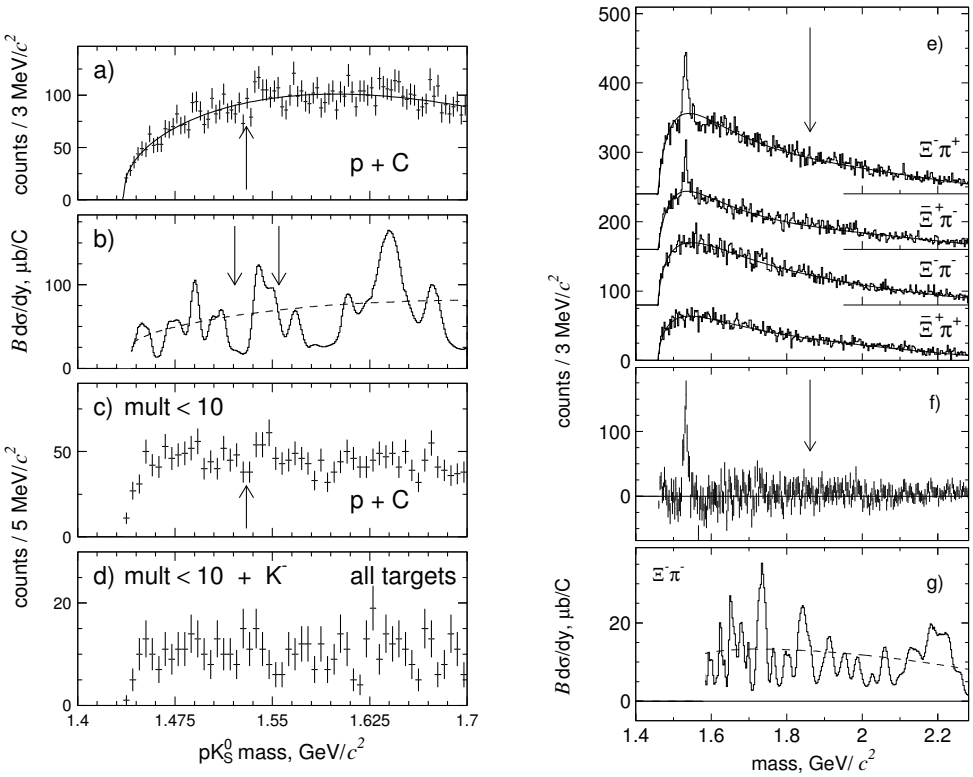

Fig. 1. Invariant mass distributions and upper limits on nuclear cross section for channels p K^0_S (left) and $\Xi\pi$ (right). Arrows denote mass region 1521 - 1555 and mass of 1530 MeV/c^2 (left) and mass of 1862 MeV/c^2 (right). Data were taken with carbon target. See text for details.

like: a) requiring a low track multiplicity in an event (Fig. 1c), b) strangeness tagging, by requiring a particle with an s quark (Λ , K^-) in an event, c) combination (Fig. 1d) of criteria a) and b), d) relaxation of the proton identification cut. None of the attempts resulted in a significant narrow peak in the mass spectrum. We checked capabilities of the HERA-B detector by reconstruction of $\Lambda(1520) \to pK^-$. Masses of Θ^+ and Λ (1520) are similar as well as geometrical acceptances for $\Theta^+ \to pK^0_S$ and $\Lambda(1520) \to pK^-$. Using RICH likelihood cut for both proton and K^- , we obtained a clean signal for Λ (1520). Assuming Br($\Theta^+ \to pK^0_S$)=1/4, we determined the UL(95%) on the particle ratio $\frac{\Theta^+}{\Lambda(1520)} < 0.92\%$ in the mid-rapidity region. This upper limit is more than one order of magnitude lower than predictions of statistical hadronization models. We also found that $\frac{\Theta^+}{\Lambda(1116)} < 0.27\%$.

We searched for members of $\Xi_{3/2}$ family in decay channels $\Xi^-\pi^-$, $\Xi^-\pi^+$ and c.c. Ξ^- candidates had to lie in $\pm 3\sigma$ mass window around the table mass. Both Ξ^- and π candidates had to point to the main vertex. Weak identification cuts with RICH and ECAL removed tracks with clear electron, kaon or proton identity from the π sample. The invariant mass spectra of $\Xi\pi$ pairs obtained from

p+C data are shown in Fig. 1e for all four charge combinations. The background shape is obtained from event mixing and is normalized to the data. The experimental resolution in the analyzed mass region is in 2.9 - 10.6 MeV/c^2 range and has value of 6.6 MeV/c^2 at the mass of 1862 MeV/c^2 . The only observed structure in the spectra are signals for $\Xi(1530)^0$ and $\bar{\Xi}(1530)^0$ in neutral channels. Fig. 1f gives sum of invariant mass distributions of all four charge channels after subtraction of background. Particularly, there is no enhancement in mass region around around 1862 MeV/c^2 , where NA49 observed $\Xi_{3/2}$ candidates. We determined UL(95%) on $Br \cdot d\sigma/dy|_{y=0}$, which at mass of 1862 MeV/c^2 are 2.5, 2.3, 0.85 and 3.1 μb/nucleon in $\Xi^-\pi^-$, $\Xi^-\pi^+$, $\bar{\Xi}^+\pi^+$ and $\bar{\Xi}^+\pi^-$ channels, respectively. The corresponding upper limits using all targets are 2.7, 3.2, 0.94 and 3.1 μb /nucleon. We also found the UL(95%) on particle ratio $Br \cdot \Xi^{--}/\Xi^0(1530) < 4\%$ and $Br \cdot \Xi^{--}/\Xi^- < 3\%$. As an illustration, the UL(95%) on nuclear cross section is presented in Fig. 1g (full line) as function of Ξ^{--} mass.

To conclude, we searched for pentaquark signals in channels $p\,K^0_S$ and $\Xi\pi$. Having found no evidence for signals we set upper limits on production cross sections and particle ratios in mid-rapidity region. If existent, strange pentaquarks (Θ^+ and $\Xi_{3/2}$) also seem to have exotic production mechanisms.

References

1. T. Nakano *et al.* (LEPS Collaboration), Phys. Rev. Lett. **91**, 012002 (2003), [arXiv:hep-ex/0301020].
2. C. Alt *et al.* (NA49 Collaboration), Phys. Rev. Lett. **92**, 042003 (2004), [arXiv:hep-ex/0310014].
3. I. Abt *et al.* (HERA-B Collaboration), submitted to Phys. Rev. Lett. (2004), [arXiv:hep-ex/0408048].

BLEJSKE DELAVNICE IZ FIZIKE, LETNIK 5, ŠT. 1, ISSN 1580–4992
BLED WORKSHOPS IN PHYSICS, VOL. 5, NO. 1

Zbornik delavnice 'Quark Dynamics', Bled, 12. – 19. julij 2004
Proceedings of the Mini-Workshop 'Quark Dynamics', Bled, July 12–19, 2004

Uredili in oblikovali Bojan Golli, Mitja Rosina, Simon Širca
Publikacijo sofinancira Ministrstvo za šolstvo, znanost in šport
Tehnični urednik Vladimir Bensa

Založilo: DMFA – založništvo, Jadranska 19, 1000 Ljubljana, Slovenija
Natisnila Tiskarna MIGRAF v nakladi 100 izvodov

Publikacija DMFA številka 1586